

UNIVERSITÀ DELLA CALABRIA



UNIVERSITA' DELLA CALABRIA

Dipartimento di Fisica

Dottorato di Ricerca in

Scienze e Tecnologie Fisiche, Chimiche e dei Materiali
in convenzione con il CNR

CICLO XXXII

TITOLO TESI

Advanced Membrane-based Technology for Treatments of Industrial Streams

Settore Scientifico Disciplinare CHIM/07

Coordinatore: Ch.ma Prof.ssa Gabriella Cipparrone


Firma oscurata in base alle linee guida del Garante della privacy

Supervisore: Dott.ssa Lidietta Giorno



Firma oscurata in base alle linee guida del Garante della privacy

Supervisore: Dott. Giuseppe Barbieri



Dottorando: Dott. Leonardo Melone


Firma oscurata in base alle linee guida del Garante della privacy

Content

Abstract	1
Sommario	4
Outline	7
1. Introduction.....	9
1.1. State of the art – Membrane Gas Separation.....	9
1.1.1. CO ₂ separation	14
1.1.2. Plasticization.....	18
1.2. Membrane gas separation technology for industrial application	19
1.3. Process intensification.....	34
1.4. Aims of the thesis.....	37
2. Fundamentals	39
2.1. Basic principles of dense membrane gas separation: Solution-Diffusion Model	39
2.2. Membrane separation performance measurements method.....	43
2.3. Mathematical models for membrane unit design: 1-D model for the multi-species steady-state permeation	47
2.4 Process Intensification Metrics	54
3. Kinetic model for high pressure adsorption measurement.....	56

3.1 Introduction	58
3.2 Method	60
3.2.1 Sieverts experimental apparatus	60
3.2.2 Equations of State	68
3.2.3 Equilibrium isotherm equation	71
3.2.4 Thermo-kinetic equations of gas adsorption	74
3.3 Results and discussion.....	79
3.3.1 Gases behaviour.....	79
3.3.2 Simulation analysis and experimental fitting	83
3.3 Conclusion.....	89
4. Membrane Permeation Performance for mixture gas separation	90
4.1. CO ₂ permeance in Matrimid membrane: Activation energy calculation.	91
4.1.2 Results and discussion	92
4.2. PIM-based membrane gas separation measures.....	96
4.2.2 Results and discussion	98
4.3. Conclusion.....	103
5. Wet CO₂-mixture analysis for CO₂/CH₄ separation	105
5.1. Results and Discussion.....	108
5.1.1. Effect of humidity at different pressure ratios	114
5.1.2. Effect of humidity on membrane area	116

5.2. Conclusion.....	118
6. Membrane Integrated Process for Trichloroethylene Mixture Separation.....	120
6.1. Results and Discussion.....	123
6.2. Conclusion.....	142
7. Conclusions.....	144
Appendix A – Publications	146
Appendix B – Training PhD school activity	147
List of figures	148
List of tables	154
References	157

Abstract

Membrane technologies have attracted attention in the last decades as a promising industrial solution in the field of gas separation. In this dissertation, membrane gas separation was analysed both mechanistically in terms of elementary steps [1] of gases permeation, i.e. adsorption and diffusion, and in terms of industrial application. Indeed, the dissertation can be divided in two parts. In the first one permeation and kinetic adsorption measurements have been carried out on membrane and solid porous materials, respectively. In the second part, the main industrial applications of membrane gas separation have been investigated. Particular attention was focused on CO₂ separation which is a hot topic in the field due to the known environmental problems related to CO₂ emissions.

Kinetic adsorption experiments showed the potential application of the Sieverts systems for solubility and gas diffusivity evaluation. In particular, the use of Redlich-Kwong equation of state allowed to model satisfactorily the system in a wide range of operating conditions and to easily predict the behaviour of gases. An analysis on membrane permeation performance was carried out using pressure drop and concentration gradient methods. Matrimid and PIM-based membranes were studied. In particular, Matrimid membrane showed a good behaviour in a wide temperature range from -25°C to 150°C, while PIM membrane, generally, showed two main disadvantages: 1) high selectivity reduction due to plasticization phenomena and 2) fast reduction of selectivity and permeation properties due to quick aging [2].

Particular attention was focused on three different membranes PIM-PI-1, PIM-PI-r-6FDA-Durene=1:6 and PIM-PI-r-PIM-PEG=4:1, which showed CO₂ permeance values of 75.1, 68.4, and 20.3 dm³(STP) m⁻² h⁻¹ bar⁻¹, respectively.

The experiments demonstrated promising separating performances of CO₂ from other gases such as N₂ and O₂. For instance, CO₂/N₂ selectivities values of PIM-PI-1 and PIM-PI-r-PIM-PEG=4:1 have been calculated 16.3 and 15.6, respectively. Moreover, no dependence of the transport properties on operating pressure has been retrieved. These results indicate that PIM-based membranes have potential in CO₂ separation from stream in a large range of operating conditions.

The second part of this dissertation deals with CO₂ separation from a biogas-based stream (CO₂/CH₄ mixture) and trichloroethylene separation from N₂ stream. Both applications have industrial relevance.

Separating CO₂ from biogas and/or natural gas aims to enrich the stream in CH₄, thus increasing the energetic value of biogas. In this regard, the effect of water vapour on the separation was studied at different CO₂/CH₄ selectivities (from 25 to 100), pressure ratio and flow rate/membrane area ratio. The presence of water vapour induced significant changes in membrane performances, with consequent repercussions in CH₄ recovery, which, in some cases, reduced from 85.3% to 80.9% from dry to wet conditions.

Trichloroethylene (C₂HCl₃) may cause cancer, causes serious eye irritation, is suspected of causing genetic defects, is harmful to aquatic life with long lasting effects, causes skin irritation and may cause drowsiness or dizziness [3].

Therefore, the recovery of C₂HCl₃ and its separation from N₂ during process transformation is very important. The simulations carried out in this dissertation aim at increasing C₂HCl₃ recovery and reducing its concentration in the stream. Moreover, the membrane integrated process was compared with traditional technologies by using process intensification metrics. Membrane integrated process showed the best solution in terms of energy intensity (61.6 kJ mol⁻¹) with respect to high pressure condensation and

cryogenic systems, which showed energy intensity of 142.9 and 110.7 kJ mol⁻¹, respectively.

Sommario

Negli ultimi anni, la tecnologia a membrane ha assunto sempre maggiore interesse come applicazione industriale nelle separazioni gassose. Durante le attività di ricerca riportate all'interno di questa tesi, sono state investigate sia le proprietà di trasporto e sia la potenzialità delle membrane per le applicazioni industriali. La tesi, dunque, può essere suddivisa in due parti correlate: la prima, prevede lo studio dei fenomeni di trasporto (adsorbimento e diffusività dei gas) che intercorrono nella separazione gassosa a membrane [1] e l'analisi della permeabilità di gas all'interno di membrane dense; la seconda fase, invece, prevede l'analisi di sistemi a membrane per le separazioni gassose in applicazioni industriali.

Particolare attenzione è stata focalizzata alla separazione della CO₂, che rappresenta una delle principali tematiche affrontate in letteratura. Lo studio cinetico dell'adsorbimento è stato condotto all'interno di sistemi volumetrici alla Sieverts. Questo ha permesso di sviluppare un modello cinetico per la determinazione dei coefficienti di diffusività in materiali solidi. Il comportamento dei gas è stato studiato e predetto attraverso equazioni di stato basate sul modello di Redlich-Kwong.

Le misure di permeabilità condotte sulle membrane in Matrimid e su quelle base PIM sono state mirate ad identificare la loro potenziale per uso industriale.

La membrana in Matrimid ha mostrato un buon comportamento in un ampio intervallo di temperature da -25 ° C a 150 ° C, evidenziando la potenzialità di impiego in molteplici processi industriali (da processi che impiegano moderate temperature criogeniche a processi che lavorano con temperature mediamente alte).

Le membrane a microporosità intrinseca (PIM) mostrano, generalmente, due svantaggi: 1) alta riduzione della selettività dovuta al fenomeno della plasticizzazione e 2) riduzione rapida delle proprietà di selettività e permeazione a causa dell'aging [2]. Particolare attenzione è stata focalizzata su tre diverse membrane PIM-PI-1, PIM-PI-r-6FDA-Durene = 1:6 e PIM-PI-r-PIM-PEG = 4:1 che mostrano delle permeanze alla CO₂ rispettivamente di 75.1, 68.4 e 20.3 dm³ (STP) m⁻² h⁻¹ bar⁻¹.

Le misure di permeabilità hanno mostrato delle promettenti prestazioni di separazione della CO₂ rispetto gli altri gas come N₂ e O₂ (ad esempio, le selettività CO₂/N₂ di PIM-PI-1 e PIM-PI-r-PIM-PEG=4:1 sono rispettivamente 16.3 e 15.6) e non è stata rilevata nessuna dipendenza delle proprietà di trasporto dalla pressione di esercizio (effetti di plasticizzazione). Questi risultati indicano che le membrane base PIM hanno un ampio potenziale di applicazioni per la separazione della CO₂ da correnti di flue gas.

Nella seconda parte della tesi, sono state studiate la separazione della CO₂ da un flusso simulato di biogas e la separazione di tricloroetilene da corrente di azoto. L'arricchimento del CH₄ ottenuto mediante separazione della CO₂, è una delle principali strade percorribili per aumentare il valore energetico del biogas e/o del gas naturale. È stato studiato l'effetto del vapore acqueo sulla separazione a diverse selettività di CO₂/CH₄ (da 25 a 100), rapporto di pressione e rapporto portata/area della membrana.

La presenza di vapore acqueo ha indotto cambiamenti significativi nelle prestazioni della membrana, con conseguenti ripercussioni nel recupero di CH₄, che in alcuni casi si è ridotto dall'85.3% all'80.9%.

Ad oggi, il tricloroetilene è un solvente di sintesi controllato normativamente a causa dell'elevato rischio ambientale e per la salute umana.

Le simulazioni effettuate hanno permesso di sviluppare strategie di processo al fine di recuperare il C_2HCl_3 e a ridurre la concentrazione nella portata emessa in atmosfera. Il processo integrato a membrane è stato confrontato con le tecnologie tradizionali utilizzando le metriche della Process Intensification. Il processo integrato a membrana ha mostrato la migliore soluzione di processo in termini di Energy Intensity (61.6 kJ mol^{-1}), comparandolo con le tecnologie tradizionali quali la condensazione ad alta pressione e la condensazione criogenica, che hanno mostrato rispettivamente una Energy Intensity di 142.9 e $110.7 \text{ kJ mol}^{-1}$.

Outline

This dissertation deals with the membrane technology application in the industrial stream treatment. Particular attention was focused on CO₂ separation from gas mixtures containing CH₄ and volatile organic compounds (VOCs).

The first chapter presents the state of the art in the field of membrane technologies for gas separation, with particular attention to CO₂ and VOCs separation. The environmental problem of the global warming caused by emission of greenhouse gases, such as CO₂ and C₂HCl₃, and the industrial membrane application for gas treatment are discussed. The second chapter describes the fundamentals of membrane gas separation, in particular, the basic principles of membrane gas separation in dense membranes (Sorption-Diffusion model). Experimental methods for membrane characterization in terms of gas permeation and separation performances, and related mathematical models are discussed.

Chapter 3 reports the kinetic analysis on high pressure adsorption apparatus carried out during a training experience abroad, at the University of Edinburgh. Appendix A and B report the publications and the training Ph.D. school activity, respectively.

Chapter 4 reports the analysis carried out on dense and mixed matrix membrane for CO₂ separation from gas mixtures.

Wet CO₂-mixture separation analysis for biogas to bio-methane enrichment is discussed in Chapter 5. Separation performance and membrane module design are studied. Chapter 6 reports an industrial case study about trichloroethylene mixture separation. Analysis was carried out by using membrane integrated process and the results were compared to traditional technologies used for VOCs capture. To this aim process intensification

metrics, such as mass and energy intensity, have been used. Finally, the main results are summarized in the last chapter of this dissertation (Conclusions).

1. Introduction

1.1. State of the art – Membrane Gas Separation

The Research Agenda published as part of the Delft Skyline Debates [4] defines the new strategies for chemical industry development based on process intensification principles. The main aims are the sustainability and efficiency process growth. On this basis, the traditional industry is pushed to develop plant and processes by using innovative equipment and methods which afford lower production costs, reduce equipment size, energy consumption and waste generation, and improve remote control, information fluxes and process flexibility. Membrane technologies can play an important role in this framework and, in particular, membrane gas separation is assuming more and more importance. Commercial scale gas separations [5] using membrane systems were applied for the first time in the late 1970s to early 1980s. Today membrane technology for gas separation (GS) is a well-consolidated technique, which in various cases is competitive with traditional operations [6]. As it will be discussed in the next paragraph (1.2 Membrane gas separation technology for industrial application), membrane gas separation is used in H₂ recovery from refinery and petrochemical industrial gases, natural gas dehumidification, and CH₄ enrichment of industrial streams.

The main advantages and specific features attributable to membrane technology with respect to traditional technologies are reported below:

1. Lower capital (devices and membranes cost) and operating (electricity, heat, etc.) cost.
2. Simplicity of operation, installation and maintenance.
3. Modularity. Easily scalable processes.

4. Membrane devices and systems are compact. The membrane plants are at lower footprint.
5. Mild operating conditions, close to ambient condition (with respect to traditional technologies, e.g. cryogenic).
6. Continuous process.
7. Easy design of membrane integrated processes. In other words, it is easy to combine membrane processes with traditional technologies.

The history of membrane gas separation development is based on several milestones (Figure 1, [7]), starting from the first observations of J. K. Mitchell in 1831 [8,9]. Mitchell observed the first gas permeation through natural rubbers. The most important contribution was made by Thomas Graham which recorded the first diffusion rate and observed that the gas diffusion rate is inversely proportional to the square root of its density [10]. He also observed that same species diffused more slowly through the polymers than other materials. The chemical nature of compounds strongly influenced their diffusion through polymers and other materials. These results brought to the discovery of dialysis. In the 1855, Fick [11] postulated the first law of diffusion (Fick's law) on the basis of his studies on gas transport through nitrocellulose membranes. However, the main quantitative analysis was carried out by T. Graham which formulated the solution-diffusion model for gas permeation through the membrane [12].

In 1879 Von Wroblewski [13] quantified the Graham's model, defining the permeability coefficient as the ratio between the permeating flux and the transmembrane pressure multiplied by the membrane thickness. He, also, defined permeability as the product between diffusivity and solubility. In 1891 Kayser [14] demonstrated the validity of the Henry's law for adsorption of CO₂ in rubber. Up to this time the progress in membrane

separation was very slow. An important step forward was done by H.A. Daynes in 1920 [15]. He developed the time-lag method which allows to determine the diffusion coefficients of gases. Only in the 70's, the first important application of membrane gas separation in an industrial plant has been reported. More details are reported in "1.2 Membrane gas separation technology for industrial application".

The membranes used in the gas separation field, can be classified in two families: organic and inorganic. Organic membranes, especially polymeric membrane, are widely used in the membrane gas separation technologies due to lower cost and lower fabrication issues than inorganic membrane [16]. Inorganic membranes are used only in specific applications, where high thermal, mechanical and chemical resistance are needed.

This thesis focuses on the polymeric membranes and their applications. For this reason, in the next discussion, only the polymeric membranes will be considered.

In the last years, the introduction of new polymers with high free volume endows the membrane with very high permeabilities values. Membrane Technology and Research, Inc. (MTR) [17] developed a new perfluoropolymers for CO₂ separation with improved resistance to contaminants.

Organic membranes can be divided into three sub-groups: liquid, mixed matrix and polymeric membranes. Liquid membranes are comprised by a selective liquid layer which allows selective separation of a specific component from the retentate to the permeate phase (18). The selective liquids have to be immiscible with the liquids in the retentate and permeate. The membranes can be self-supported or with solid support (usually the selective liquid is kept inside the pore of solid supports). The main disadvantage is due to the very low mechanical resistance, as high pressure can cause easy entrainments of the membrane liquid.

Mixed matrix membranes are a new generation of membranes comprised of solid inorganic particles embedded in a polymeric matrix. Mixed matrix membranes provide both high perm-selectivity (due to presence of the polymer) and high permeability (thanks to the performances of the inorganic particles) [19,20].

The polymeric membranes generally follow solution-diffusion transport law. For gas separation purposes, polymeric hollow fibres is the best technology available which provide significant advantages thanks to their high surface area and the relatively low cost [16,21].

Unfortunately, the efficiency of polymeric membranes decreases with time, due to compaction, chemical degradation and thermal instability [16,22]. One of the main issues is the plasticization phenomenon that will be discussed later. Polymer progress allowed to discover new types of polymers with ultra-high intrinsic microporosity (PIM) and thermal rearranged (TR) [23,24] which have shown exceptional transport properties.

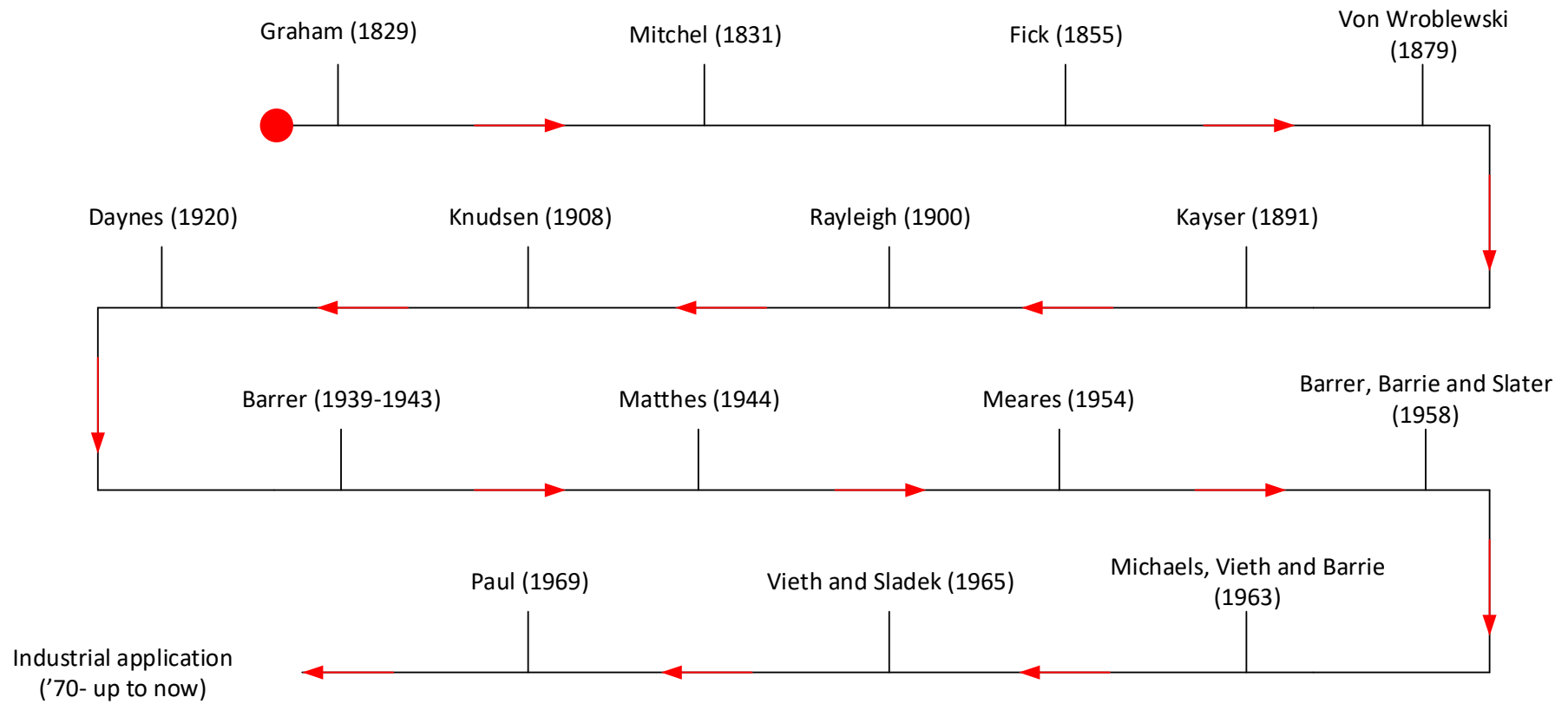


Figure 1 - Milestone of membrane gas separation [7].

1.1.1. CO₂ separation

CO₂ separation is, up to now, one of the main challenges of membrane technology.

The conventional CO₂ separation processes are absorption (by using amines, such as mono-ethanolamine), adsorption, and cryogenic separation [25,26].

Absorption is the more widely diffused process among them. Owing to fast kinetics and high absorption capacity CO₂ capture reaches very high efficiencies (90% or more). In the absorption processes in amines two important issues have to be considered. Amines can be highly corrosive and accelerate the degradation of the plant devices together with other components such as H₂S [27]. The second issue is the high energy demand. This is particularly true as far as the regeneration step is concerned, which requires large scale equipment for the CO₂ removal and the handling of chemicals. The Department of Energy – National Energy Technology Laboratory (DOE/NETL) has estimated [28] that the monoethanolamine (MEA) based process for CO₂ capture will increase the cost of the electricity for a new power plant by about 80–85%, also reducing the plant efficiency of about 30% [27,29].

These disadvantages promoted the recent industrial use of cryogenic processes for the removal of CO₂ from natural gas.

Great advantages of cryogenic CO₂ capture with respect to absorption are that no chemical absorbents are required, and that the process can operate at atmospheric pressure. The main disadvantage is due to the water content which condense during the cryogenic step and, consequently, high pressure drop or plugging occurs. Moreover, owing to solid formation, the heat transfer efficiency is lower. Regeneration cycles are needed to operate at higher temperature than the cryogenic ones (regeneration should be carried out with great care to avoid excessive mechanical stresses).

The adsorption systems are widely employed in industry, for different gases and concentrations. Depending on the type of interaction between the material and the target molecule, adsorbents can be used to separate gases in a wide range of possible process configuration. The main issue is due to the unsteady-state process because the adsorbent accumulates gas up to its saturation. Like regeneration in the absorption, the desorption process is therefore expensive, similarly to the regeneration step in the absorption process. Moreover, the method used to regenerate the adsorbent could influence the sorbent capacity in the following separation step.

Owing to the limit of traditional technologies, the membranes have gained more and more importance for the CO₂ separation and capture. Thanks to the low energy requirement for compressing CO₂, the low corrosion problems due to the weak CO₂ acidity, and the high stream value in terms of heat power, membranes are used in several separation industrial plants. Natural gas and biogas separation for CH₄ enrichment are the main chemical processes which perform membrane CO₂ separation.

Electricity production from fossil fuel in power plants will be challenged by the growing concerns about anthropogenic emissions of greenhouse gases, such as carbon dioxide, and to the consequent global climate change. The regulation of the carbon dioxide emissions implies the development of specific CO₂ capture technologies that can be retrofitted to existing power plants and designed into new plants, with the goal to achieve 90% of CO₂ capture [29]. Therefore, the recovery of CO₂ from large emission sources is a scientific challenge which has received considerable attention for several years [30, 31, 32]. In particular, the identification of a capture process which fits the needs of target separation performances, together with a minimal energy penalty, is a key issue.

Despite the aforementioned numerous advantages, there are a number of issues associated with the membrane based capture of carbon dioxide from flue gases which limit the application of this technology. The concentration of CO₂ in flue gases is low, which means that large quantities of gases will need to be processed. The high temperatures of flue gases will rapidly destroy a membrane, so the gases need to be cooled below 100 °C, prior to membrane separation. Likewise, the membranes will need to be resistant to the harsh chemicals contained into the flue gases, or at least these chemicals must be removed prior to the membrane separation step. Additionally, creating a pressure difference across the membrane will require significant amounts of power, which will in turn lower the thermal efficiency of the power plant. The composition of flue gases varies greatly depending on the fuel source, power plant and prior treatment. For instance, the flue gas coming out from a power and a steel production plants exhibit significant differences in CO₂ concentration. The use of membrane technology for CO₂ separation is, thus, also strictly related to the conditions of the stream to be treated. However, both membrane properties and the operating conditions of the whole process play the key role in evaluating the convenience of a membrane separation process at industrial scale.

Natural gas composition varies from source to source. CH₄ content is always the major component and the typically concentration is 75-90%. The second component in the natural gas mixture is CO₂ whose concentration ranges between 0-20%. Today, the membrane technologies are applied for less than 5% to natural gas treatment, and almost all the market is oriented toward CO₂ removal for CH₄ enrichment.

Using CH₄ as energy source is very important in industry, even if renewable energy sources are nowadays of major importance for long-term sustainability. In this context, biogas obtained via microbial digestion of farm or sewage wastes is a promising

compromise. The biogas produced consists of several gases. Out of these, CH₄ and CO₂ are the major components (up to 50%), while other gases including H₂S, N₂ and O₂ are also present [33] (bio-methane membrane treatment will be discussed in Chapter 5).

Inorganic and polymeric membranes are both used in the natural gas treatment for CH₄ enrichment. One of the most promising inorganic membranes is the zeolite membrane which shows the best CO₂/CH₄ selectivity and CO₂ permeability, when compared to other inorganic membranes reported in literature [34]. For instance, DDR membrane shows the highest CO₂/CH₄ selectivity close to 670 at 26 °C [35]. However, due to manufacturing issues, only few zeolite membranes are used in industry, despite high CO₂/CH₄ selectivity values up to 100 , [36] have been achieved during experimental measurements in laboratory [37,38]. In the last years, the new polymeric membranes reached more and more interest for application in CO₂ separation owing to chemical and thermal resistance and easier industrial scale-up compared to zeolite membranes. Particular attention is focused on polymeric membrane with high free volume and high permeability [39]. In this family, PIM-based membranes are the most promising membranes for gas separation [40]. McKeown et al. had successfully developed the first polymer with intrinsic microporosity and large surface area [41] and had synthesised the materials PIM-1 and PIM-7 for membrane applications [42]. These membranes have high CO₂ permeability of 2300 (PIM-1) and 1400 Barrer (PIM-7). Only ultrahigh free volume polymers, such as PTMSP [42], show higher CO₂ permeability. Dense polymeric membranes are the most common used membrane for gas separation application [43]. Owing to their lower permeability [44] and instability in terms of separative performance in presence of condensable gases, they are marginalized for natural gas applications [45].

1.1.2. Plasticization

The plasticization is an important phenomenon that can occur during polymer processing or during separation stages. In the first case, plasticization increases the capability of gases to flow through the polymer. Usually, due to the low molecular weight compounds introduced into glassy polymers, it increases the processability of the material [46]. The low molecular weight compounds allow a more polymer flexibility with increased rate of segmental motion and chain flexibility [47]. On the other hand, plasticization is one of the main issues during gas separation. Here, plasticization is a pressure dependent phenomenon caused by dissolution of certain penetrant species within the polymer matrix. The mobility chain increases and enhances inter-segmental mobility of polymer chains [48]. Literature reports on membrane plasticization during gas separation is wide and detailed [20,49,50,51,52,53,54,55]. Horn et al. [56,57] developed a carefully experiment to explore the effects of the film thickness on CO₂ induced plasticization on glassy polymers [56,57]. Results were used for physical aging evaluation. Plasticization and physical aging phenomena are function of film thickness, aging time, exposure time, pressure and prior history [58,59].

Plasticization, therefore, should be taken into account to correctly describe changes in thermal, mechanical and gas permeation properties of the membrane [47,60,61].

1.2. Membrane gas separation technology for industrial application

Commonly in industrial scale gas separation processes, the main traditional technologies used are cryogenic distillation, absorption and adsorption. The first method is generally used in large scale oxygen/nitrogen enrichment from atmospheric gases. The separation of components from the gaseous mixture occurs by liquefaction of the gases which are distilled at cryogenic temperatures. In order to remove carbon dioxide and water from natural gas, the absorption method is a suitable and well consolidated process. In this case the separation is realized through gas-liquid contacting devices which enable the contact between the gas mixture and a chemical or physical solvent. One or more compounds of the gas mixture are absorbed and, consequently, the un-reacted or not absorbed species can be separated from the mixture. Both cryogenic distillation and absorption are complex, capital intensive, but cost competitive methods.

The adsorption isolates the component by contact between the gas mixture and a solid characterized by a very high surface area. This type of process is used to produce high purity gases or to remove impurity. However, switching this process from cyclic to continuous, is challenging as the correspondent industrial plant requires more than one adsorbent bed. New rules were discussed to replace the traditional industrial growth with a sustainable one [4] and to apply Process Intensification principles in many sectors such as water, energy, food, health, etc.

Industrial plants adopt membrane technologies for several scopes such as the separation of air components, separation of H₂ from refinery industrial gases, natural gas dehumidification, separation and recovery of CO₂ from biogas and natural gas [62]. In this century, other promising applications were largely investigated, such as the recovery

of hydrocarbons, including olefins, paraffins, halo-hydrocarbons from waste gas streams [63,64], H₂, CH₄ and hydrocarbons (C₃+) from petrochemical gaseous streams. Generally, the main classes of polymer membranes used in gas separation are Si-containing rubbery polymers (silicone rubber, etc.), polyacetylenes, polynorbornenes, copolyimide siloxanes, para-substituted polystyrenes, Si-containing polyvinyl class poly(vinyl trimethylsilane). Generally, the first three classes are considered appropriate for hydrocarbons separation, whilst the other are often used in air and hydrogen separation. In the last decades, the separation of air into nitrogen- and oxygen-enriched streams is promptly rising up. The membranes used in this kind of separation, are generally oxygen selective, obtaining the nitrogen rich stream in the high pressure side (retentate side), and the O₂ enriched stream at a low pressure in the permeate side. The first literature study [65], reported a low O₂/N₂ selectivity of ca. 4, due to the close kinetic diameters of both gases (nitrogen (3.64 Å) and oxygen (3.46 Å)). In this century in order to enhance O₂/N₂ selectivity of the polymeric membranes, significant efforts have been made and nitrogen separation by membrane systems is the largest gas separation process industrially used. Thousands of compact membrane systems to obtain nitrogen gas are installed in the offshore and petrochemical industry. One of the most popular manufactory of gas separation membrane system for N₂ is Air Products.

The available data show that the Air Products Norway industry has sold more than 670 PRISM® systems N₂ for different ship applications, and more than 160 PRISM® systems for offshore installations [66]. In December 2006, Air Products started with another PRISM® production plant in Missouri (USA) [67]. One of the most famous user in this field, is the Air Liquide [68] which installed in Dalian (China) a new air separation unit with a capacity of 550 tons/day of oxygen. However, further improvements are on the

way, as in Japan, where the Ube Industries [68] is enhancing the polyimide hollow fibres production useful for nitrogen separation to introduce a number of ethanol refining plants mainly in the USA and Europe, driven by the rapid increase in the demand for bio-ethanol as an additive for oil products.

Besides the aforementioned plants, one of the most significant membrane system technologies is the PermSelect® [69] which uses silicone membrane (PDMS). In this system, the oxygen is approximately two times more permeable than nitrogen, therefore the permeate is rich in oxygen and, consequently, the retentate stream is rich in nitrogen. This system gives several advantages, firstly a high N₂ purity is obtained from permeate (>99.9%) and a retentate enriched in O₂ with a low amount of N₂ is attained.

For example, air with oxygen enriched with only the 9% of N₂ can be useful for processes where nitrogen has a ballast effect.

Recently, another goal was achieved by GRASYS Company by introducing a new silicone membrane in the market. In addition, this popular manufacture company industrialised a new configuration system with hollow fibre membrane modules (Figure 2) for several chemical industries, such as Exxon Mobile, ENI, Shell, Gazpron, etc.

The hollow fibre membrane system consists of two polymer layers: a porous and a rubbery polymer one. The latter is the separation layer. The composition of the fibre is similar to the above mentioned PermSelect® technologies.

The Figure 3 shows the PermSelect plant used [70] to the air separation and enrichment nitrogen stream by in-fibre air injection configuration.

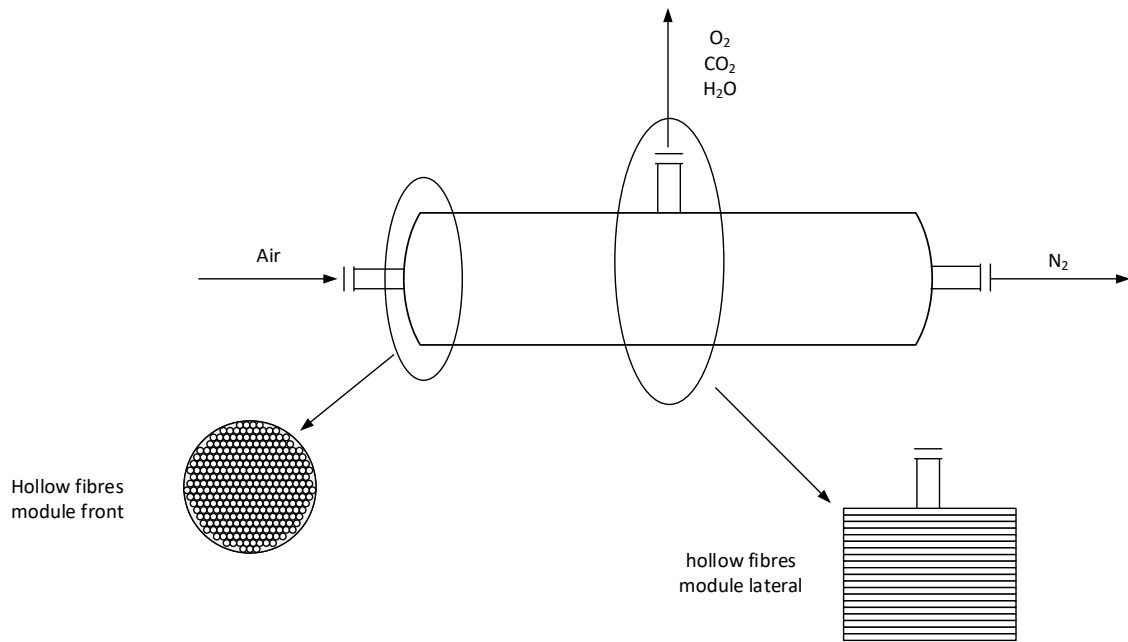


Figure 2– PermSelect module for the oxygen capture.

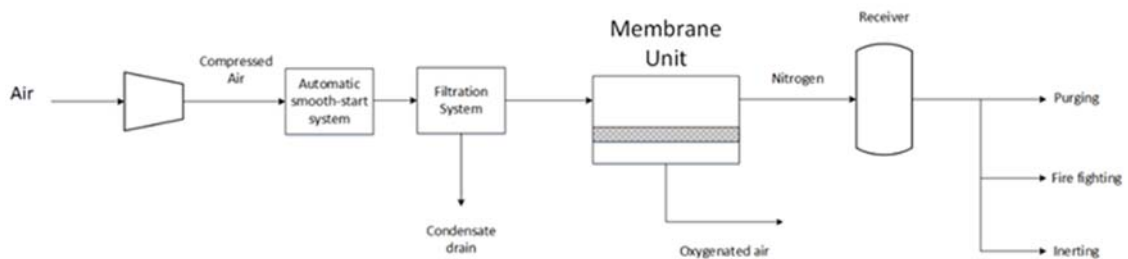


Figure 3– Scheme of PermSelect plant for the air separation and enrichment nitrogen stream [70].

In detail, to remove the impurities, the compressed air is fed into the air pre-treatment system as showed in Figure 3. In order to reach the right work temperature needed to enhance the separation process, the pre-treated air is sent into an electric heater. Then, to obtain the nitrogen enriched gas on retentate, the hot and compressed air is fed into the membrane gas separation modules. This system is able to reach nitrogen gas purity ranging from 90 to 99.9% and a nitrogen production capacity of 10 to 150 Nm³/h. This type of plant developed by GRAYS is industrially adopted for production of inert gas

mixtures from atmospheric air, to be used in chemical, petrochemical and petroleum industry, as well as in food and pharmaceutical industries, microelectronics and other sectors.

Several research groups moved the attention, also, to the H₂ production due to the increasing request from many industry processes in the framework of green energy. In this century the increasing H₂ demand encountered membrane technology because the separation of hydrogen is the most important aspect in its production and because is a cheaper process than the cryogenic distillation and PSA.

Permea Prism™ systems represent the first membrane devices used to separate hydrogen in ammonia purge streams. To this aim, up to now several membrane processes were developed i.e. from UOP with the Polysep systems and Monsanto with PRISM [71] systems. In both cases, the membranes consist of a layer of PSF and PDMS. The PRISM is nowadays the most popular (more than 500 plants used) membrane technology for hydrogen system. This membrane system consists of hollow fibres (230 systems plants in the world) [72]. The H₂ recovery from ammonia stream is an essential part of the ammonia synthesis process. This process produces inert by-products which accumulate and requires purge streams. In this contest, the PRISM membrane systems is necessary to treat the purge stream of the reaction system equipped with a water scrubber unit in order to recovery ammonia. The gas stream is fed in a membrane gas separation unit with hollow fibre design maintained at high pressure (110-130 barg). The starting gas presents high concentration of hydrogen (about 66.5%) and nitrogen (about 22.2%). Obviously, the scope of this unit is to obtain a stream enriched in hydrogen. The hydrogen recovery occurs on permeate side of the hollow fibre membranes at lower pressure system (25-70 bars) reaching a hydrogen concentration of up to 94% and hydrogen recovery up to 90%.

In order to reuse it inside the ammonia reactor, the retentate is fed to a compressor unit and recycled to the reactor. In 1977, the PRISM membrane system was for the first time developed and used for the SynGas (H_2/CO) ratio adjustment. The syngas stream composition presents 48% of hydrogen and 51% of carbon monoxide and the PRISM is used to strip hydrogen out of the syngas in order to reduce the H_2/CO ratio obtaining a permeate stream with 88% of hydrogen and 11% about of carbon monoxide and a retentate stream at very high concentration of CO (about 95%) [6].

Another user of this system are the refineries, interested to H_2 recovery to reuse and for environmental regulations. Generally, the hydrogen content in refinery purges and off-gases ranges from 30 to 80% in a stream containing prevalent light hydrocarbons (C_1-C_5). The goal needed to can reuse the H_2 enriched stream is with a purity of ca. 90-95%. Unfortunately, in this process the crucial point is the difficulty to remove 4 mol of hydrogen per mol of hydrocarbon. However, showing remarkable selectivities, at the moment, the PrismTM system is the principal system available on the market suitable for this kind of separation.

Recently, new technologies were developed by MTR, called VaporSep [73]. The application of this system allows to increase the ammonia production of ca. 4-5% with respect to the traditional one, maintaining the same gas feed to the reformer. The most important advantages of this devices are a lower gas consumption, facile operations, mild temperature conditions, simple installation and compact dimensions (6m length x 3m wide x 2.5m height) [6]. Figure 4 and Figure 5 show the scheme of VaporSep [74] and PRISM [75] technologies, respectively. In addition, downstream to the hydrotreater and hydrocracking units the VaporSep [76] system is used for hydrogen capture, due to the compact system and the high performance (Asian refinery, Figure 6).

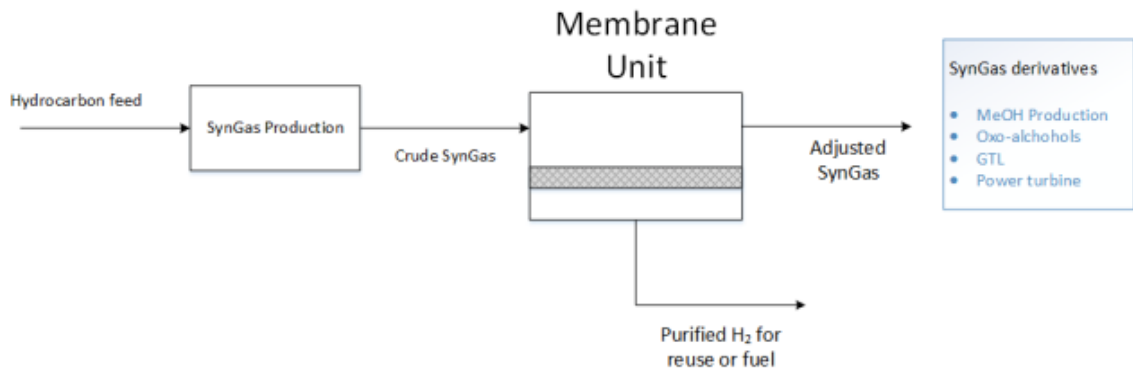


Figure 4– VaporSep plant for the SynGas ratio adjustment [74].

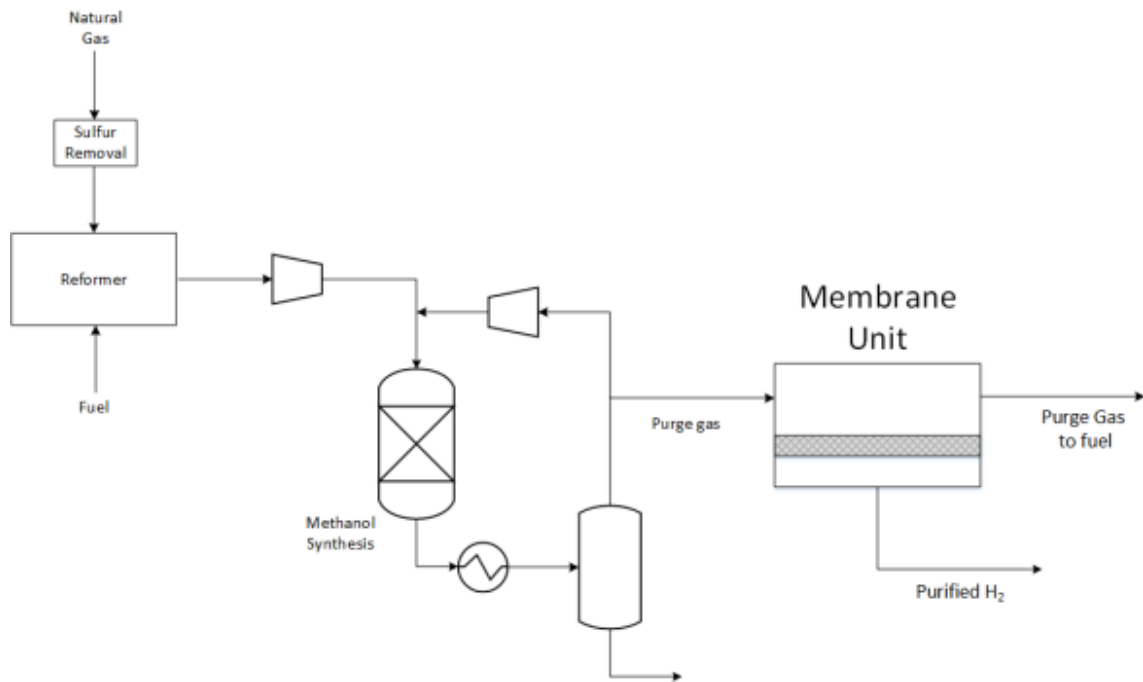


Figure 5 – VaporSep plant for the Methanol enrichment [75].

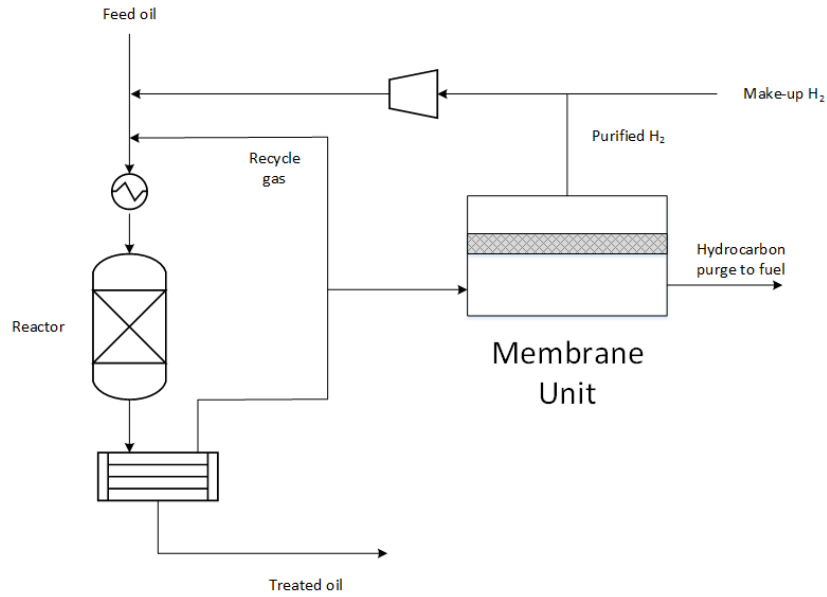


Figure 6 – VaporSep plant for the hydrogen recovery by hydrotreater downstream [76].

The industrial hydrocarbons separation are today performed successfully by using membranes containing Si [6], mainly produced by MTR (United States) and licensees of GKSS technology (Europe). The main industrial hydrocarbons separation are [77]:

- Ethylene recovery
- Polyolefin plant resin degassing
- Gasoline vapour recovery systems at large terminals
- Polyvinyl chloride manufacturing vent gas
- Natural gas processing/fuel gas conditioning

The silicone rubbery membranes (PDMS), having an adequate vapour/inert gas selectivity for most of the applications and a high permeability which permit to obtain a smaller membrane area with respect to glassy polymers, represent the highest commercially diffused system. As discussed before, ethylene recovery is the principal application of vapour separation membranes. In detail its use is necessary in the

polyolefin resin process synthesis in order to separate the unreacted monomer and hydrocarbon solvents from the reaction mixture and re-use the polymer. In the traditional separation process, the monomer is stripped with hot nitrogen in a column known as a “degassing bin”. The Now day, replacing the traditional process, is a membrane system containing two membrane units in series where the off-gas from the “bin” is compressed at 200 bar.

The compressed stream is sent inside a first membrane module which allows to obtain a permeate current rich in propylene and a retentate rich in nitrogen (97-98%). The propylene stream is sent back to the compressor, which through inter-cooled compression, allows the propylene recover in condensed phase. Nitrogen-rich stream (retentate), on the other hand, is sent in a second module in series, in order to recover further hydrocarbons. Thanks to series-configuration N₂ concentration increases up to 99%. This unit allows to recover about 450 kg/h of hydrocarbons [66]. Thanks to their potentialities and simplicity, more than 50 units have been installed in the last 20 years [78]

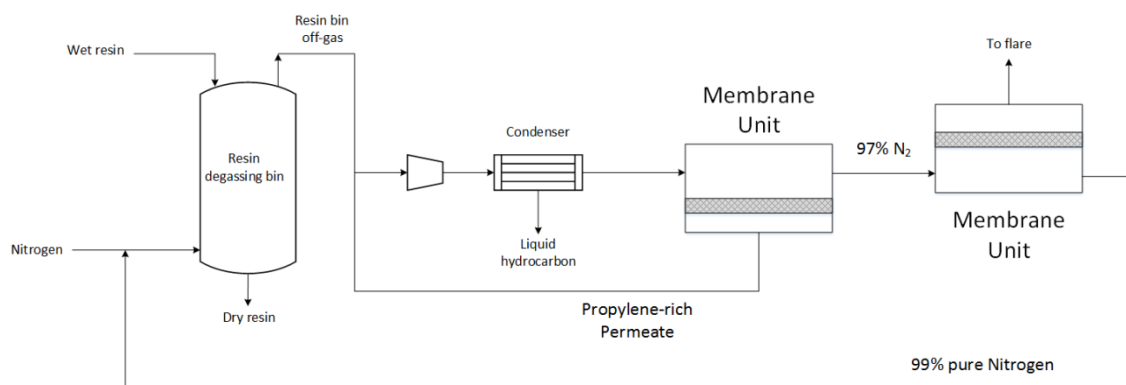


Figure 7– Membrane recovery of hydrocarbon in a hydrocarbon/nitrogen plant [78].

Similar membranes can be used in ethylene recovery from ethylene oxide production cycle [78].

Ethylene oxide is synthesised through the catalytic oxidation of ethylene with 99.6% pure oxygen. The mixture is fed into a scrubber to recover the ethylene oxide in the aqueous phase. However, the gaseous stream is fed into the reactor, after removing the CO₂ by means of the basic stream with potassium carbonate. Owing to the argon, part of the current is purged. The purge gas for a typical ethylene oxide plant contains approximately 20-30% ethylene, 10-12% argon, 1-10% carbon dioxide, 1-3% ethane, 50% methane and 4-5% oxygen (a similar current of purge is obtained in the synthesis of vinyl acetate). The stream, therefore, is fed into a membrane system, which allows the permeation of ethylene, which can be sent back to the synthesis reactor. The retentate enriched in Argon comes to purge.

Membrane application became recently very important in the field of gasoline vapours recovery. Several hundred retail gasoline station used small membrane system vaporous hydrocarbon recovery during the transfer of hydrocarbons from tankers to holding tanks and then to trucks. there are two main issues related to vapour emission. The first one is due to environmental and health problems. Usually, hydrocarbon concentration in the emitted gas is in the range 10-30%. This is very dangerous because this concentration of hydrocarbon in air could cause explosions. Thanks to the collaboration between OPW Vaporsaver (system builder) and MTR (PDMS membrane producer), a hydrocarbon recovery system has been developed that reduces emissions up to 95-99% [78].

The volatile organic compounds (VOCs) recovery is an important application in the chemical [79] and petrochemical industries [6].

As process discussed before, MTR [6,80], OPW and Vaporsaver have developed plants that use silicon rubber (PDMS) and PTMSP polymer membranes which exhibit higher VOCs/air selectivity. VOCs separation through membrane technology has two large advantages, in addition to those typical of membrane technology, which are the low maintenance request and the low operating costs of the utilities. In particular, VOCs are removed from the air stream and condensed into a concentrated liquid (volume reduction). Moreover, even if you don't want the recovery and reuse of VOCs is not required, the stream at higher VOCs concentration recovered is more flammable with respect to the feed stream, so it can be more easily burned.

For example, the MTR plants allow to recover the VOCs, obtaining an air current with less than 10 ppm by weight of VOCs [80]. The technology uses composite membranes characterized by a microporous layer coated with a dense selective layer in spiral units. The modules can be connected in series and/or in parallel, according to the process requirements. The power supply is previously compressed (~13 bar) and sent to a heat exchanger [6]. Owing to temperature reduction in the heat exchanger, the air is dehumidified (the initial vapour content is 1-2%). The stream is fed into a membrane separator where the VOCs are recovered in the permeate. In the other side, the stream at lower VOCs (retentate) concentration than the feed is fed in a second membrane unit. The enriched stream is recycled to the process. The permeate obtained from the first separation module is fed to a condenser which allows to recover the VOCs in the liquid phase. The residual stream is fed in a third membrane module. Here the permeated current is recycled to the module, and the retentate is fed to the head of the process.

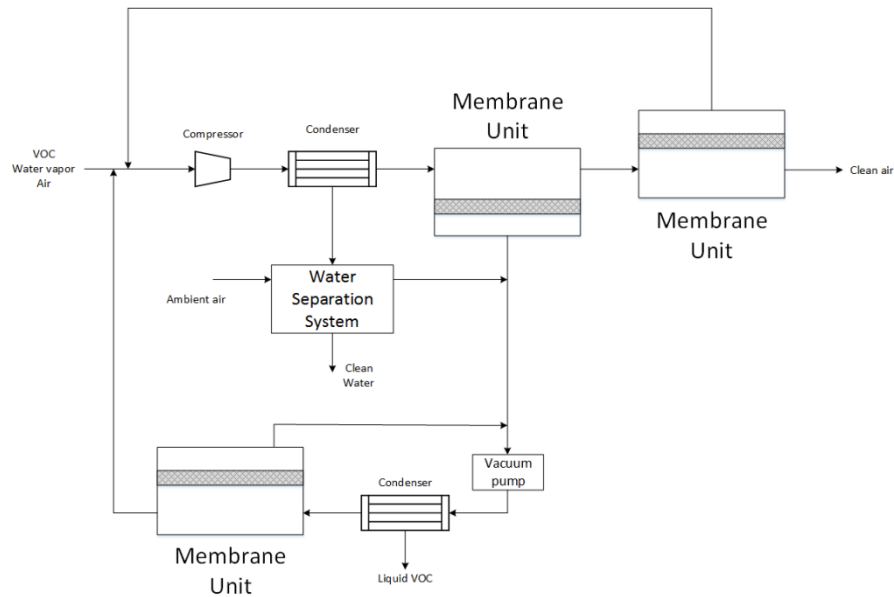


Figure 8 – Membrane recovery of VOCs for clean air production by air/VOCs mixture [80].

CO₂ industrial application emerged in the last years. Particular attention has been focused on CO₂ separation from natural gas [81], by using commercial or lab/pilot-scale devices [82]. Membrane technologies is one of the most promising implemented technology for the CO₂ removal and CH₄ enrichment. Even if membrane technologies do not ensure the same CO₂ separation efficiency demonstrated by traditional technologies (e.g. amine absorption), other advantages can be displayed. Polyimide and cellulose acetate membranes are the most common used in industrial plants [83]. Polyimide was commercialized by DuPont and Ube Industries Ltd. for hydrogen recovery and, subsequently and successfully, used for CO₂ separation [81]. UOP, instead, developed commercially cellulose acetate membrane which is considered the best industrial membrane solution for CO₂/CH₄ separation [83]. Industrial membrane plant for CH₄ enrichment from natural gas consists in two membrane unit (Figure 9).

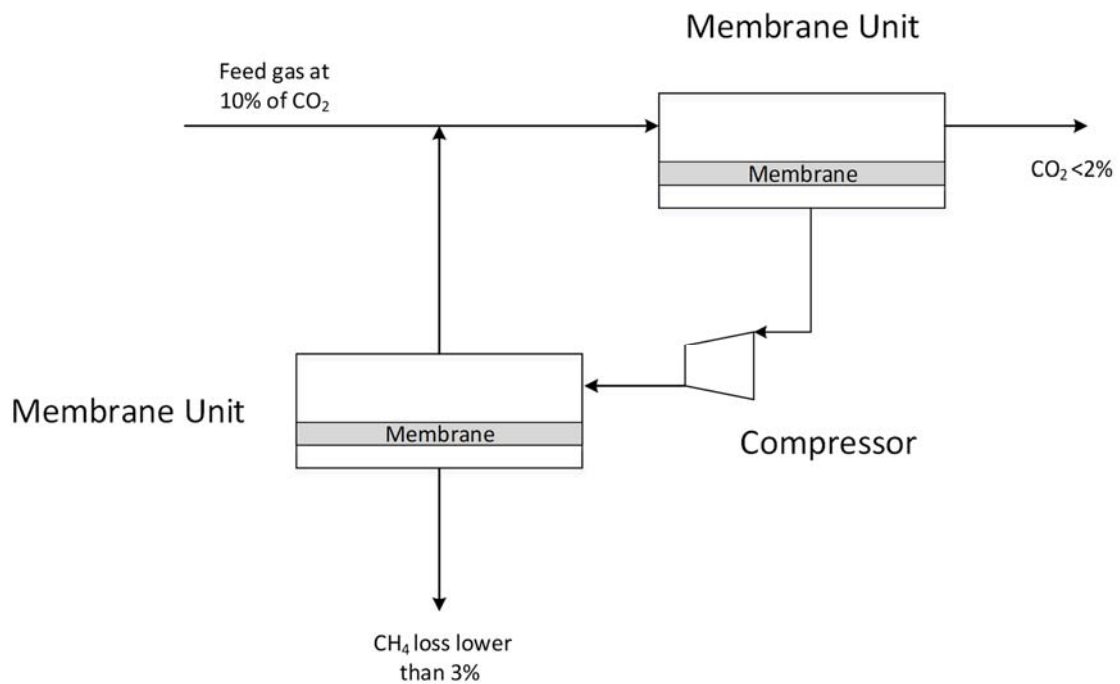


Figure 9 - Scheme of natural gas sweetening membrane based technology [82].

Another important application of CO₂ separation for CH₄ enrichment is the biogas treatment. One of the most important problem is due to H₂S and water and pre-treatment is needed in order to avoid membrane failure. The main aim in the biogas separation is represented by a process to achieve simultaneously high CH₄ concentration and low CH₄ loss. Various pilot and pre-industrial plants have been developed in recent years in order to test membrane performance over long periods in biogas separation. Two relevant membrane-based technology for biogas separation are installed in Europe. In Norway a carbon membrane module was exposed to 10 Nm³/h of a raw biogas stream (CH₄ of 63%, H₂S about 1 ppm and CO₂ less than 37%). The plant showed a stable separative performance during the test, reaching CH₄ concentration of 96% and CH₄ recovery of 98% [81]. Tecno Project Industriale srl (SIAD group) installed in Italy an innovative membrane based plant for biogas treatment coming from biomass digestion (Figure 10)

[84]. The membrane modules adopt polyimide membranes commercialised by Evonik Group. The plant can treat up to $4 \cdot 10^5$ tons per year of biomass with a biogas generation capacity of $6 \cdot 10^3$ m³/h [84]. The pre-treated stream is fed into three-stage membrane system. The retentate of the first stage is CH₄ rich, while the permeate is rich in CO₂. The CH₄ stream is fed in a second membrane stage where the retentate reaches the required composition by the bio-methane standards, while the permeate stream is recycled to the feed of the first stage. The permeate of the first stage is fed in a third membrane stage. Then, the CO₂-rich permeate is recovered. The retentate is fed in the feeding of the first stage.

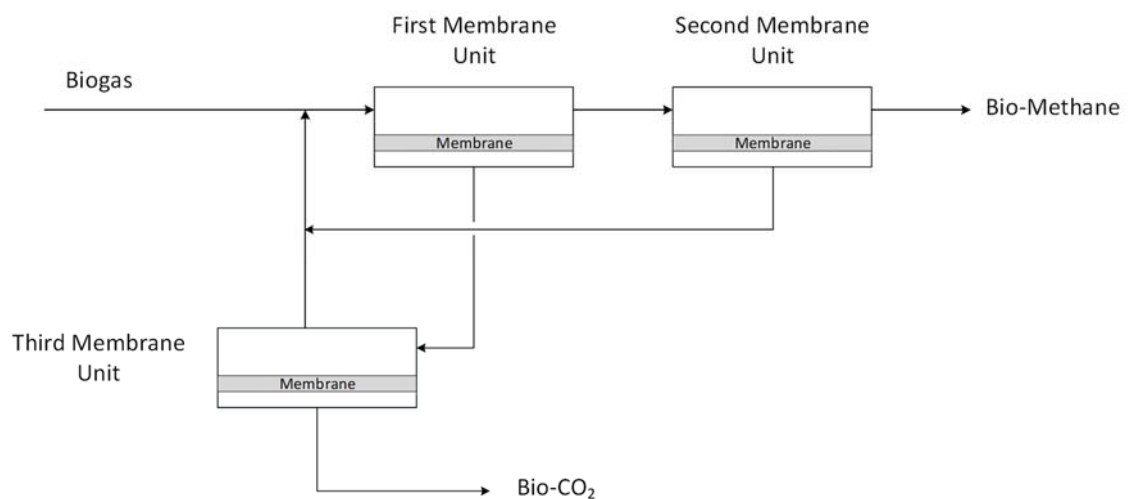


Figure 10 – Scheme of the membrane system installed by Tecno Project Industriale srl in Italy.

Pre-combustion CO₂ separation is currently applied in oil refineries [81]. Pre-combustion separation is based on CO₂ capture and it involves three stage: 1) CH₄ or coal converted into SynGas (CO and H₂), 2) CO transformed into CO₂ and H₂ via water gas shift reaction and 3) H₂ enrichment thanks to CO₂ separation [85,86]. Generally, membranes used in

pre-combustion applications are inorganic membranes, ceramic and metallic. Both CO₂-selectivity and H₂-selectivity membranes are adequate for separation process. Regarding dense metallic membrane, the most important application is in the water gas shift where Pd-based membranes for H₂ separation from reaction system are used [87]. Pd-based membranes show very high H₂ selectivity but they suffer contamination and poisoning by H₂S, CO and other compounds such as unsaturated hydrocarbons.

With respect to the pre-combustion separation, post-combustion separation has, already, a higher application in the chemical industry. An important Europe action (Nanoglowa project) started in 2006 and coordinated by KEMA Nederland BV shows the potentiality of CO₂ capture and separation from flue gas using membrane technology [88]. In 2011, two CO₂ capture power plants were integrated in power plants in Germany and Portugal. The membrane modules use the fixed-side carrier (FSC) membranes which showed a permeance of 5 m³ (STP) m⁻² h⁻¹ bar⁻¹ and CO₂/N₂ selectivity higher than 1000 [89]. Similar pilot plant was installed in Norway for stream treatment containing CO₂ concentration up to 17%. The plant was integrated in a cement industry and uses polyvinylamine (PVAm) membranes and they showed stable separative performance also under high SO₂ and NO_x concentration exposure in long time [90]. The Helmholtz Zentrum developed a membrane plant for CO₂/N₂ separation based on ionic liquid membranes. The future direction for membrane based CO₂ separation development in industrial application is based on a cost reduction. US department of energy's (DOE) targeted the aim at reduction cost up to 20 \$ per ton of CO₂ [91,92].

1.3. Process intensification

Since the last century, the scientific community and the chemical industry are focused particular attention on several trials in order to reduce the energy consumption, the waste generation, and to enhance the environmental and economic aspects of the process. In this context, the Process Intensification (PI) appears a valid and promising methodology, largely studied in the last twenty years [93,94,95,96] in reactive distillation, rotating packed beds, and microreactors. In all of these processes some aspects can be improved such as in the reactive distillation case, where the reaction and separation occurs by filling a distillation column with a catalyst [97], in order to simultaneously remove the vapour products from a boiling reacting mixture [98]. Even if in this process, the equilibrium is generally draw to reach high conversions [99], the application of PI can, in one hand, minimise the energy request (80%) and the investment cost (20%) [100], and, in the other hand, improve both global reaction rates and selectivity of reactive distillation [101]. Similar situation is that of rotating packed beds, where, by means of centrifugal acceleration, the mass-transfer limiting steps can be overcome [102]. Inducing centrifugal acceleration on the packed beds reactor increases the volumetric mass transfer coefficient of 1–2 orders by uniform dispersion and high turbulence [103]. This device, compared with the conventional one, decreases the required volume [102]. Similar improvements could be reached in the case of microreactor design by a PI point of view. This kind of reactors are characterized by a micrometric size and a low reaction volume to surface area ratio, which consents to obtain both high heat transfer rates [104] and reaction temperature control [105]. The great results achieved in this century induced the scientific community to formulate also the Process Optimization and Process Synthesis methodology. Briefly, the first provides a significant advancement in the speed and

robustness of NLP and MINLP algorithms [106] and modelling environments enabling the formulation and solution of large-scale optimization applications [107]; the PS offers great improvements in synthesis tools and techniques, mostly for heat exchangers and separation networks[106]. It appears clear that all of these processes investigate several aspect, but their improvements and developments are correlated by the same methodology that can be applied, as reported the Table 1 [108].

Table 1 - Basic features of Process Optimization, Process synthesis , Process Intensification [108]

	AIM	FOCUS	Interdisciplinary
Process optimization	Performance improvement of existing concepts	Model, numerical method	Weak (interface with applied mathematics)
Process system engineering	Multiscale integration of existing and new concepts	Model software	Model (mostly applied mathematics, informatics, chemistry)
Process intensification	Development of new concepts of process steps and equipment	Experiment, phenomenon, interface	Strong (chemistry and catalysis, applied physics, mechanical engineering, material science)

PI was generally defined as “process development leading to reduction in equipment size” [109]. Nevertheless, nowadays the PI meaning include also business, process, and environmental aspects [109] and it is regarded as a holistic approach to improve a process. Methods adopted to perform a PI, Process optimization and Process system as well are classified into heuristic (and knowledge-based), mathematical optimization, and hybrid approached. The heuristic approach is characterized through rules on procedures grown by experience and process insights at the unit operations scale [110] confirmed by simulation or experimentation. Data models, data mining models, and application models

are the main categories of the heuristics approach. In general, this method aims to understand and consequently to recommend the possible enhancements for target processes [111].

Membrane systems is one of the most promising technologies for industries growth in terms of PIs [112]. Thanks to the intrinsic properties of membrane processes, membranes can be replaced to conventional energy-intensive techniques in order to increase processes efficiency. Two different approaches are used to compare membrane technologies and traditional ones: exergy analysis way and PI indicators. Exergy is an energy contribute which takes into account the amount of entropy produced into the physical and/or chemical transformation. The exergetic efficiency of a process is based on calculation of entropic loss (or production of entropy) [113] and it allows to evaluate the lower work obtained or a higher work required in a process.

Various PI indicators have been developed in the past years which evaluate their impact on environment, economy and society [114,115]. Both development of new membrane systems and improvements of membrane properties resulted in a wide membrane technology application. For example, the water deoxygenation step in the electronic industry for semiconductor manufacturing is today carried out by membrane contactors [116]. Membrane contactors find application also in the beverage market [113].

1.4. Aims of the thesis

The membrane gas separation overview discussed up to now testify the increasing attention of the industry for this technology. Up to now, high free volume PDMS or organic polymers have been used in industrial plants. The main aim of this dissertation is to evaluate the possibility to apply membrane technology to industrial gas mixture stream treatment.

The starting point of the dissertation was to identify the transport and separative properties of new materials, such as polymers to intrinsic microporosity (PIM), and investigate new methods and operating conditions to characterize the materials. Particular attention was focused on CO₂ separation, especially, in the flue gases separation. The material characterizations were carried out by following two approaches: adsorption and diffusion analysis of innovative solid material and membrane permeation characterization. One of the most important challenges in terms of material characterization for gas separation is the measure carried out at high pressure. The permeation measures on the membrane module were carried out and the separative performance was calculated. Particular attention was focused on polymers known also for industrial application, such as Matrimid, and new polymers, as mentioned before, like PIMs.

In the second part of the dissertation, industrial applications of membrane separation were investigated. In the first case, the problem of humidity in CO₂ separation was studied which is an important issue in CO₂ separation and CH₄ enrichment by natural gas and biogas streams. With the aim of membrane separation industrial application, trichloroethylene mixture separation analysis was carried out.

The results discuss in the dissertation will not only provide essential data for the membrane industrial application, but also an optimization of traditional technologies in terms of process intensification.

2. Fundamentals

2.1. Basic principles of dense membrane gas separation: Solution-Diffusion Model

Today, the solution-diffusion model is the most appropriate model accepted by the scientific community to describe the trans-membrane transport in dense membranes. The model is valid for different separation processes (dialysis, reverse osmosis, gas permeation and pervaporation) and this makes the solution-diffusion model a unified approach [1]. The model assumes that the gas is adsorbed on the surface of the membrane and, diffuses under a chemical potential (concentration, pressure gradient and potential) within the membrane. The separation between the species takes place thanks to the difference of concentration of the species and diffusion rate through the material.

Therefore, the solution-diffusion model consists in a three-steps process for gas transport through a polymer: 1) gas adsorption and solution in the membrane matrix in the high pressure side (or high chemical potential); 2) gas diffusion through the polymer; 3) desorption from the low-pressure side (i.e., low chemical potential) [117].

The solution-diffusion model is based on two fundamental assumptions (shown in Figure 11):

- 1) The gas inside the bulk of the fluid phase is in equilibrium with the gas adsorbed at the interface of the membrane and so, the chemical potential between the adsorbed gas and that in the fluid phase are equal ($\mu_{i0}^{bulk} = \mu_{i0}^{memb.}$). As a consequence, adsorption and desorption gas rates are much faster than the penetration rate through the matrix, making diffusion the rate-determining step of the process.

- 2) The second assumption is that the pressure inside the membrane is uniform and that the potential difference, therefore, is due only to the difference in gas activity.

The gas flux through the membrane is shown in Eq. 1, where $\frac{d\mu_i}{dx}$ is the gradient in chemical potential of the component “i” along the membrane axis and L_i is a coefficient of proportionality (not necessarily constant).

Restricting ourselves to driving forces generated by concentration and pressure gradients, the chemical potential can be written according to Eq. 2.

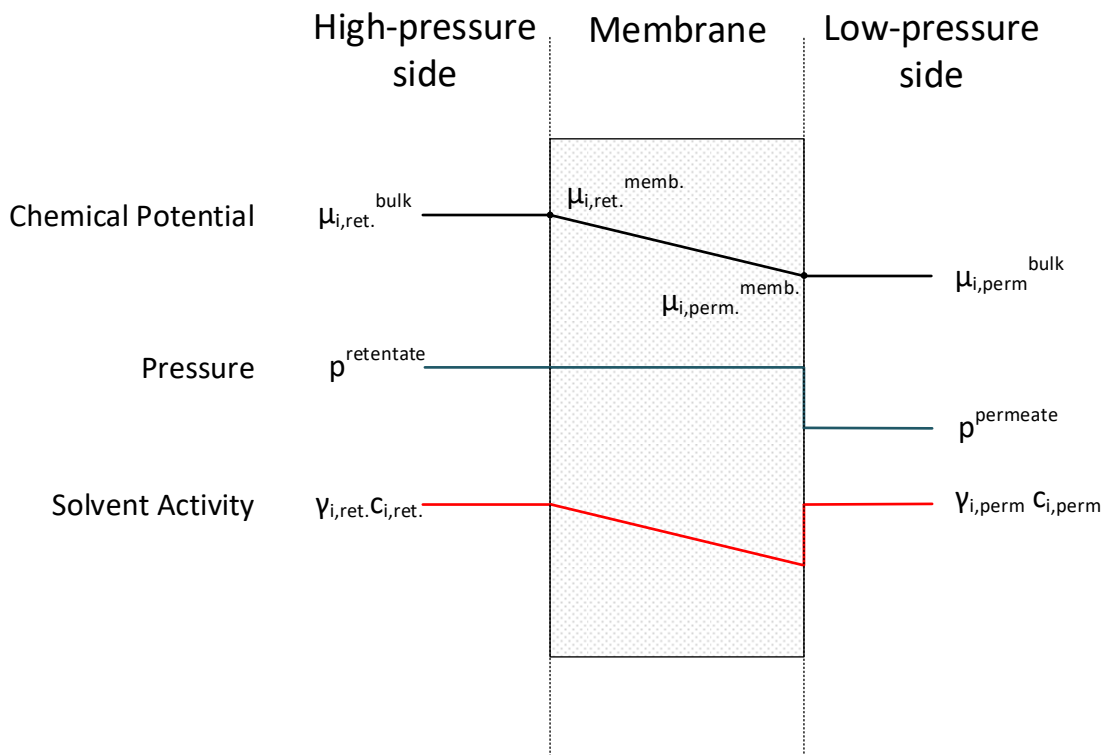


Figure 11 – Driving force and concentration gradient through membrane according to solution-diffusion model.

Flux	$J_i = -L_i \frac{d\mu_i}{dx}$	Eq. 1
------	--------------------------------	-------

Driving force	$d\mu_i = RTd\ln(\gamma_i c_i) + v_i dp$	Eq. 2
---------------	--	-------

	$\mu_{i,ret} + RT\ln(\gamma_{i,ret} c_{i,ret}) + RT \ln\left(\frac{p^{retentate}}{p_i^{sat.}}\right)$	Eq. 3
	$= \mu_{i,ret} + RT\ln(\gamma_{i,ret}^{memb.} c_{i,ret}^{memb.}) + v_i(p^{retentate} - p_i^{sat.})$	

	$c_{i,ret}^{memb.} = \frac{\gamma_{i,ret}}{\gamma_{i,ret}^{memb.}} \frac{p^{retentate}}{p_i^{sat.}} c_{i,ret} \exp\left(\frac{-v_i(p^{retentate} - p_i^{sat.})}{RT}\right)$	Eq. 4
--	---	-------

	$c_{i,ret}^{memb.} = \frac{\gamma_{i,ret}}{\gamma_{i,ret}^{memb.}} \frac{p_i^{retentate}}{p_i^{sat.}}$	Eq. 5
--	--	-------

Combining the first assumption ($\mu_i^{bulk} = \mu_i^{memb.}$) previously reported and using ideal gas flow, the integrated Eq. 2 becomes Eq. 3 which, in turn, can be rearranged into Eq. 4. v_i is the molar volume of “i” dissolved in the membrane phase and not the molar volume in the gas phase [1]. Therefore, v_i is approximately close to the molar volume of liquid “i” and the exponential terms (Poynting correction) is close to 1. Moreover, partial pressure of “i” in the retentate phase is obtained by combining the retentate pressure and concentration of “i” in the retentate phase. This simplification affords Eq. 5. By defining K_i , the sorption coefficient, equal to the term $\frac{\gamma_{i,ret}}{\gamma_{i,ret}^{memb.} p_i^{sat.}}$, Eq. 5 can be written as Eq. 6.

The concentration of the i-specie at the membrane/permeate interface follows the same mathematical analysis and results are reported in Eq. 7.

$$c_{i,ret.}^{memb.} = S_i p_i^{retentate} \quad \text{Eq. 6}$$

$$c_{i,per.}^{memb.} = S_i p_i^{permeate} \quad \text{Eq. 7}$$

$$J_i = \frac{D_i(c_{i,ret.}^{memb.} - c_{i,per.}^{memb.})}{l} \quad \text{Eq. 8}$$

Eq. 8 is the Fick's law, where l is the membrane thickness and D_i is the i -specie diffusion coefficient. The equation is a different mathematical interpretation of Eq. 1. Combining Eq. 6, Eq. 7 and Eq. 8, the widely used gas membrane permeation equation (Eq. 9) is obtained, where the permeability Pe_i is defined as the product between the diffusivity (D_i) and solubility (S_i).

$$J_i = \frac{D_i S_i (p_i^{retentate} - p_i^{permeate})}{l} = \frac{Pe_i (p_i^{retentate} - p_i^{permeate})}{l} \quad \text{Eq. 9}$$

2.2. Membrane separation performance measurements method

The membrane performance can be analysed in terms of permeating flux (Eq. 10) and permeance (Eq. 11). The first parameter is defined as the ratio between the permeate flow rate and the active membrane area available for the gases permeation. The permeance is the straight line slope, passing through the origin of the axes, i.e. the ratio between the permeating flux and the driving force. The driving force (Eq. 12) is the partial pressure difference of the penetrant species. The selectivity (Eq. 13) defines the separation performance of the membrane, showing the capabilities of the membrane of separating two different gases. In particular, it is defined as the ratio between the permeances of two gases.

$\text{Permeating flux}_i = J_i = \frac{\text{Permeate flow rate}_i}{A^{\text{Membrane}}}, \text{dm}^3 (\text{STP}) \text{m}^{-2} \text{h}^{-1}$	Eq. 10
$\text{Permeance}_i = \frac{\text{Permeating flux}_i}{\text{Driving force}_i}, \text{dm}^3 (\text{STP}) \text{m}^{-2} \text{h}^{-1} \text{bar}^{-1}$	Eq. 11
$\text{Driving force}_i = \Delta P_i = P_i^{\text{Feed}} - P_i^{\text{Permeate}}, \text{bar}$	Eq. 12
$\text{Selectivity}_{i/j} = \frac{\text{Permeance}_i}{\text{Permeance}_j}$	Eq. 13

Two experimental methods for the measurement of the membrane separative performances are used: pressure drop and concentration gradient method.

The pressure drop method is used for the permeation measurement with a single gas. In the pressure drop method, an absolute pressure difference was applied through the membrane. The retentate side is closed and the trans-membrane pressure difference (ΔP) is set by controlling the pressure at the feed side by means of a forward pressure

controller, keeping atmospheric the permeate side pressure. The membrane module is placed in the oven for temperature control and the permeate stream, for its evaluation, is fed to the bubble soap gas flowmeter (Figure 12).

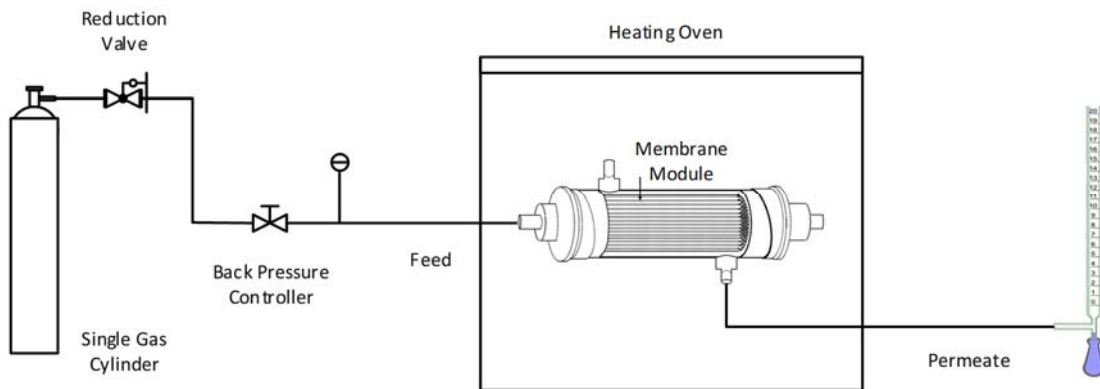


Figure 12- Experimental plant scheme for single gas permeation measurements (Pressure drop method).

Figure 13 schematically shows the experimental set-up for permeation measurements on mixtures of gases (concentration gradient method). The gas mixture was fed to the membrane module by means of mass flow controllers, opportunely tuned for assuring a set composition of feed flow rate to the membrane. In the case of wet mixture, the dry feed stream is fed in the humidifier. In any case the retentate line is open.

A back pressure regulator on the retentate line and a manometer on the feed line allow the required trans-membrane pressure difference to be operated and measured in the membrane module. The retentate and permeate flow rates were measured by means of two soap bubble gas flow meters. The retentate and permeate flow rates were analysed with a gas chromatography (in the permeation measurements on mixture gases that will be discussed in the chapter 4, Agilent 7890A GC was used).

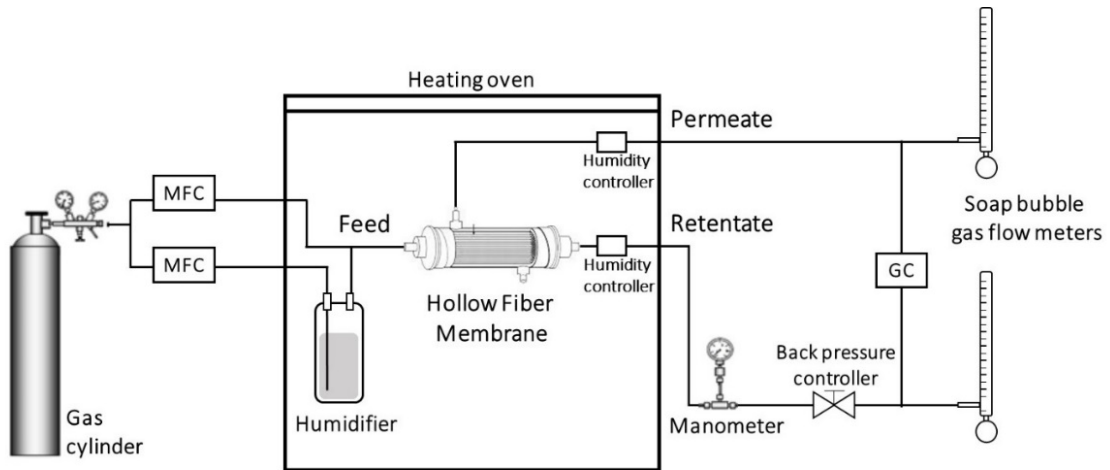


Figure 13 - Schematic of concentration gradient method experimental set-up used for measuring mixed gas permeation properties of membranes: MFC, mass flow controller; GC, gas chromatography.

An important analytical method to characterize membranes, which was not used during this doctoral research activities, is the time lag method which can evaluate diffusion, solubility, and permeability coefficients from a single experiment [118]. Owing to the nature of the measurement, transport parameters can be directly obtained [119]. The method has been applied to study permeation phenomena in terms of diffusion and adsorption in polymeric and porous membranes, respectively [119].

The time lag method is based on the determination of the "delay" (θ) obtained from the time difference observed between the beginning of the measurement, when the gas starts to enter the membrane and, the time in which the permeate gas flow is constant.

The diffusivity is calculated as reported in Eq. 14 for a slab sample with thickness "l".

Assuming the validity of Solution-Diffusion mechanism, the solubility is calculated in Eq. 15, at known permeability "P".

Diffusivity	$D = \frac{l^2}{6\theta}$	Eq. 14
-------------	---------------------------	--------

Solubility	$S = \frac{P}{D}$	Eq. 15
------------	-------------------	--------

2.3. Mathematical models for membrane unit design: 1-D model for the multi-species steady-state permeation

Several studies [120,121,122,123,124,125,126,127,128] developed models to understand and predict the membrane gas separation phenomenon. In this thesis, the model developed by Brunetti et al. [27] will be taken into account due to its easy and flexible application. 1D dimensionless model for the multi-species steady-state permeation in no sweep mode and co-current configuration is discussed. The model was developed and already validated elsewhere [27]. The membrane gas separation devices have been studied and the influence of different parameters affecting the membrane system performance has been introduced in terms of general maps (will be discussed below).

Figure 14 shows a schematic membrane system for mixture gas separation system. The model was developed by using plug flow fluid dynamics along the membrane. The mixture gas flows down on feed side along membrane to retentate side. The mixture follows two ways: one part goes through the membrane layer and it is recovered in the permeate side, the rest in the retentate is recovered.

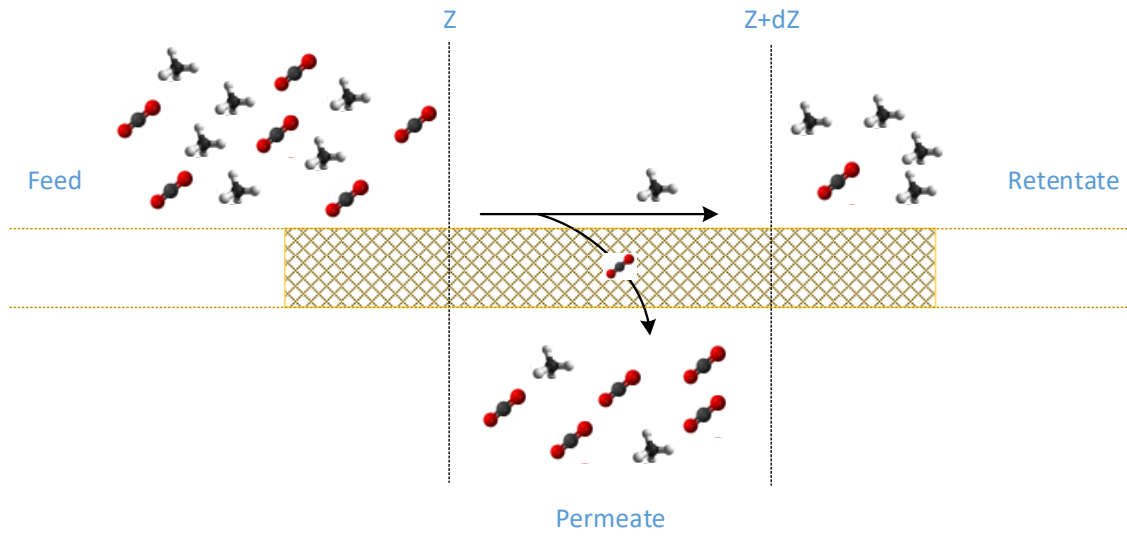


Figure 14 – Membrane system geometry for model development.

In the case of binary mixtures (a CO₂/CH₄ mixture is used here) the model consists of a system of 2 ordinary differential (for the retentate side) and 2 algebraic (for the permeate side) equations, i.e. Eq. 16-19 [27].

Feed/Retentate side

$$\frac{d\varphi_{CO_2}^{Retentate}}{d\zeta} = -\theta_{CO_2}(\phi x_{CO_2}^{Retentate} - x_{CO_2}^{Permeate}) \quad \text{Eq. 16}$$

$$\frac{d\varphi_{CH_4}^{Retentate}}{d\zeta} = -\frac{x_{CO_2}^{Feed}}{x_{CH_4}^{Feed}} \frac{1}{\alpha_{CO_2/CH_4}} \theta_{CO_2}(\phi x_{CH_4}^{Retentate} - x_{CH_4}^{Permeate}) \quad \text{Eq. 17}$$

Permeate side

$$\varphi_{CO_2}^{Permeate} = \varphi_{CO_2}^{Feed} - \varphi_{CO_2}^{Retentate} \quad \text{Eq. 18}$$

$$\varphi_{CH_4}^{Permeate} = \varphi_{CH_4}^{Feed} - \varphi_{CH_4}^{Retentate} \quad \text{Eq. 19}$$

In the equations φ_{CO_2} and φ_{CH_4} (Eq. 20), are the dimensionless molar flow rates in the feed, retentate and permeate, and ζ (Eq. 21) is the dimensionless module length. θ_{CO_2} (Eq. 22) and ϕ (Eq. 23) are the permeation number and pressure ratio, respectively. Permeation number is a dimensionless group representing the ratio of permeating flux through the membrane and the convective flux fed to the membrane module. Higher permeation number corresponds higher residence time for the stream and higher permeation through the membrane than total flux along the module.

Pressure ratio is a dimensionless group representing the feed/permeate pressure ratio.

$$\varphi_{CO_2} = \frac{Q_{CO_2}}{Q_{CO_2}^{Feed}} \quad \text{Eq. 20}$$

$$\varphi_{CH_4} = \frac{Q_{CH_4}}{Q_{CH_4}^{Feed}}$$

$$\zeta = \frac{z}{L} \quad \text{Eq. 21}$$

$$\theta_{CO_2} = \frac{\text{Permeance}_{CO_2} A^{Membrane} p^{Permeate}}{x_{CO_2}^{Feed} Q^{feed}} \quad \text{Eq. 22}$$

$$\phi = \frac{p^{Feed}}{p^{Permeate}} \quad \text{Eq. 23}$$

Feed composition, membrane properties (such as CO₂ permeance and CO₂/CH₄ selectivity), module geometry (total membrane area and module length) and operating conditions (feed flow rate and pressure) fix the equation solutions in term of dimensionless flow rate profile along the module dimensionless length for both membrane sides (feed/retentate and permeate side). Species concentration and its

recovery in both membrane sides can be easily calculated. As a consequence, overall membrane module performance in terms of final species purity and total recovery can be obtained. Thanks to the dimensionless solution, variable membrane properties combination, module geometry and operating conditions lead to the same solution for the membrane system (dimensionless species profiles along the membrane module and overall membrane module performance). Table 2 reports the feed composition and operating condition used in this section for following maps. A binary CO₂/CH₄ gas mixture separation was simulated at pressure ratio of 10, 50 and 100 and CO₂/CH₄ selectivity of 1, 5, 10 and 50.

Table 2 – Feed condition and operating parameters

CO ₂ :CH ₄ feed composition, %	50:50
Pressure ratio, bar	5, 10, and 50
CO ₂ /CH ₄ selectivity, -	5, 10 and 50

Figure 15 displays global maps showing all the possible solutions for CO₂:CH₄ feed composition of 50:50, pressure ratio of 50 and CO₂/CH₄ selectivity of 5, 10 and 50. In particular, CO₂ permeate and CH₄ retentate concentration are plotted as a function of their recovery for different CO₂/CH₄ selectivities and fixed pressure ratio of 50. All the curves at constant CO₂/CH₄ selectivity follow the same trend: at high CO₂/CH₄ selectivity correspond higher CO₂ concentration in the permeate side. Same behaviour is shown for CH₄ concentration trend. Increasing the CO₂/CH₄ selectivity, the curves move up, which means that a higher purity is achieved at the same CH₄ (or CO₂) recovery.

At a given permeation number (Figure 15, dashed line), higher CO₂/CH₄ selectivity allows higher CO₂ permeate concentration while the CO₂ recovery decreasing. At higher CO₂/CH₄ selectivity the membrane allows a better separation between CO₂ and CH₄ (higher purity for CO₂ and CH₄ in permeate and retentate, respectively). The partial pressures difference of each species reduces along the membrane length. As a consequence, the permeation driving force is lower (lower permeation flow rate) and the same recovery is reached at higher permeation number. This effect is more evident in the right side of the CO₂ concentration trend (Figure 15, above) where the driving force is lower with respect to the feed side.

As showed in the upper part of Figure 15, all the curves converge always to the CO₂ feed composition at total recovery.

The space of solution for different membrane selectivity at a given pressure ratio can be divided into two spaces: at low CO₂ recovery, the CO₂ permeate concentration is strongly affected by the CO₂/CH₄ selectivity and at high CO₂/CH₄ selectivity higher CO₂ permeate concentration can be obtained. In the second space, the membrane selectivity does not affect the membrane separation performance and the permeate concentration is controlled only by the pressure ratio.

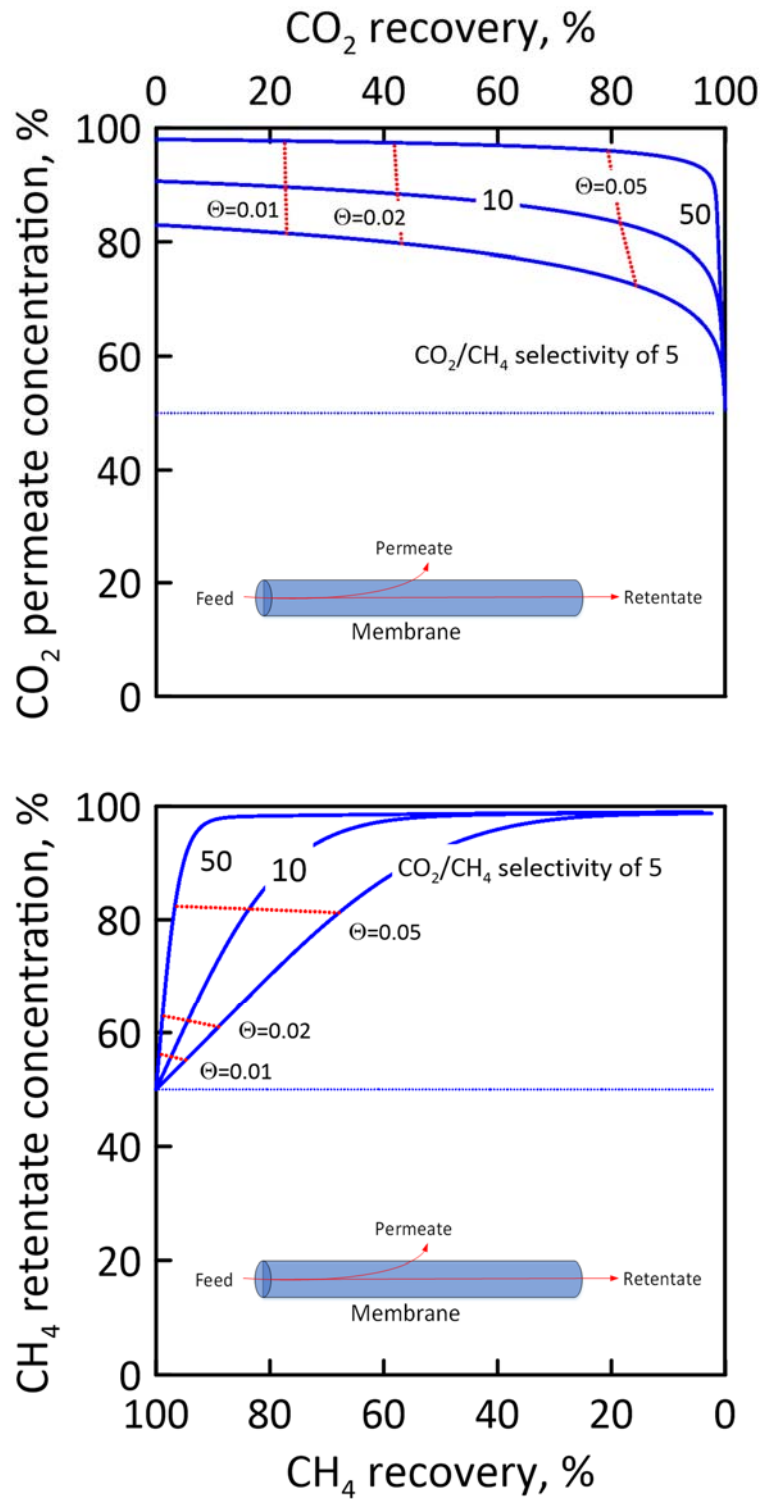


Figure 15 – CO₂ permeate concentration and CH₄ retentate concentration as a function of CO₂ and CH₄ recovery, respectively. Dashed line (red): Permeation number of 0.01, 0.02 and 0.05; Pressure ratio of 50; CO₂/CH₄ selectivity of 5, 10 and 50.

Figure 16 shows the effect of CO₂/CH₄ selectivity (CO₂/CH₄ selectivity of 5) at different pressure ratio of 5, 10 and 50. At higher CO₂ recovery, the CO₂ permeate concentration approaches asymptotically a limit trend, converging to the feed composition. On the other side, CH₄ recovery reduces and the CH₄ concentration in the retentate increases.

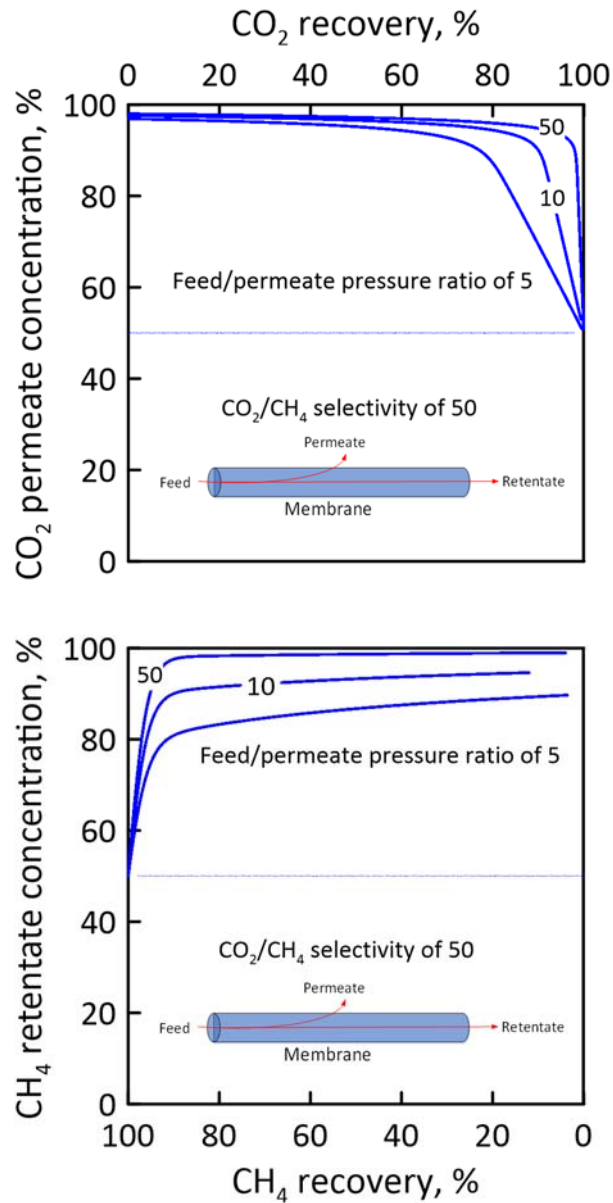


Figure 16 – CO₂ permeate concentration and CH₄ retentate concentration as a function of CO₂ and CH₄ recovery, respectively. Pressure ratio of 50; CO₂/CH₄ selectivity of 5, 10 and 50.

2.4 Process Intensification Metrics

Criscuoli and Drioli [113] reported the role of membrane operations for re-designing industrial productions in the logic of the process intensification. Particular attention is focused on the use of metrics for the quantification of productive and environmental parameters. Membrane and traditional operations were compared using new metrics. One of the most important aim for innovative chemical plants is the maximisation of productivity/size plant ratio. The first metrics proposed by Criscuoli & Drioli [113] (productivity/size plant ratio) compare the membrane plant productivity/size ratio with traditional plant productivity/size ratio (Eq. 24). Similarly to the metric PS (Eq. 24), it is possible to define the same parameters as a function of weight (productivity/weight plant ratio, Eq. 25) and not of the volumetric size. This metric is particularly important for offshore plants or for plants that must be built in remote areas.

$$PS = \frac{\text{Productivity/Size (membrane)}}{\text{Productivity/Size (traditional)}} \quad \text{Eq. 24}$$

$$PW = \frac{\text{Productivity/weight (membrane)}}{\text{Productivity/weight (traditional)}} \quad \text{Eq. 25}$$

$$MI = \frac{\text{Productivity}_2}{\text{Productivity}_1} \quad \text{Eq. 26}$$

$$M = \frac{(\text{area}_2/\text{area}_1 - MI) (\text{membrane})}{(\text{area}_2/\text{area}_1 - MI)(\text{traditional})} \quad \text{Eq. 27}$$

Modularity index (Eq. 26) is evaluated as a function of change of productivity. It is defined as ratio between two productivities at different plant productivity configuration.

Modularity takes into account the changes of the plant size due to variations of the plant productivity (Eq. 27). This metric compares the variations of the area (for membranes) with those of the volume (for conventional systems). The membrane system has a higher modularity if the modularity metric is lower than 1; modularity values higher than 1 are in favour of the traditional system.

The application of metrics will be shown in the following chapters in order to compare the production potential of integrated membrane processes and traditional processes (6. Membrane Integrated Process for Trichloroethylene Mixture Separation).

3. Kinetic model for high pressure adsorption measurement

As discussed in Section 2.1, adsorption and diffusion are the fundamental stages of membrane separation in dense membrane [1]. Therefore, the knowledge of the properties of membrane materials is required to design and predict their behaviour in relevant applications. In recent years, high microporosity membranes, enabling high trans-membrane flow rates, and mixed matrix membranes have gained increasing interest. In particular, the latter display selective performances and high adsorption capacity thanks to the inclusion of micro- and/or mesoporous particles within the polymeric network. Controversial reports have been published on these membranes as far as the sorbent capacity is concerned. Consequently, their application has been limited by a diffused scepticism among the scientific community [129]. The demanding synthesis procedures, the different experimental conditions, and the difficulty in carrying out high pressure adsorption measurements (up to 140 bar) on small samples (~100 mg), are the main reasons for the discrepancies reported in the relevant literature [129].

The research activity described in this Chapter has been carried out at the University of Edinburgh under the supervision of Dr. M.C. Ferrari and Prof. S. Brandani. The aim of the research was to develop a kinetic model for the accurate analysis of diffusivity and sorption of high pressure gas on porous matrices in Sieverts volumetric systems [130]. Volumetric systems (as Sieverts apparatuses) are flexible devices used to accurately evaluate adsorption phenomena (equilibrium analysis) and kinetic diffusivity (dynamic analysis) [131].

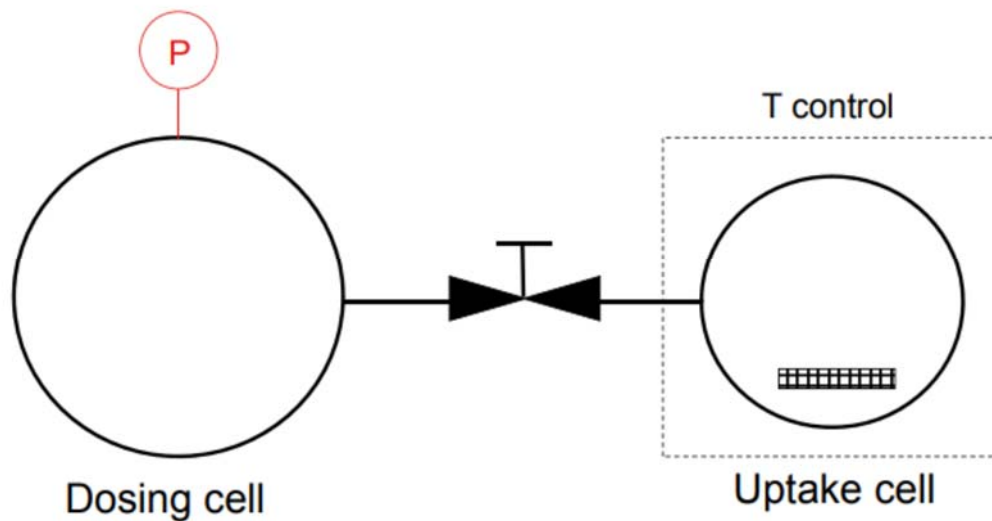


Figure 17 - Sieverts schematic apparatus [130].

Figure 17 shows the scheme of the Sieverts apparatus used in this work. It basically consists of two volumes, dosing and uptake volume, separated and isolated by means of a valve.

The dosing cell is the section in which the gas is pressurized, while the uptake cell is the cell containing the sample upon which adsorption takes place. During adsorption experiments, the pressurized gas flows from the dosing to the uptake cell, which is at lower pressure and where gas adsorption occurs. During desorption measurements, the dosing cell is at lower pressure than the uptake cell, thus the gas flows backwards and gas desorption from the sample occurs due to pressure reduction. During the transient phases, both during adsorption and desorption steps, kinetic parameters such as gas diffusivity and global heat exchange coefficient can be evaluated. At the equilibrium, instead it is possible to calculate the absolute amount of gas adsorbed [132]. Pressure and temperature have been monitored and recorded both during transient and equilibrium phases and in both the dosing and uptake volumes. The main parameters intervening are the volumes

of the two sections and the mass of the sample, which can be determined by means of helium expansion tests.

Owing to the non-ideality of the system studied, the Redlich-Kwong cubic equations of state (EoS) have been used to simulate the gas behaviour at high pressure. EoS parameters were evaluated from the National Institute of Standards and Technology (NIST) database. By combining EoS, material and energy balances, adsorption constitutive equation, etc. it is possible to develop a kinetic model describing the gas diffusivities in the solid material network.

3.1 Introduction

As discussed before, one of the most important social issue is the global warming effect caused by the excessive emissions of greenhouse gases, especially CO₂, into the atmosphere. The main activities contributing to this problem are related to the generation of energy from fossil fuels, but also to the cement production, refining, petrochemical, iron and steel industry, and transports. The most important technology available to mitigate CO₂ emission is based on carbon capture and storage (CCS). In this framework, understanding the CO₂ adsorption onto microporous solids is a relevant task in the fields of gas separation, gas purification, but especially for environmental remediation [133,134]. Zeolites, activated carbon, metal organic frameworks (MOFs), carbon nanotubes and nanofibers have been recently considered as promising high-capacity sorbent materials.

Thanks to the high adsorbent capacity demonstrated in several studies [135,136,137,138], zeolite 13X is one of the best commercial zeolites for post combustion applications and

it is very often used as benchmark to compare other materials potentially applicable for CO₂ separation processes.

Even if data reported in literature from different research groups [139] are often controversial, most of them agree on the accuracy improvement obtainable by using volumetric systems. In this regard, many studies focused on minimizing the uncertainties on the system variables and increase the sensitivity. Particular sensitivity problems arise when light gas adsorption is considered, due to the significant experimental errors [140,141]. Measurements carried out in volumetric systems [142] showed remarkable problems about adsorption errors and discordant data [143,144]. Two types of Sievert's volumetric systems are generally used: the first one is based on single manifold and only total pressure analysis [145,146,147,148,149,150], while the second type is a differential unit, i.e. two mirror-image single-sided units connected via a differential pressure transducer which are studied simultaneously [151,152,153]. For small sample volumes, many uncertainties during the measurement occur, such as errors detected in the dosing and uptake volumes, uncertainty in the calibration of the volumes once the sample is loaded, possibility of significant variation of the sample mass during the pre-treatment, and weighing difficulty due to the sensitivity of the scales in-situ. Tibbetts et al. [129] have shown how these problems are even more evident in high pressure measurements. Thanks to the use of a differential transducer, the differential unit differs from the single-volume unit for greater accuracy. Using a differential transducer allows to decrease the measurement scale by 10 times compared to an absolute one, thus making the measurement 10 times more sensitive [142].

3.2 Method

3.2.1 Sieverts experimental apparatus

Figure 18 shows the scheme of the experimental apparatus used for the kinetic and adsorption tests on microporous materials [154]. The system is composed by five sections:

1. Feed section: Gas is fed by a pressure cylinder regulated by its supplied reducer. The storage cylinder can be sectioned from the rest of the system through the V01 valve.
2. Vent section: A section which bring the system from high to atmospheric pressure.
3. Vacuum section: Vacuum pump bring the system to a pressure lower than atmospheric pressure.
4. Dosing section (dashed blue line reported in Figure 18).
5. Uptake section (dashed red line reported in Figure 18).

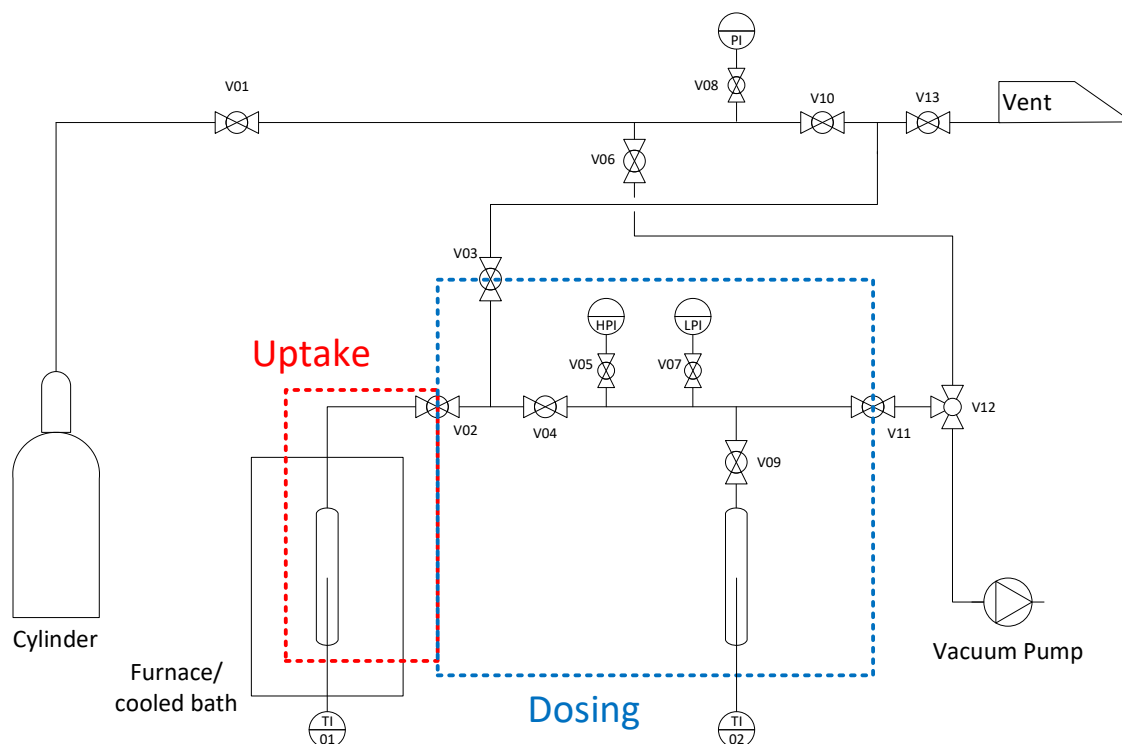


Figure 18 - Schematic Volumetric adsorption unit used during kinetic and adsorption measurements.

The dosing cell volume can be determined by expanding a known quantity of gas and, knowing gas density and temperature, by measuring the volume through the pressure displayed on the pressure transducer.

Once the dosing volume is determined, the uptake cell volume, V_U , can be found with a helium expansion from the dosing section, when a certain pressure is achieved, to the uptake cell. The moles of gas in the uptake and dosing sections at the equilibrium can be calculated through the state equation of gas, by taking into account the non-ideal gas behaviour, and by using the gas density from the NIST Webbook and the measured pressure and temperature.

Selected gas is fed from the cylinder to the pre-dosing volume through the valves V01 and V10. Once the pre-dosing line section is filled, the valve V03 is opened, in order to fill the dosing volume up to the desired pressure. The pressure is controlled through two

different absolute pressure indicators with different reading ranges (Table 3), in order to improve the accuracy of the analysis in the studied pressure ranges. The correct pressure in the dosing is regulated either through the V13 valve, when working at pressures higher than the atmospheric ones, or through the V11 and V12 valves, which supply the gas to the vacuum pump (Table 3). Once the gas has been correctly loaded into the dosing volume, the gas expands into the uptake volume by opening the V02 valve. Thereafter, the pressure is reduced in the dosing volume and consequently increases in the uptake section. By following the transient phase of gas expansion within the uptake volume, it is possible to investigate all the gas diffusion kinetic parameters through the adsorbent matrix and both the heat exchange coefficients.

After the equilibration, i.e. when pressure and temperature values are constant, the cells are disconnected from each other by closing the valve V02 and the manifold is re-pressurized. As the temperature is constant, each amount of adsorbed or desorbed gas at a certain pressure defines a point of an isotherm of adsorption or desorption, respectively (Every step defines a point of isotherm).

Adsorption measurements can be represented by three different steps in which the adsorption, desorption and regeneration of the sample are studied.

Table 3 – Instrumentation used in adsorption apparatus

Vacuum pump	Triva E2
Pressure transducers	MKS instruments: 127AA-25000B (up to 33.3 bar) 127AA-01000B (up to 1.33 bar)
Thermostatic bath	Jencon-PLS

	Julabop F25-MA (-28 - +200 °C)
Thermocouples reader	Tenna 72-2065 A
Furnace	Custom made (from 0°C to 350°C)

The volume of the dosing is:

For pressure range up to 1.33 bar, $V_{LP}=83.299 \text{ cm}^3$

For pressure range up to 33.33 bar, $V_{HP}=67.316 \text{ cm}^3$

Volume difference as a function of pressure range is due to the interception of the low pressure transducer (higher pressure than 1.33 bar could damage the membrane) via the V07 valve (Figure 5) with a consequent reduction in the available volume. Thanks to the pressure reduction during gas expansion in the uptake section, it is possible to evaluate the exact uptake volume.

As mentioned before, the moles that have to be in the uptake section at the equilibrium can be calculated through the gas equation of state, by taking into account the non-ideal gas behaviour.

Zeolite 13X pellets (UOP Honeywell International Inc, type 13X APG 8X12) have been used to test gas adsorption.

Metallic beads (1/8 " diameter) were used to reduce the free volume in the uptake section. A lower free volume allows to maximize the gas volume adsorbed on the sample and, consequently, to enhance the accuracy of the data due to the greater pressure difference observed through adsorption. Using metallic fillers instead of glass or other inert materials allows to quickly disperse the generated adsorption heat and to reach fast equilibrium conditions.

Table 4 - Material properties of beads, sample and steel materials

	Volume steel		Beads	Sample (zeolite 13X)	Thermocouple
	Dosing	Uptake			
Density, kg m ⁻³	7990	7990	7990	1650	8610
Heat capacity, J kg ⁻¹ K ⁻¹	500	500	500	920	523
Void degree, %	N.A.	N.A.	N.A.	N.A.	35.69
Tortuosity, -	N.A.	N.A.	N.A.	N.A.	2.2

Table 5 – All system components geometry (dosing, uptake, beads, sample and thermocouple)

	Dosing	Uptake	Beads	Sample (zeolite 13X)	Thermocouple
Volume, cm ³	83.23	18.367	13.12	1.2	0.197
Mass, g	933.4	933.4	N.A.	0.73	N.A.
Length, cm	15	15	N.A.	N.A.	N.A.
Internal diameter, cm	1.56	1.56	N.A.	N.A.	N.A.
External diameter, cm	2.23	2.23	N.A.	N.A.	N.A.
Internal surface, cm ²	206	73	N.A.	N.A.	N.A.
External surface, cm ²	300	105	-	-	5

Table 4 and Table 5 report material properties and system geometry used in the adsorption measurements.

It is possible to distribute the fillers and the samples in the uptake column in stratified or dispersed configuration. In the first case, the column is filled with three different layers.

A first layer, on the bottom of the column, is composed of metal beads, a second layer, close to the hot joint of the thermocouple, is filled with the sample, and a third layer, on the top of the column, comprised of metal beads (Figure 19, left). This packing method causes an accumulation of localized heat in the sample layer and, consequently, heat dispersion is not efficient and the equilibrium is reached slowly.

The second filling method (Figure 19, right) provides a more uniform distribution of the sample inside the column where it is dispersed together with the metal beads and allows a better thermal distribution in the uptake. However, in this case, the temperature read in the uptake volume has considerable uncertainty. In fact, while in the stratified configuration the hot joint of the thermocouple is in contact with the sample, in the dispersed configuration the column is filled randomly, and the hot joint can be in contact with metal beads, with sample, or with both parts (Figure 19, right).

Dispersed configuration was used in the CO₂ adsorption measurements, which will be discussed in the next paragraphs.

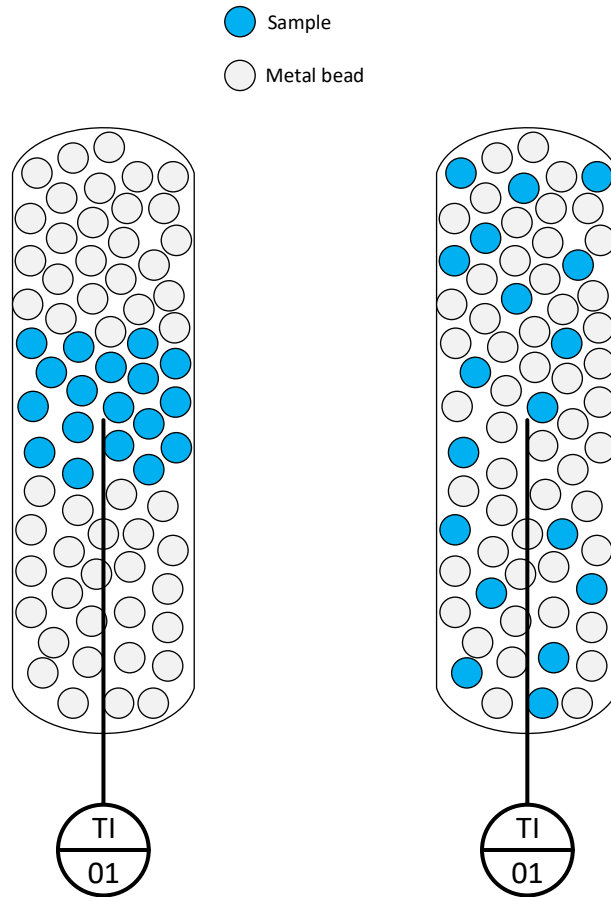


Figure 19 - Packaging method. Left: stratified filling; right: dispersed filling. Blue circle: sample; grey circle: metal beads.

It is important to identify a strategy to process the data obtained for a correct analysis of the amount of adsorbed gas. Three different types of adsorption are defined within the micropores of the solid [155,156]: absolute, net, and excess adsorption. The total number of molecules contained within a microporous crystal is given by the sum of the molecules adsorbed onto the external surface of the solid body itself (n_s), considered as inaccessible to gas, and the molecules contained in the micropores (n_A). The total amount of adsorbed moles n^{tot} by a given crystal is the sum of n_A and n_s (Eq. 28) by considering V_s , as the volume of the crystal by considering full and empty spaces.

Total number of moles	$n^{Tot} = n_A + n_S$	Eq. 28
-----------------------	-----------------------	--------

In absolute adsorption the solid is removed: Absolute adsorption n^{Abs} considers only the amount of gas adsorbed onto the micropores, as if the solid would be removed, and it can be calculated according to Eq. 29

Absolute adsorption	$n^{Abs} = n^{Tot} - n_S = n_A$	Eq. 29
---------------------	---------------------------------	--------

Net adsorption (Eq. 30) is defined by subtracting from the absolute adsorption, the equivalent gas moles that would be present in the same volume of solid (V_S) at the same pressure and temperature of the system (c : gas concentration under these conditions).

Differently from net adsorption, excess adsorption also takes into account volumes not accessible by gas (V_{NA}) as shown in Eq. 31.

Net adsorption	$n^{Net} = n^{Abs} - V_S c = n_A - V_S c$	Eq. 30
----------------	---	--------

Excess adsorption	$n^{Ex} = n^{Abs} - (V_S - V_{NA})c = n_A - (V_S - V_{NA})c$ $q^{Ex} = \frac{n^{Ex}}{V_S}$	Eq. 31
-------------------	--	--------

Absolute adsorption determination is possible by using techniques such as NMR [157] or impedance spectroscopy [158], while it is not accessible with the most common adsorption techniques [155]. On the other hand, helium expansion experiments are usually used to evaluate the volume of solid, which is then used to estimate the excess adsorbed amount [155]. Therefore, excess adsorption is easily calculated [159,160,161] with volumetric techniques such as those used in this work. However, isotherm equations, such as the Langmuir equation which will be discussed later, are based on absolute

adsorption. Therefore, excess adsorption obtained by volumetric methods has to be converted in absolute adsorption (Eq. 32).

Absolute adsorption	$q^{Abs} = q^{Ex} + \varepsilon^{Void} c$	Eq. 32
---------------------	---	--------

3.2.2 Equations of State

On the basis of the equations of state (EoS) based on Helmholtz free energy (Eq. 34 - Eq. 36), which is expressed in function of measurable variables such as temperature, pressure and density, it is possible to define the thermodynamic fluid properties (the thermodynamic fluid properties used in the work were reported in the equations Eq. 37 - Eq. 41). In the last decades, multi-parameter EoSs have been obtained by modifying BWR equation [162], which led to semi-empirical equations of up to 38 parameters [163,164,165]. Over the years, a huge literature has been developed based on multi-parameter equations of state [166] for single and mixture gases [167].

The main idea that places the EoS at the basis of the various studies is the need to describe all the experimental data of the thermodynamic properties through a single equation, considering an uncertainty of the data due to the approximation of each model to the calculated physical data. The EoS would become the true reference of all of the thermodynamic properties of the examined species. This would make possible to transform the state equation into the new reference for the study of all the thermodynamic properties of the fluid without requiring experimental validation tests [166]. In this way, the EoS could be implementable to calculate thermodynamic properties in process analysis (as it will be discussed later, the EoS have been used for the calculation of the fugacity in order to evaluate Langmuir adsorption isotherm parameters), and for the

calibration of accurate scientific instruments (correct assessment of uptake and dosing volumes by means of gas expansion processes). The main issue to this aim is the accuracy of the EoS. As anticipated previously, modified BWR equation is the first EoS equation in literature, published in 1973, which successful reach the accuracy target [162].

In the 1980s, reference equations with optimized functional forms resulted in significantly increased accuracies [168,169].

More recently, new experimental techniques allowed to accurately determine thermodynamics properties, such as speed of sound [170]. Moreover, new optimization algorithms development [170] and the introduction of new EoS parameters allowed to improve the properties representation in the critical region [171].

Thanks to these development, new EoS can be used in a wide range of conditions, up to the limits of chemical stability of the substances.

Redlich-Kwong equation	$z = \frac{1}{1 - \rho b} - \frac{\varepsilon(T)b\rho}{RT(1 + \rho b)}$ $\varepsilon(T) = \varepsilon_0 + \varepsilon_1 (T - T_0)$	Eq. 33
Helmholtz Energy	$a = a^{id} + a^r$	Eq. 34
Ideal Helmholtz contribution	$a^{id} = h^{id} - RT - T s^{id}$	Eq. 35
Residual Helmholtz contribution	$a^r = \hat{a} - RT \ln z$ $\hat{a} = RT \int_0^\rho \frac{z - 1}{\rho} d\rho = RT \ln \left(\frac{1}{1 - \rho b} \right) + \varepsilon(T) \ln \left(\frac{1}{1 + \rho b} \right)$	Eq. 36

	$g(T, p) = h - Ts$	
Gibbs Energy	$g = g^{id} + g^r = g^{id} + (a^r + RT(z - 1))$	Eq. 37
	$s(T, \rho) = -\left(\frac{\partial a}{\partial T}\right)_v$	
Entropy	$s = s^{id} + s^r = s^{id} - \left[R \ln\left(\frac{1}{1 - \rho b}\right) + \varepsilon_1 \ln\left(\frac{1}{1 + \rho b}\right) - R(\ln z - 1) \right]$	Eq. 38
	$h(T, p) = u + pv$	
Enthalpy	$h = h^{id} + h^r = h^{id} + (g^r + Ts^r)$	Eq. 39
	$u(T, \rho) = a + Ts$	
Internal Energy	$u = u^{id} + u^r = u^{id} + [h^r - RT(z - 1)]$	Eq. 40
	$g(T, p) - g^{id}(T, p) = RT \ln \frac{f}{P}$	
Fugacity	$\ln \frac{f}{P} = a^r + RT(z - 1)$	Eq. 41

In this work, EoS will be used to develop a simple approach which can be extended on the study of mixtures. Cubic equations, in particular the Redlich-Kwong equation (Eq. 33), was chosen, to determine all the thermodynamic properties of the single gases (Eq. 34 - Eq. 41). The two parameters of the Redlich-Kwong equation, the co-volume “ b ” and the energy parameter “ $\varepsilon(T)$ ” were obtained by fitting the experimental data present on the NIST Webbook [172] based on the previously discussed multi-parameter equations. The fitting of the parameters was obtained by analysing a temperature range of 0 - 100 °C and a pressure range of 0 - 30 bar.

3.2.3 Equilibrium isotherm equation

More and more adsorption isotherm models have been developed so far. Linear isotherms and Langmuir based model isotherms are generally used due to their thermodynamic consistency. The linear isotherm is expressed by Eq. 42

$$q_s = Hf = H_0 e^{\frac{-\Delta H_s}{RT_s}} f \quad \text{Eq. 42}$$

where:

- q_s , absolute amount adsorbed
- H , Henry's law constant
- H_0 , pre-exponential factor
- $-\Delta H_s$, heat of adsorption
- f , fugacity.

The Langmuir equation, used in this work, allows a wide range of adsorption cases. Different equations can be derived by considering single-site (Eq. 43), dual-site (Eq. 46), or triple-site (Eq. 50) adsorption.

The use of different mathematical expressions derives from the presence of sites more active than others, according to the Langmuir saturation model. In other words, the most favourable site/s will be filled first, followed by the less favourable site/s [173].

Eq. 44 describes Langmuir adsorption on single-site:

$$q_s = q_{s,1} \frac{b_1(T)f}{1 + b_1(T)f} \quad \text{Eq. 43}$$

where:

- q_s , absolute amount adsorbed
- $q_{s,1}$, saturation adsorption. It only depends on the material in terms of available sites

- $b_1(T)$, temperature-dependent equilibrium constant
- f , fugacity.

At very low pressures (close to 0), behaviour of gases is satisfactorily described by the ideal gases law. This allows to assume the fugacity equal to the pressure of the gas.

Under these conditions the single-site Langmuir isotherm can be written as in Eq. 45:

$$q_s = q_{s,1}b_1(T)f = q_{s,1}b_1(T)P \quad \text{Eq. 44}$$

where $q_{s,1}b_1(T)$ assumes the meaning of the Henry law constant, $H(T)$.

$$q_s = H(T)P \quad \text{Eq. 45}$$

In the case of dual-site Langmuir adsorption (Eq. 46) each site must be modelled by a separate equilibrium constant, $b_1(T)$ and $b_2(T)$, being $\Delta H_{i,ads}$ the heat of adsorption (Eq. 47 and Eq. 48, respectively) for each site.

$$q_s = q_{s,1} \frac{b_1(T)f}{1 + b_1(T)f} + q_{s,2} \frac{b_2(T)f}{1 + b_2(T)f} \quad \text{Eq. 46}$$

$$b_1 = b_{1,0} e^{\frac{-\Delta H_{1,ads}}{RT_s}} \quad \text{Eq. 47}$$

$$b_2 = b_{2,0} e^{\frac{-\Delta H_{2,ads}}{RT_s}} \quad \text{Eq. 48}$$

where:

- q_s , absolute amount adsorbed;
- $q_{s,i}$, saturation capacities. It only depends on the material in terms of available sites;
- $b_i(T)$, temperature-dependent equilibrium constant;
- f , pressure.

As discussed before, at very low pressure the fugacity tends to 0 and Eq. 47 can be rewritten as in Eq. 50, where $q_{s,1}b_1(T)+q_{s,2}b_2(T)$ assume the physical value of Henry law constant, $H(T)$.

By extending the same procedure for the triple-site model, Eq. 51 can be written

$$\lim_{f \rightarrow 0} \frac{q_s}{f} = q_{s,1}b_1(T) + q_{s,2}b_2(T) = H(T) \quad \text{Eq. 49}$$

$$q_s = q_{s,1} \frac{b_1(T)f}{1 + b_1(T)f} + q_{s,2} \frac{b_2(T)f}{1 + b_2(T)f} + q_{s,3} \frac{b_3(T)f}{1 + b_3(T)f} \quad \text{Eq. 50}$$

$$b_3 = b_{3,0} e^{\frac{-\Delta H_{3,ads}}{RT_s}} \quad \text{Eq. 51}$$

Analogously, at pressure values tending to 0 for the triple-site model it can be demonstrated that

$$\lim_{f \rightarrow 0} \frac{q_s}{f} = q_{s,1}b_1(T) + q_{s,2}b_2(T) + q_{s,3}b_3(T) = H(T) \quad \text{Eq. 52}$$

The isosteric heat of adsorption is, generally, constant for adsorption following the linear and single site models Langmuir isotherm. Differently, for more complex models described by multiple site Langmuir isotherms, the heat produced is not constant (isosteric heat of adsorption is a function of fugacity) and it is thermodynamically described by the following equation (Eq. 53) [174]:

$$\Delta H_{ads} = \frac{\Delta H_1 q_{s,1} b_1 (1 + b_2 f + b_3 f)^2 + \Delta H_2 q_{s,2} b_2 (1 + b_1 f + b_3 f)^2 + \Delta H_3 q_{s,3} b_3 (1 + b_1 f + b_2 f)^2}{q_{s,1} b_1 (1 + b_2 f + b_3 f)^2 + q_{s,2} b_2 (1 + b_1 f + b_3 f)^2 + q_{s,3} b_3 (1 + b_1 f + b_2 f)^2}$$

Eq. 53

3.2.4 Thermo-kinetic equations of gas adsorption

The thermo-kinetic model can be developed on mass and energy equations based on a volumetric system [154], as discussed in paragraph 3.2.1. In this paragraph the equation discussion was carried out considering adsorption steps, where gas is loaded in the dosing volume and expanded into the uptake volume. However, equations are consistent also in the desorption step. Therefore, the model is always valid during adsorption/desorption measures.

A known gas amount is initially loaded into the dosing volume. At time $t = 0$ the valve, that separates the two volumes, is opened. The gas flow rate through the valve is a linear function of the pressure difference (difference between dosing (P_D) and uptake pressures (P_U)) (Eq. 54). χ is the kinetic constant of the valve which indicates the dependence of the gas flow rate through the valve ($\frac{dn}{dt}$) on the pressure difference ($P_D - P_U$).

Gas concentration within the dosing volume gradually decreases (Eq. 55), while the pressure in the uptake volume increases with time (Eq. 56). The higher quantity adsorbed corresponds to the equilibrium conditions of the process [130]. The amount of gas that expands in the uptake volume is partially adsorbed ($V_S \frac{d\bar{q}}{dt}$), following its adsorption isotherm, and in part is expanded in the free uptake volume (ϵV_U).

According to these considerations, it is possible to write the mass balance equations written below (Eq. 54 - Eq. 59).

Valve	mass	$\frac{dn}{dt} = \chi(P_D - P_U)$	Eq. 54
balance			

Dosing balance	mass	$V_D \frac{dc_D}{dt} = -\frac{dn}{dt}$	Eq. 55
Uptake balance	mass	$\varepsilon V_U \frac{dc_D}{dt} + V_S \frac{d\bar{q}}{dt} = \frac{dn}{dt}$	Eq. 56

c_D and c_U are the dosing and uptake concentration, respectively. In this way it is possible to retrieve the total amount of gas adsorbed on the solid (\bar{q}) as a function of time. At equilibrium conditions, the gas adsorbed on the solid is equal to the adsorbed quantity calculated through adsorption isotherm (q^*). The film theory is based on the linear driving force hypothesis, i.e. a linear dependence of dq/dt on the difference between the amount of gas adsorbed at equilibrium (q^*) and gas adsorbed punctually (\bar{q}) at different time (Eq. 57). For porous matrices the linear model (or film model) does not satisfactorily describes the variation of the adsorbed concentration of gas on solid. In this case two models can be used instead, depending on the limiting diffusive regime: micropore diffusion control (Eq. 58) and macropore diffusion control (Eq. 59).

The limiting diffusion stage can be determined by comparing the time diffusion in micropores and in macropores.

Generally, the diffusion in macropores is 2-4 orders of magnitude higher than that of micropores. However, the characteristic length, which for spherical geometries is the radius, is at least three orders of magnitude greater for macropores than for micropores. From this it can be deduced that, in many adsorbent materials, the limiting diffusive regime is the diffusion in macropores (Eq. 59).

Within this work, the diffusion model based on the macro-diffusion control was used. The model assumes the macropore diffusion control and the instantaneous adsorption in micropores. The whole gas that diffuses from the external surface of the sample inwards

$(\varepsilon_p D_p \left(\frac{\partial^2 c}{\partial r_p^2} + \frac{2}{r_p} \frac{\partial c}{\partial r_p} \right))$, occupies the volume of the macropores $(\varepsilon_p \frac{dc}{dt})$ and adsorbs instantly on the crystals $((1 - \varepsilon_p) \frac{d\bar{q}}{dt})$.

Linear driving force (LDF) –	$V_p \frac{d\bar{q}}{dt} = K_{LFD} A_S (q^* - \bar{q})$	Eq. 57
------------------------------	---	--------

Micropore diffusion control	$\frac{d\bar{q}}{dt} = \frac{1}{r^2} \frac{\partial}{\partial r} \left(r^2 D_c \frac{\partial \bar{q}}{\partial r} \right)$	Eq. 58
-----------------------------	--	--------

Macropore diffusion control	$(1 - \varepsilon_p) \frac{d\bar{q}}{dt} + \varepsilon_p \frac{dc}{dt} = \varepsilon_p D_p \left(\frac{\partial^2 c}{\partial r_p^2} + \frac{2}{r_p} \frac{\partial c}{\partial r_p} \right)$	Eq. 59
-----------------------------	--	--------

$\frac{\frac{R_{macropore}^2}{D_{macropore}}}{\frac{R_{micropore}^2}{D_{micropore}}} = \frac{t_{macropore}}{t_{micropore}} \gg 1$	Eq. 60
---	--------

The isosteric heat of adsorption, the Joule-Thomson phenomenon for the expansion/compression of the gas and the consequent thermal exchanges require also the introduction of the energy balance (Eq. 61 - Eq. 68) along with the mass balance equations. For example, the gas that expands in the dosing volume (Eq. 61) causes a reduction in temperature linked to the Joule-Thomson effect, contained within the variation of real enthalpy (h_{out}) and, a consequent exchange with the external environment ($h_w^T A_w (T_{w,D} - T_D)$). More complicated, however, is the description of the phenomena taking place in the uptake volume. To better identify the thermal phenomenon, the energy balance is studied by dividing the contribution of the empty volume (Eq. 62) and the adsorbent solid (Eq. 63). The pressure inside the uptake volume increases resulting in higher temperatures due to the gas compression. The consequent

heat exchange takes place between the compressed gas and the metal beads but also with the uptake walls and the sample. The sample, on the other hand, increases its temperatures due to both adsorption and the heat exchange with the gas. The thermal capacities of inert solids such as stainless steel beads (Eq. 64), dosing (Eq. 65) and uptake volume (Eq. 66) have been included in the energy balance. In order to study in depth the adsorption phase it was necessary to take into account, also, the response time of the thermocouples (Eq. 67 and Eq. 68).

Dosing energy balance	$V_D \frac{du_D}{dt} = -\frac{dn}{dt} h_{out} + h_w^T A_w (T_{w,D} - T_D)$	Eq. 61
Uptake energy balance	$\varepsilon V_U \frac{du_D}{dt} = \frac{dn}{dt} h_{in} + h_w^T A_w (T_{w,U} - T_U) + h_{f-s}^T A_s (T_s - T_U) + h_{f-b}^T A_b (T_b - T_U)$	Eq. 62
Solid energy balance	$c_s V_s \frac{dT_s}{dt} = V_s \frac{d[\bar{q}(-\Delta H_{ads})]}{dt} + h_{f-s}^T A_s (T_U - T_s)$	Eq. 63
Stainless Steel beads	$c_b V_b \frac{dT_b}{dt} = h_{f-b}^T A_b (T_U - T_b)$	Eq. 64
Dosing solid volume	$c_s V_D^{Solid} \frac{dT_D^{Solid}}{dt} = h_D^T A_D (T_{amb} - T_D^{Solid})$	Eq. 65
Uptake solid volume	$c_s V_U^{Solid} \frac{dT_U^{Solid}}{dt} = h_U^T A_U (T_{bath} - T_U^{Solid})$	Eq. 66

Thermocouple in the Dosing Volume	$\frac{c_{TC}V_{TC}}{h_f^T A_{TC}} \frac{dT_{TC}}{dt} = (T_D - T_{TC})$	Eq. 67
---	---	--------

Thermocouple in the uptake Volume	$\frac{c_{TC}V_{TC}}{h_f^T A_{TC}} \frac{dT_{TC}}{dt} = (T_U - T_{TC})$	Eq. 68
---	---	--------

3.3 Results and discussion

3.3.1 Gases behaviour

As previously discussed, the EoS parameters (Table 6) were obtained through fitting the data present in the NIST webbook [175].

In particular, the analysis was carried out by fitting 100 points in a wide range of operating conditions: temperatures from 0 °C to 100 °C and pressure from 0.1 bar to 30 bar. In this way, the co-volume b and the energy parameter $\varepsilon(T)$ (Eq. 33) were obtained at $T=0$ °C in the pressure range of 0-30 bar. The subsequent fitting, at 30 bar and temperature range of 0-100 °C, obtained ε_0 and ε_1 (in according to functionality between $\varepsilon(T)$ and T) as reported in Eq. 33. The fitting was carried out on gas density evaluation.

Table 6 - EoS co-volumes and energy parameters for each gases

Species	$b, \text{m}^3 \text{mol}^{-1}$	$\varepsilon(T) = \varepsilon_0 + \varepsilon_1 (T - T_0)$	
		$\varepsilon_0, \text{J mol}^{-1}$	$\varepsilon_1, \text{J mol}^{-1} \text{K}^{-1}$
He	$1.21 \cdot 10^{-5}$	100	1.57
Ar	$2.17 \cdot 10^{-5}$	$4.51 \cdot 10^3$	-8.85
H ₂	$2.26 \cdot 10^{-5}$	901.36	1.02
N ₂	$2.57 \cdot 10^{-5}$	$3.18 \cdot 10^3$	-8.87
O ₂	$2.34 \cdot 10^{-5}$	$4.43 \cdot 10^3$	-8.23
CO ₂	$3.47 \cdot 10^{-5}$	$1.23 \cdot 10^4$	-29.2
CH ₄	$2.57 \cdot 10^{-5}$	$6.99 \cdot 10^3$	-14.24
CO	$2.32 \cdot 10^{-5}$	$3.66 \cdot 10^3$	-12.30

Different points were selected within the range of operating conditions studied, in order to verify the correct prediction of the model. Table 7 shows the comparison between the

thermodynamic properties of the gases with those estimated using the EoS. Deviations were calculated using Eq. 69

$$Deviation = \frac{NIST\ webbook - Simulated\ data}{NIST\ webbook}, \% \quad Eq. 69$$

Data fitting allowed to obtain very accurate EoS in terms of density prediction. Thermodynamic parameters calculated using the cubic EoS are extremely accurate for all the gases studied. The maximum calculated deviation is associated to the real enthalpies and internal energies, and it was generally less than 1%. CO₂, especially in conditions of low temperatures (0 °C) and high pressure (30 bar), shows the greatest errors (up to 6% for real internal energy). In this condition, CO₂ shows a behaviour very far from ideal gas state.

Table 7 – Deviation calculation between NIST data and cubic EoS

Reference thermodynamics properties	Deviation, %							
	He	Ar	H ₂	N ₂	O ₂	CO ₂	CH ₄	CO
Density	0.01	0.02	0.02	0.02	0.03	0.4	0.05	0.03
Ideal Enthalpy	0.02	0.02	0.02	0.02	0.02	0.02	0.2	0.02
Real Enthalpy	0.05	0.6	0.2	0.4	0.4	5	0.6	0.2
Real Internal Energy	0.05	0.8	0.3	0.45	0.5	6	0.8	0.4

In order to identify the correct prediction of thermodynamic properties by cubic EoS, a comparison was made between the adsorption isotherms present in the University of Edinburgh database. The CO₂ isotherm was studied on a polymer sample of 0.274 g (whose name and nature cannot be disclosed). Within this work, the polymer will be called Polymer A. The measurements were carried out at 20 °C in a pressure range of 0-

30 bar. Excess adsorption was reported because the vacuum degree of the polymer is unknown and the absolute adsorption is not an accessible parameter. Figure 20 shows excess adsorption (Eq. 31) as a function of the equilibrium pressure.

The deviation of the excess adsorption was reported as a function of the equilibrium pressure by using cubic and Wagner equations, as shown in Figure 20. In fact, the greatest deviation was found at pressures close to the highest range pressure (30 bar). Under these conditions, the maximum deviation between the excess adsorption calculated through the NIST data and that calculated through the EoS is about 0.4%, with a low overestimation calculated by using the cubic state equation.

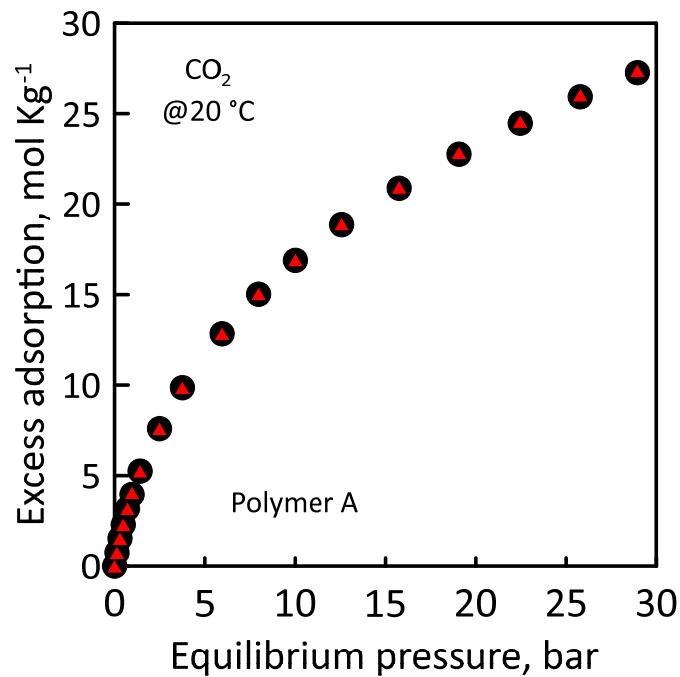


Figure 20 – CO₂ isotherm in terms of excess adsorption as a function of equilibrium pressure. Circle: excess adsorption obtained by cubic EoS data; Triangle: excess adsorption obtained by NIST webbook. Adsorption gas: CO₂; Sample: Polymer A; Temperature of 20 °C.

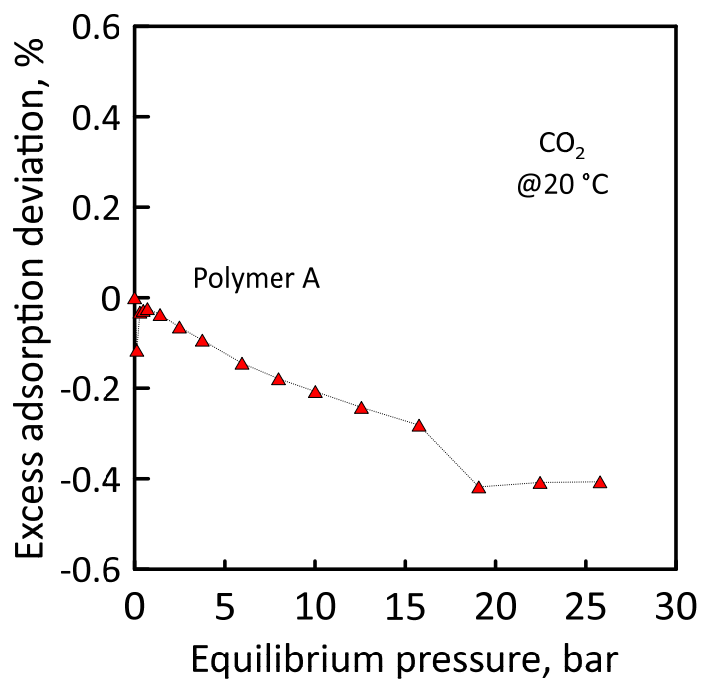


Figure 21 – CO₂ excess adsorption deviation as a function of equilibrium pressure. Adsorption gas: CO₂; Sample: Polymer A; Temperature of 20 °C.

3.3.2 Simulation analysis and experimental fitting

This section reports simulation and experimental measurements on diffusion of gases in a solid macroporous sample (zeolite 13X) during adsorption measurements. This investigation is intended as a preliminary analysis and further studies are required.

As reported in the mass and energy balance equation in Section 3.2.4 Thermo-kinetic equations of gas adsorption, the mathematical model takes into account several parameters, such as global heat exchange coefficient, thermocouples time delay and valve characteristic parameter which defines valve open velocity.

On a first approximation, all the parameters were evaluated using He expansions. In this way the mathematical model results simplified because He adsorption can be safely neglected. Figure 22 and Figure 23 show the dosing pressure decay as a function of the time during expansion measurements.

The measurements were carried out in series. At the beginning, the system was brought at very low pressure (0.13 Pa). Subsequently, the valve was closed between the dosing and uptake volumes (V02, Figure 18) and the He loaded into the dosing volume (the pressure increase up to 31.33 kPa). The valve was quickly opened to let the gas into the uptake volume (expansion). Dosing pressure was monitored and the valve characteristic was calculated (χ equal to $2.2 \cdot 10^{-8} \text{ mol Pa}^{-1} \text{ s}^{-1}$). The system reached the equilibrium pressure of 25.77 kPa (Figure 22). The same measurements of gas expansion and pressure dosing monitoring was carried out, as previously discussed. Initially, the valve between the volumes was closed (an initial uptake pressure of 25.77 kPa was used). Subsequently, the dosing volume was loaded up to 82.99 kPa. The valve was opened and the gas was allowed to expand. The resulting characteristic of the valve is $3.7 \cdot 10^{-8} \text{ mol Pa}^{-1} \text{ s}^{-1}$ (Figure 23).

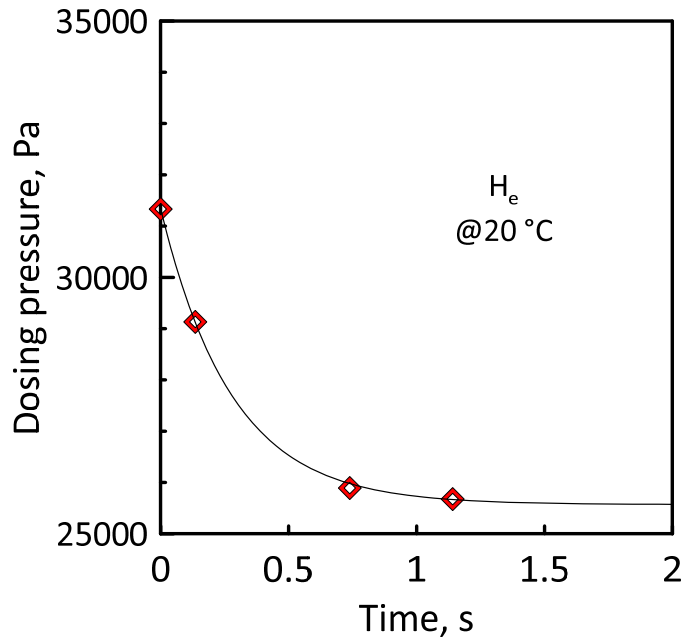


Figure 22 – Pressure decay as a function of time during open valve measurements. Gas: Helium; Diamond (red): experimental measurements; solid line (black): simulation dosing pressure. Temperature of 20 °C. Initial pressure of 31.33 kPa; Initial uptake pressure of 0.13 Pa. Valve constant χ : $2.2 \cdot 10^{-8} \text{ mol Pa}^{-1} \text{ s}^{-1}$.

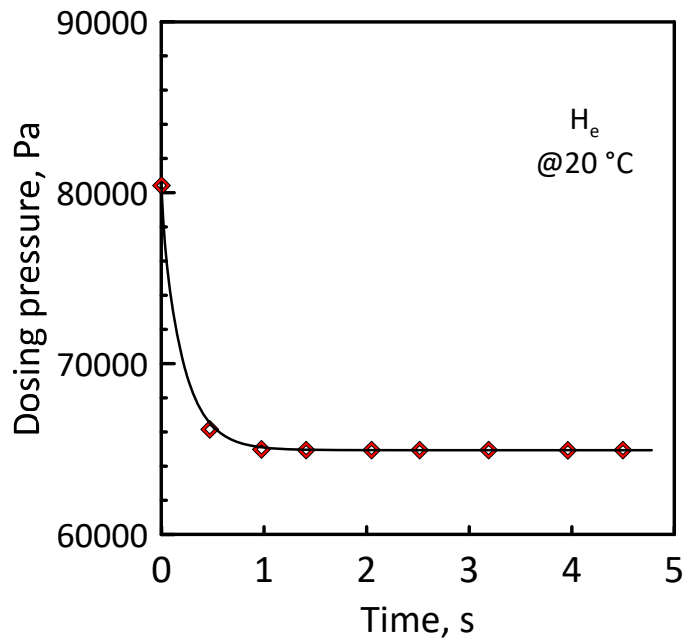


Figure 23 – Pressure decay as a function of time during open valve measurements. Gas: Helium; Diamond (red): experimental measurements; solid line (black): simulation dosing pressure.

Temperature of 20 °C. Initial dosing pressure of 80.4 kPa; Initial uptake pressure of 25.77 kPa. Valve constant χ : $4.7 \cdot 10^{-8} \text{ mol Pa}^{-1} \text{ s}^{-1}$.

Owing to the pressure difference between the measurements reported in Figure 22 and Figure 23 and the manual opening speed of the valve, the calculated valve constants are different. Therefore, in order to better interpret the valve behaviour, it is necessary to use automatic actuators that allow to uniform valve opening, in order to safely attribute the differences only to gas behaviour [176].

Gases conductivity, which is different between CO₂ and He such as viscosity, influence the heat coefficient calculation during fitting experimental data. In fact, CO₂ and He present different gas conductivity and viscosity, differently influencing the heat coefficient.

Valve constant and the energetic parameters were obtained by the same expansion measurements (CO₂ expansion measurements) and the pressure dosing trend can be obtained as shown in Figure 24.

The dual-site Langmuir isotherm (Eq. 46) was used to simulate the experimental behaviour (Table 8).

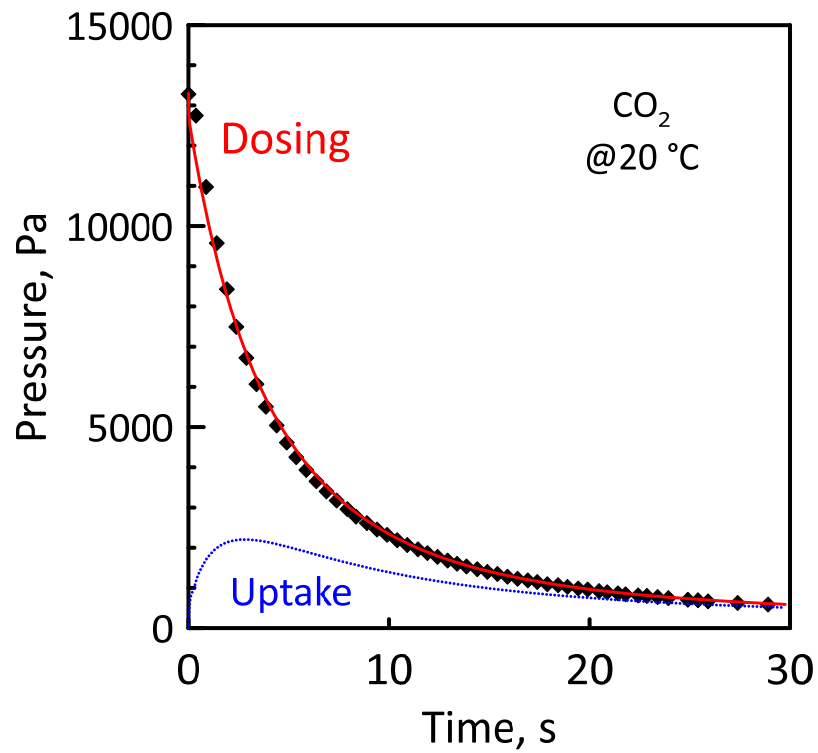


Figure 24 – Dosing and uptake pressure as a function of times. Gas: CO₂. Diamond: experimental measurements; solid line (red): simulation dosing pressure; dashed line (blue): simulation uptake pressure. Initial dosing pressure: $13.28 \cdot 10^3$ Pa; initial uptake pressure: 0.13 Pa. Temperature: 20 °C.

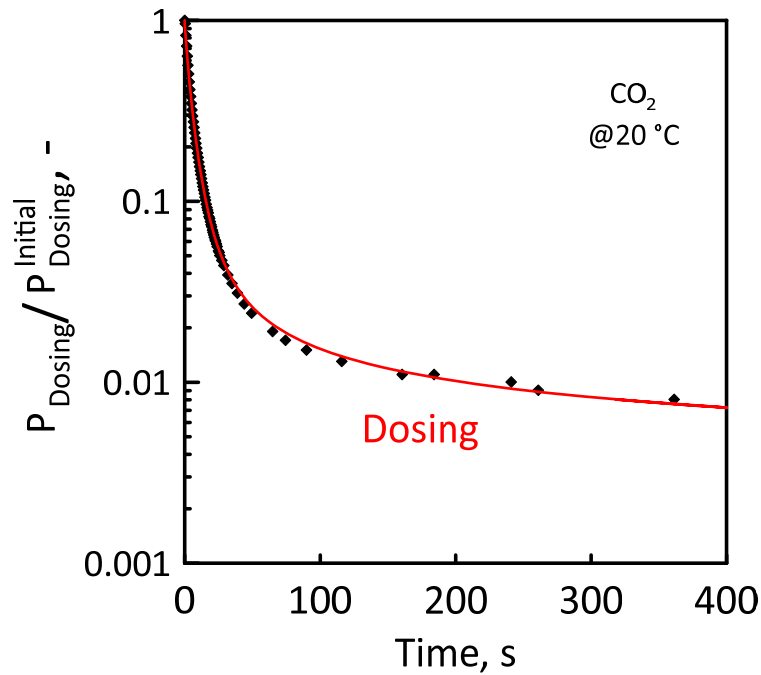


Figure 25 – Dosing pressure normalised as a function of times. Gas: CO₂. Diamond: experimental measurements; solid line (red): simulation dosing pressure. Initial dosing pressure: 13.28 10³ Pa; initial uptake pressure: 0.13 Pa. Temperature: 20 °C.

Figure 24 shows dosing and uptake pressure as a function of time (measurements and operating condition are reported in Table 9). The simulations satisfactorily describe the experimental data (the corresponding evaluated diffusivity is 4.5 10⁻⁶ m² s⁻¹). The uptake pressure simulation is also shown in Figure 22. The pressure dosing response is in agreement with the literature data [130]. In particular, the presence of a maximum in uptake pressure response suggests a high ratio between the characteristic time of valve opening and the diffusivity of the gas in the sample [130]. When the characteristic time of the valve approaches the characteristic mass transfer time, the system tends to equilibrium, therefore, no reliable kinetic measurements can be obtained. The best measurements conditions are reached when the valves can be modelled with a rump function. Here, the gas diffusion inside the pores is the only mass transfer phenomenon

shown. When the valve dynamics is slow, instead, the dosing pressure monitoring leads to wrong kinetic analysis because the mass transfer inside the sample is not the dominant mechanism [176].

Table 8 – Dual-site Langmuir isotherm parameters

$q_{s,1}$, mol kg ⁻¹	2.7976
$q_{s,2}$, mol kg ⁻¹	1.2374
b_1 , Pa ⁻¹	$1.95 \cdot 10^{-4}$
b_2 , Pa ⁻¹	$1.05 \cdot 10^{-2}$
$-\Delta H_1$, kJ mol ⁻¹	32.194
$-\Delta H_2$, kJ mol ⁻¹	33.055
Heat of adsorption, kJ mol ⁻¹	32.6

Table 9 - Operating condition and system geometry

Initial dosing pressure, Pa	$13.28 \cdot 10^3$
Initial uptake pressure, Pa	0.13
Initial dosing temperature, °C	20.5
Initial uptake temperature, °C	20

3.3 Conclusion

In this research activity, the preliminary analysis of kinetic diffusivity measurements in the Sieverts apparatus was carried out. The work was developed in two phases. The first phase involved a thermodynamic analysis in order to identify cubic EoS, easily manipulated, that satisfactorily interpreted the behaviour of the gases studied. Cubic equations have been obtained by using the Redlich-Kwong model which allows a good thermodynamic interpretation of gas parameters in the range of pressure and temperature studied. Thanks to the comparison with the data reported in the literature (NIST webbook [175]), the EoS is reliable to determine the behaviour of gases through its thermodynamic properties. During the second phase, the analysis was carried out on kinetic adsorption measurements. The model used allows a good experimental data fitting. In this second case, further investigation is required in order to improve the parameters evaluation and, consequently, simulations accuracy.

4. Membrane Permeation Performance for mixture gas separation

In this chapter the membrane gas separation performances were studied by using experimental measurements by means of pressure drop and concentration gradient, as discussed in the paragraph “2.2 Membrane separation performance measurements method”. Transport phenomena and membrane behaviour at different operating conditions were analysed. Two different membranes were studied: 1) polyimide dense membrane (MATRIMID) and 2) PIM-based membrane. In the first case, the CO₂ permeance through MATRIMID membrane was studied in a large temperature range, i.e. from -25 °C to 150 °C. In the second case, Single gas and flue gas separation measures were carried out to evaluate the performance of PIM-based membrane gas separation.

At the highest temperature of 150 °C, polymer chain rearrangement occurs and the CO₂ permeance reduces up to 35%, at temperature higher than 70°C.

PIM membranes have two main disadvantages: high selectivity reduction owing to plasticization phenomena [177] and fast reduction of selectivity and permeation properties due to quick aging. Particular attention was focused on three different membranes PIM-PI-1, PIM-PI-r-6FDA-Durene=1:6 and PIM-PI-r-PIM-PEG=4:1, which showed CO₂ permeance of 75.1, 68.4 and 20.3 dm³(STP) m⁻² h⁻¹ bar⁻¹, respectively. These membranes were tested after thermal treatment at 40°C for 3 hours, in order to remove traces of residual solvent. The experiments demonstrated good separating performances of CO₂ from other gases such as N₂ and O₂ (e.g., CO₂/N₂ selectivities of PIM-PI-1 and PIM-PI-r-PIM-PEG=4:1 were 16.3 and 15.6, respectively) and no dependence of

transport properties from the operating pressure. These results indicate that PIM-based membranes have great potential in separation of CO₂ from a flue stream in a large range of operating conditions.

4.1. CO₂ permeance in Matrimid membrane: Activation energy calculation.

Matrimid®5218 is currently one of the most studied types of polyimide, materials particularly applied for hydrogen [178,179,180,181,182] and CO₂/CH₄ separation [183,184,185].

The Matrimid®5218 hollow fibre membranes here investigated were prepared into the ITM-CNR laboratory as reported in Falbo et al. [186]. The hollow fibre preparation method is briefly reported below.

Hollow fibre membranes were prepared via the dry-wet spinning technique through the phase inversion process. The polymer solution (dope), prepared by adding the polymer to the solvent under mechanical stirring at 50 °C, was then stored in a thermostatic vessel for the entire spinning run. Before starting, the polymer solution was degassed under vacuum. In fact, the presence of air inside the polymer solution can cause defects in the dense separating layer. At the end of the spinning test, carried out at room temperature, the continuous bundle of the spun fibres was cut in pieces of ca. 30 cm and kept in distilled water for at least 24 hours in order to remove residual solvent [186]. The fibres were then dried at room temperature for 48 hours.

4.1.2 Results and discussion

Figure 26 shows the CO₂ permeance as a function of temperature. Experimental measures were carried out in three steps: during the first one (see Figure 26, circles) CO₂ permeance was analysed at temperature ranging between 65°C and 150 °C. Thereafter, in the second step (see Figure 26, diamonds), CO₂ permeance was studied from cryogenic to room temperatures. Finally, CO₂ permeation measures were carried out at the same temperature range of the first step (Figure 26, squares). The comparison between the first and the third measure sets allows to evaluate the effect of the temperature on the membrane.

The first set of measurements evidences that the permeance of CO₂ linearly increases with the inverse of the temperature, which is a typical Arrhenius behaviour. Subsequently the module was cooled to room temperature and then cooled down to -20 ° C (second set of measures) in order to estimate the permeance trend at cryogenic temperatures. Also in this case, in the range between -20 and 24 ° C, the permeance of CO₂ shows a typical Arrhenius behaviour, i.e. linear with the inverse of the temperature. Finally, the system was heated to room temperature and the permeation measurement was repeated. The same permeance obtained at 25 °C before and after the cryogenic measurements confirming the reproducibility of the measurements at 24 °C.

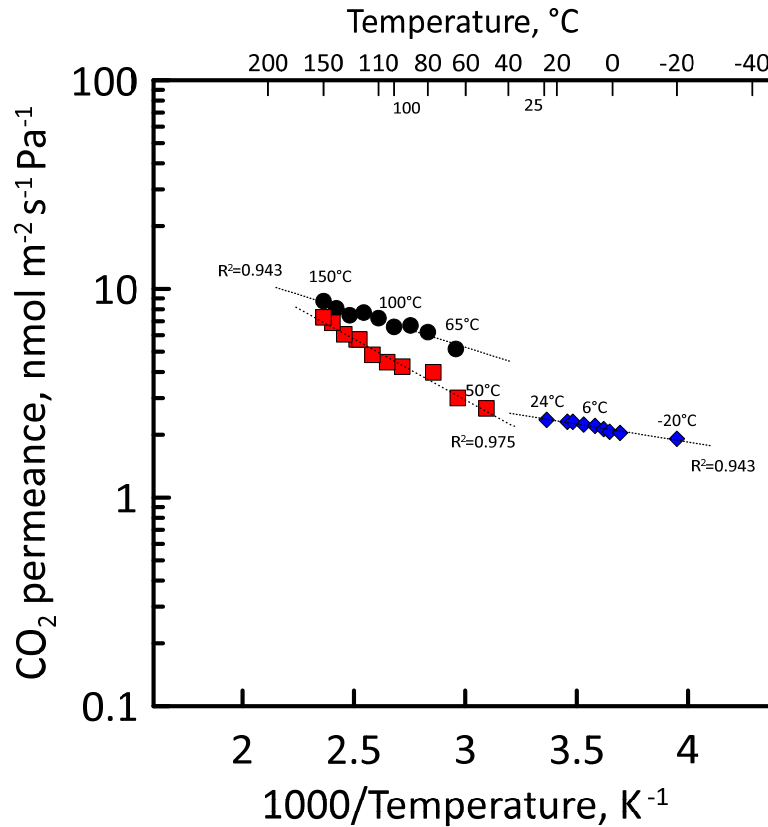


Figure 26 – CO₂ permeance as a function of temperature.

A new measures set was carried out at higher temperatures up to 150°C ((Figure 26, squares). In this case a reduction in permeance compared to the first set of measurements. In particular, for temperatures above 80 °C, the permeance decreases of about 35%.

Ansaloni et al. [187] have shown how a thermal pre-treatment of Matrimid membranes (at temperature close to 150 °C) causes a change in the transport properties of the material. In particular, it is highlighted how the temperature induces a rearrangement of the polymer chains, which causes both an increase in the rigidity of the chains themselves and a reorganization, with consequent reduction of the free volume. The study of Ansaloni et al. [187] suggests that the permeation measurements carried out at 150 °C could have

had a "heat treatment" effect on the Matrimid fibres which caused the reduction of the CO₂ permeance.

The second set of measures also highlights a change in the slope of the functionality of the CO₂ permeance with the inverse of the temperature in a range between 60 and 80 °C. A probable explanation can be inferred from the work of Comer et al. [188], who investigated the dynamic relaxation characteristics of Matrimid. Three transition temperatures that influence the mobility of the polymer chains were shown [188]: one related to the glassy-rubbery transition (α transition, 313 °C) of the polymer and two to "sub-glass" transitions (β transition, 80 °C; γ transition, -110 °C). Therefore, the change in the permeance slope observed in Figure 26 at temperatures close to 80 °C could be due to β transition of the polymer.

Table 10 reports the permeance parameters for each set of measures. The evaluation of the parameters was carried out by fitting the experimental data with Eq. 70.

$$Permeance = Permeance_0 \exp\left(-\frac{E_P}{RT}\right), mol\ m^{-2}s^{-1}Pa^{-1} \quad \text{Eq. 70}$$

where $Permeance_0$ is the pre-exponential factor ($mol\ m^{-2}s^{-1}Pa^{-1}$), E_P is the activation energy of permeation ($J\ mol^{-1}$), T is the temperature (K) and R is the ideal gas constant ($8.314\ kJ\ mol^{-1}\cdot K^{-1}$). E_P for the transport of CO₂ through membrane were determined from the slopes ($-E_P/R$) of the best curve-fits through the permeation data in Figure 26.

Table 10 – Pre-exponential factor and activation energy of permeation.

Set of measures	$E_p, kJ/mol$	$Permeance_0,$ $nmol m^{-2} s^{-1} Pa^{-1}$	R^2
First (from 65°C to 150°C)	+6.4	53.8	0.943
Second (from 25°C to -20°C)	+3.3	9	0.943
Third (from 50°C to 150°C)	+11.1	166	0.975

The activation energy of permeation can be represented as the sum of the activation energies of diffusion and sorption. The activation energy of diffusion is positive, which means the diffusivity increases with the temperature. Instead, the sorption enthalpy is negative, as expected since the sorption is an exothermic process [189]. In each case the activation energy of permeation is positive, which means that the energy of diffusion is greater than the enthalpy of sorption.

Owing to the first set of measures and, consequently, polymer chain rearrangement due to high temperature treatment, permeance parameters change drastically from the first to the third set of measures. The activation energy of permeation increase from 6.4 to 11.1 kJ/mol (+72.9) in the same temperature range. Owing to polymer chain rearrangement, the contribution of CO₂ diffusion increases with respect to contribution of CO₂ solubility.

4.2. PIM-based membrane gas separation measures

Thanks to the high interconnected free volumes which allow to define PIMs as microporous materials, according to IUPAC classification (pore size < 2 nm) [190], polymers with intrinsic microporosity (PIMs) have attracted much interest as novel materials for membrane-based gas separation. The rather unique macromolecular structure of PIMs results in remarkable gas-separation behaviour as separation technology, exceeding Robeson's upper bounds [191,192].

As reported previously, the most important problems regarding to PIMs are due to plasticization and aging phenomena. Highly sorbing gases, such as CO₂, can induce plasticization, leading to a large increase of the gas permeability with increasing pressure and, consequently, selectivity reduction during separation in gas mixtures. As reported in Section 1.1.1, the plasticization of the polymer matrix by penetrant gases can be attributed to the swelling stresses on the polymer network. Carbon dioxide absorption in glassy polymers is known to facilitate local segmental organization with a reduction in permselectivity [192,193]. Therefore, plasticization is a phenomenon widely occurring in polymer systems for CO₂ separation where membranes are exposed to a high concentration of CO₂ in the feed stream. One of the most popular way to improve the performance of a polymer is by blending it with another polymer to combine the best properties of the two individual materials [194]. Also in the PIMs synthesis, it is one of the most important way to improve the PIM properties.

In an effort to combine the high free volume of amorphous PIMs with the excellent chemo-physical properties of PIs, a series of polyimides was designed [195,196,197].

The transport properties of PIMs obtained by random copolymerisation synthesis with polyimides are reported in this chapter. The main aim is to obtain polymeric membranes

that exhibit slow aging and good separative performances at higher pressure. High pressure permeability measures (close to 10 bar) with single and mixture gases were carried out.

The membranes were synthesized in the “Synthesis of Organic Materials” laboratories of the University of Incheon, South Korea [198]. Permeability measures were carried out on membrane disks possessing the geometric characteristics listed in Table 11.

Membranes were characterized by pressure drop and concentration gradient method (both methods were widely discussed in paragraph 2.2 Membrane separation performance measurements method).

Table 11 – Membranes size

Membrane	Area, cm ²	Thickness, μm
PIM-PI-1	3.8	40
PIM-PI-r-6FDA-Durene=1:6	3.8	30
PIM-PI-r-PIM-PEG=4:1	3.8	33

Table 12 - Operating condition

Temperature, °C	25
Feed pressure, bar	3 – 9.4
Permeate pressure, bar	1 bar
Feed stream mixture composition, %	CO ₂ :N ₂ :O ₂ =15:80:5

Table 12 reports the operating conditions used for the permeability measurements. In particular, pressure drop method was used to evaluate the permeance of single gases. Thanks to the evaluation of the thickness of the membranes, the permeability of the

membrane was calculated. The results were compared with literature data using the Robeson diagram [199]. It is possible to compare membranes that have a high free volume, such as polynorbornenes, PTMSP and PIMs. Subsequently, the concentration gradient method was used in order to analyse the separative performances of the membranes on gas mixtures simulate flue gas mixture, as reported in Table 12.

The membranes were tested after thermal treatment at 40°C for 3 hours, in order to remove the residual synthesis solvent in the polymeric matrix.

4.2.2 Results and discussion

PIM-PI-1 permeability measurements were carried out in order to evaluate the effects of random copolymerization on the separative properties of the membranes based on PIM-PI. In fact, the permeance measurements were compared with the PIM-PI-r-6FDA-Durene = 1: 6 and PIM-PI-r-PIM-PEG = 4:1 property.

Gases permeance and, consequently, selectivities were determined thanks to permeability measurements reported in Table 13. As discussed before, single gas and mixture gases measures were carried out. CO₂/N₂ selectivity reduces from 22.5 (ideal selectivity calculated by CO₂ and N₂ permeability ratio evaluated during single gas measurements) to 16, obtained by gases mixture separation measurements.

Membrane permeability was calculated by membrane thickness evaluation, using micrometre. PIM-PI-1 membranes showed a good CO₂ permeability of 30 GPU and 28.1 GPU for single gases and mixtures, respectively. Single gas measurements, using PIM-PI-r-6FDA-Durene=1:6 membranes, were carried out in the pressure range 3-8.3 bar. No dependence of permeance with the feed pressure was observed neither with CO₂ nor with

N₂ and O₂, as confirmed in Figure 28 where the permeating flux of each gas is fully linear with the relative permeating driving force.

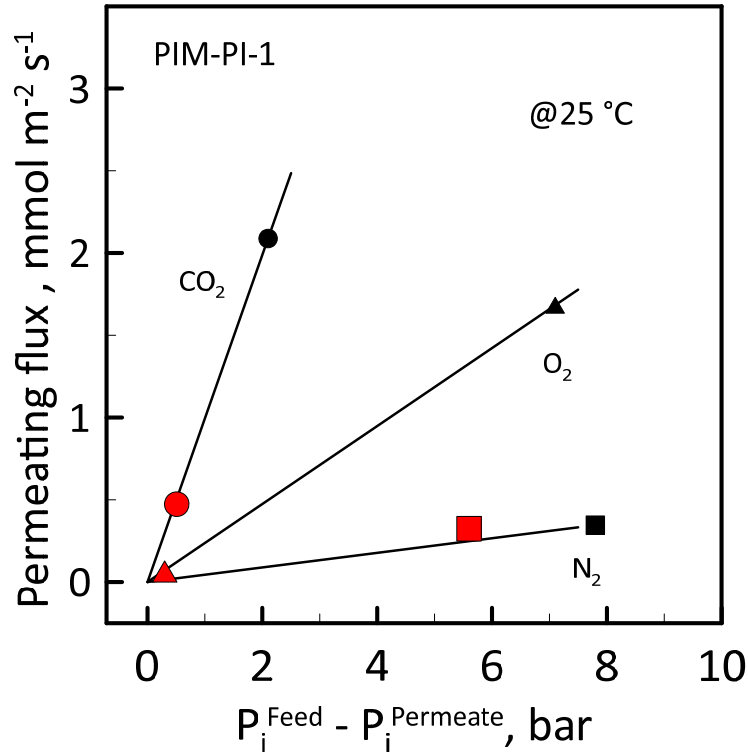


Figure 27 – Permeating flux of *i*-species as a function of correspondent partial pressure difference. Circle: CO₂; triangle: O₂; square: N₂. Single gas (black), Mixed gas (red).

Mixed gas experiments carried out at a feed pressure of 9.3 bar, showed no significant differences in the permeance values measured for CO₂, N₂ and O₂ if compared with single gas. Permeability measurements showed no change in the CO₂ permeance between single gas and mixture. In particular, the permeance of CO₂ is 22.8 and 22.3 GPU for single gas and mixture measurements, respectively. The permeability of N₂, on the other hand, decreases from 1.8 to 1.4 GPU in single gas and mixture gas separation measurements. Thanks to this reduction, CO₂/N₂ selectivity is greater during the separation

measurements of mixtures compared to the individual gases (selectivity increases from 13.5 to 16.1, Table 13)

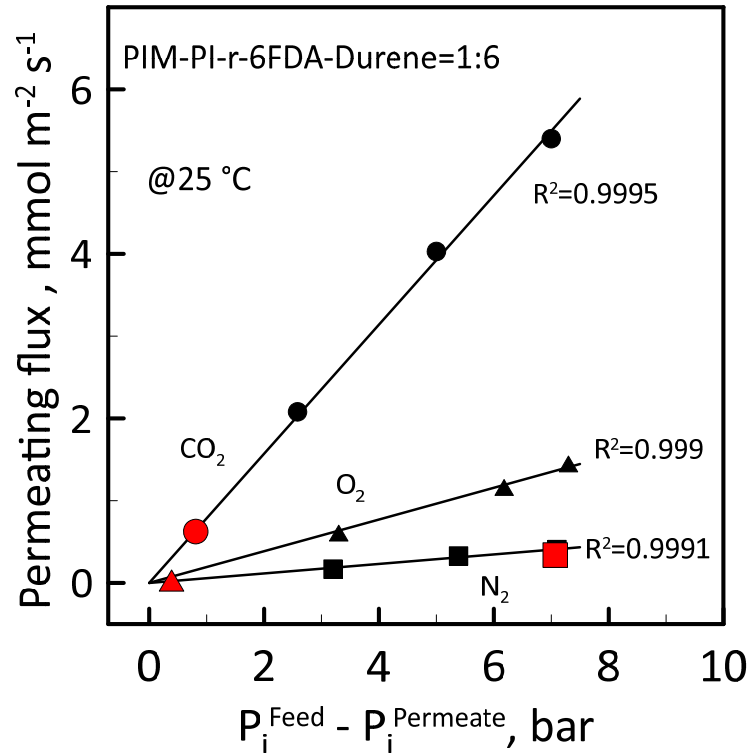


Figure 28 – Permeating flux of *i*-species as a function of correspondent partial pressure difference. Circle: CO₂; triangle: O₂; square: N₂. Single gas (black), Mixed gas (red).

In the case of the PIM-PI-r-PIM-PEG=4:1, single gas measurements were carried out in the pressure range 3-8.1 bar. Nor with CO₂ nor with N₂ and O₂ a dependence of permeance with feed pressure was observed, as confirmed in Figure 29 where the permeating flux of each gas is fully linear with the relative permeating driving force. Mixed gas experiments carried out at a feed pressure of 9.4 bar, showed no significant differences in the permeance values measured for CO₂, N₂ and O₂ if compared with single gas. Selectivity in mixture was a bit greater than ideal one with a CO₂/N₂ value of 17 (Table 13). Similarly, to the results obtained for the PIM-PI-r-6FDA-Durene membrane

= 1: 6, also for the PIM-PI-r-PIM-PEG = 4: 1 membrane, the CO₂/N₂ selectivity increase in mixture due to permeance reduction. In this case, the change in permeance, which causes an increase in CO₂/N₂ selectivity from 17 to 18.

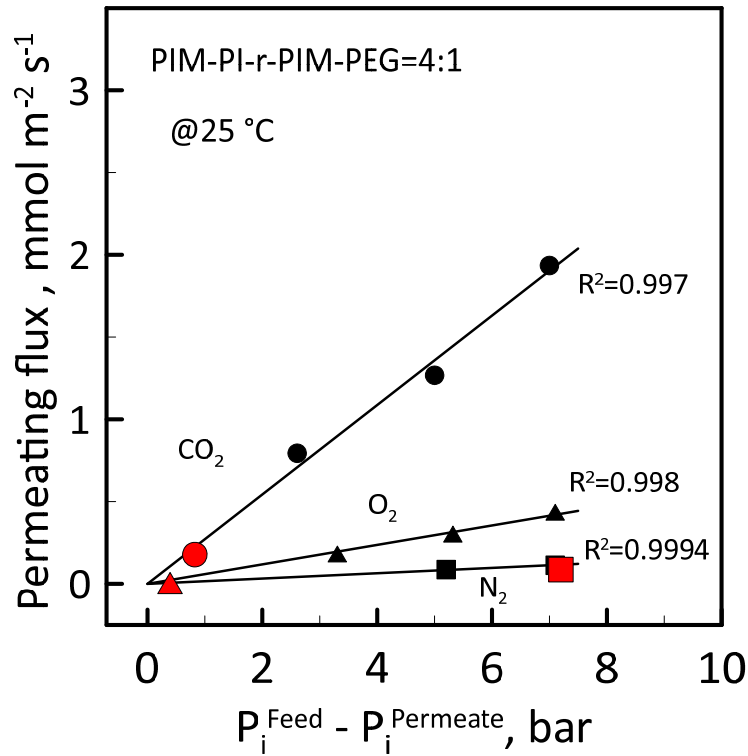


Figure 29 – Permeating flux of i-species as a function of correspondent partial pressure difference. Circle: CO₂; triangle: O₂; square: N₂. Single gas (black), Mixed gas (red).

Figure 30 shows the CO₂/N₂ selectivity as a function of the CO₂ permeability of the membranes studied and the Robeson upper bound [199].

Permeability measures results were compared with literature data, in particular, of polymers with a high free volume. All literature data concerned glassy polymers [189,192,200,201,202,203,204,205,206,], except for the PDMS [202], which has been taken into account due to its importance in numerous industrial applications [6]. The PIM-PI-1 membrane shows separative properties, compared with the data present in the

literature [189]. The membrane obtained by random poly-condensation with 6FDA-Durene shows performances similar to 6FDA-Durene, due to the high 6FDA-Durene concentration. However, the presence of PIM-PI improves the CO₂ permeance with respect to the same CO₂/N₂ selectivity.

Table 13 - PIM-based membrane separative properties.

Membrane	Measures	CO ₂ Permeance, GPU	CO ₂ Permeability, Barrer	Selectivity, -	
				CO ₂ /N ₂	O ₂ /N ₂
PIM-PI-1	Single gas	30	1200	22.5	5.4
	Mixture gases	28.1	1122	16	3.7
PIM-PI-r-6FDA-Durene=1:6	Single gas	23.8	712.9	13.5	3.3
	Mixture gases	23.3	700.1	16.1	1.6
PIM-PI-r-PIM-PEG=4:1	Single gas	8.2	271.7	17	3.7
	Mixture gases	6.54	215.8	18	1.1

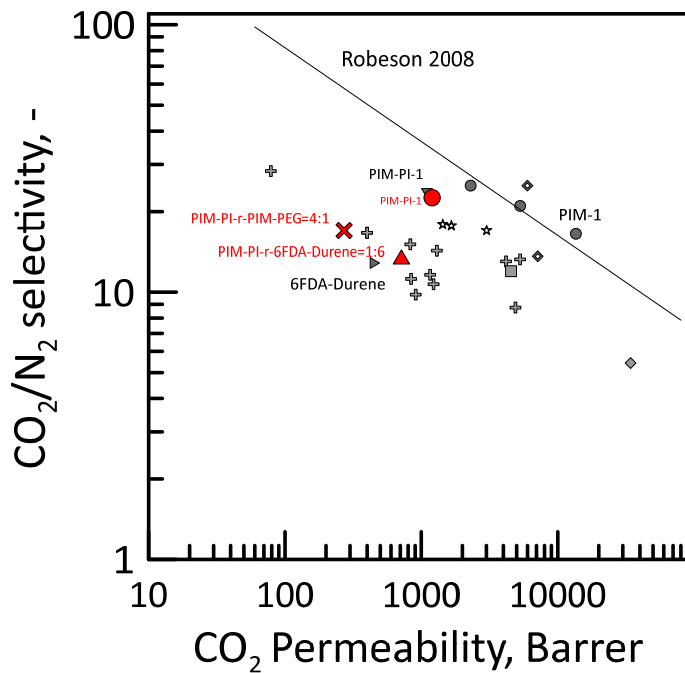


Figure 30 – Robeson diagram for CO₂/N₂ for high free volume polymers. The lines represent the 2008 upper bounds for each gas pair.

4.3. Conclusion

In conclusion, the experimental activities for the gaseous separation measurements showed a potentiality of the membranes studied for industrial applications. The Matrimid membranes presented a monotonous Arrhenius trend in the temperature ranges studied. Particular interesting is the good thermal resistance at high temperatures (150 °C). Permeance fitting as a function of temperature allowed to highlight a logarithmic linearity with an average square deviation of 0.975 (slightest variation in linearity is attributable to experimental errors). The good membrane operability at different temperatures allows to use them in different industrial fields, such as in combustion systems for the production of electricity which contain a high CO₂ concentration. These are cooled inside cooling columns through mixing with air at room temperature. This is necessary because

temperature and CO₂ concentration have to decrease before atmospheric emission. The possibility of operating at a temperature of 150 ° C suggests that the membrane can be applied in the system area where the streams to be treated has a much higher concentration of CO₂ (improving the driving force of the separation).

PIM-based membranes have shown significant separative advantages. In particular, the membranes obtained by random copolymerization have shown an increase in selectivity due to a tendency of reduction in permeability during the separation of gas mixtures. The membranes showed a linear behaviour at different pressures, not showing plasticization phenomenon induced by the presence of CO₂ in the operating conditions studied. All the membranes have good separative performances, even if all positioned under the Robeson upper bound, and the copolymerization allowed to reach new separative properties depending on the properties of the initial polymers used (such as PIM-PI and 6FDA-Durene). The results show a high potential of this new type of PIM-based polymers and, in particular, indicate that our PIM-PI random copolymer membranes have remarkable potential to be used for CO₂ gas separation.

5. Wet CO₂-mixture analysis for CO₂/CH₄ separation

Bio-methane production from biogas upgrading is becoming more and more an attractive route for alternative energy sources utilization. Bio-gas is mainly constituted by methane in a concentration variable from 55% to 70% and carbon dioxide, whose concentration ranges between 30% and 45% [207]. Often, other species such as H₂S, N₂, O₂, H₂, halides, siloxanes are present in low concentration or in traces [207]. The separation of bio-methane leads to an increase of the calorific value and to a reduction of the corrosion phenomena induced by acidic species (e.g. CO₂ and H₂S). Absorption, adsorption and cryogenic techniques are technologies usually used in the treatment of natural gas or biogas but they suffer of various drawbacks such as, high energy intensity, large equipment, use of organic solvent and adsorber, and complex control auxiliary systems [208]. Moreover, in most of the cases they produce low pressure CH₄ streams, which then need re-compression. The intrinsic advantages of membrane technologies, as discussed previously in the Introduction chapter, incentivized their installation in different plants for bio-methane production [209, 210]. Sahota et al. [209] showed the advantages of biogas upgrading solutions for small upgrading plants (less than 100 Nm³/h), where membrane integrated systems are particularly efficient and the main assets of membrane technology (modularity, low plant size, etc.) become more and more important. Cellulose acetate, polyimides and perfluoro polymers [208], currently used for natural gas separation are today used as membranes for biogas processing. As widely reported in literature [211, 212, 213, 214], the presence of water vapour in the gaseous stream strongly influences the performance of polymeric membranes affecting both permeability and selectivity. Falbo et al. [186] studied the effect of humidity using Matrimid hollow

fibre membranes for CO₂/N₂ and CO₂/CH₄ gas mixtures separation, observing a reduction of CO₂/N₂ and CO₂/CH₄ selectivity in wet condition with respect to dry condition. Polysulfone and polyimide fibre membranes performance was studied by the central waste water treatment plant in Prague, where biogas is produced by anaerobic fermentation of sewage sludge [215]. Real biogas that contained 70–100 mg m⁻³ of H₂S with a relative humidity of 40–50% was used in the experimental measures.

In this chapter, the water vapour effect on the membrane gas separation performance in CO₂/CH₄ mixture was studied. Analysis was carried out at different CO₂/CH₄ selectivities (from 25 to 100), pressure ratio and flow rate/membrane area ratio and performance maps were opportunely developed. The presence of water vapour reduced the CO₂/CH₄ selectivities up to 28%, due to competitive sorption between CO₂ and water vapour, and this influences the separation stage design. Moreover, the CH₄ retentate recovery, which in dry conditions was 85.3% (CO₂/CH₄ selectivities of 25), was reduced to 80.9% (CO₂/CH₄ selectivities of 18) in wet conditions, with a loss of 4.4%, at the methane concentration stream of 90%.

The simulation model developed by Brunetti et al. [27], widely discussed in paragraph 2.3, was here used for investigating the performance of a single stage membrane for separating a saturated biogas stream. We studied the performance of a Matrimid 5218 hollow fibre membrane module fed by mixed-gas (CO₂:CH₄= 40:60) in both dry and humidified conditions, at different pressure ratio. Specifically, we focused on the effect of humidity in terms of recovery and purity of CH₄ and CO₂ and on membrane area.

The mass transport properties used for simulations are based on Matrimid 5218 membranes studied by Falbo et al. [186], measured in mixed gas conditions (Table 14).

In the case of saturated mixed gas conditions, they observed that the membrane module used for experimental measurements shows a loss of selectivity with respect to measures carried out in dry condition. Table 2 summarizes the operating conditions used for simulations in this thesis.

Table 14. Membrane properties of Matrimid® 5218 hollow fibres considered in the simulations [186]

Feed composition	CH ₄ Permeance, dm ³ (STP) m ⁻² h ⁻¹ bar ⁻¹	CO ₂ /CH ₄ Selectivity, -
CH ₄ :CO ₂ =60:40	~2	25
CH ₄ :CO ₂ =60:40 at RH=100%	1.4	18

Table 15 - Operating condition

Temperature, °C	25
Feed/permeate pressure ratio, -	10 - 20
Feed stream composition, %	CH ₄ :CO ₂ =60:40 (dry and RH=100%)

The results presented in this chapter have been published in (see reference [216]):

Melone L., Giorno L., Brunetti A., Barbieri G. "Analysis of membrane unit performance in presence of wet CO₂-containing mixtures"; Chem. Eng. Res. Des., 2020, 153, 721–727; DOI: 10.1016/j.cherd.2019.11.034

5.1. Results and Discussion

Figure 31 shows CH₄ concentration in the retentate as a function of recovery in dry (red line) and wet (blue line) conditions. Falbo et al. [186], as before mentioned, showed the CO₂/CH₄ selectivity from 25 to 18 (CO₂/CH₄ selectivity reduction of 28%) due to presence of water vapour with respect to dry conditions. CH₄ concentration in the retentate side in wet conditions is lower than in dry ones, but this reduction did not significantly affects the curves (Figure 31) which resulted very close to each other.

A CH₄ concentration of 90% in dry condition corresponds to CH₄ recovery of 85.3% (point A in Figure 31). Owing to humidity the CH₄ recovery reduces to 80.9 (Point B) at the same CH₄ concentration of 90%. For the same recovery, methane retentate concentration reduces from 90% (dry condition) to 87.5% (wet condition) (Point C).

Higher CO₂/CH₄ selectivity of 50 and 100 were considered for the new polymeric membranes discussed in the introduction chapter which showed separation performance higher [217,218] than Matrimid5218 membranes [186]. In all cases, CO₂/CH₄ selectivity reduction of 28% from dry to wet condition was used. Analogous trends could be observed for CO₂/CH₄ selectivity of 25 at CO₂/CH₄ selectivity of 50 and 100 (Figure 32 and Figure 33, respectively).

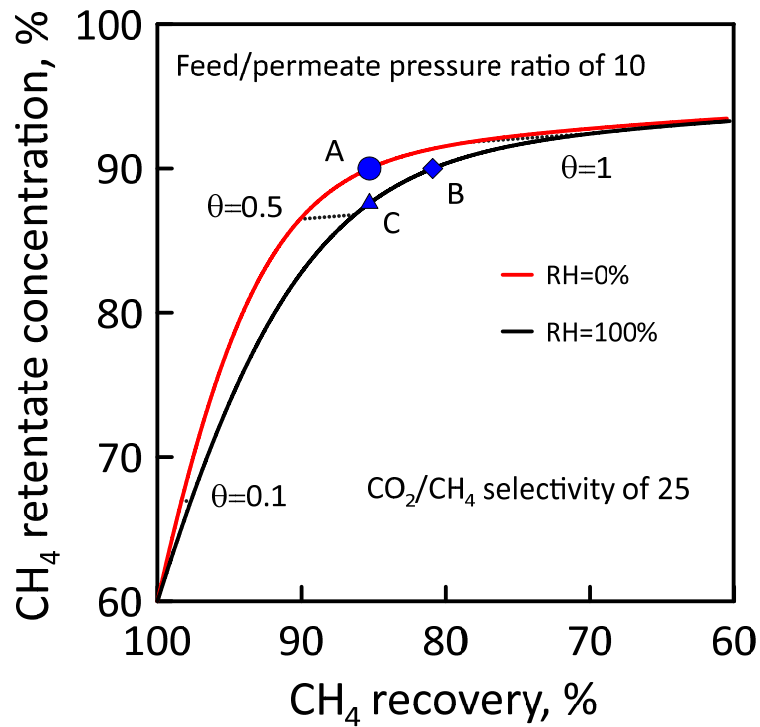


Figure 31 – CH₄ retentate molar concentration as a function of recovery in dry (red line) and wet (black line) condition. Pressure ratio of 10. CO₂/CH₄ selectivity of 25. Dashed line: permeation number. Symbol: circle (A), CH₄ retentate molar concentration of 90% at RH=0%; diamond (B), CH₄ retentate molar concentration of 90% at RH=100%; triangle (C), CH₄ retentate molar concentration of 87.5% at RH=100%.

CO₂/CH₄ selectivity reduction occurs from 50 (in dry condition) to 36 (in wet condition), (Figure 32), and from 100 (in dry condition) to 72 (in wet condition), as shown in Figure 33. Figure 32 and Figure 33 show the same target of methane concentration of 90% (Point A' and A'', respectively), as assumed in Figure 31.

Point A' (Figure 32) corresponds to CH₄ recovery in dry condition of 91.6%, against 89% (Point B') obtained in wet conditions. For the same recovery, methane retentate concentration reduces from 90% (dry condition) to 88% (wet condition) (Point C').

At the same target of CH₄ concentration of 90%, a methane recovery of 95.2% (Point A''), Figure 33) is reached in dry conditions, while methane recovery of 93.7% (Point B'') was obtained in wet conditions for CO₂/CH₄ selectivity of 100.

For the same recovery, methane retentate concentration reduces from 90% (dry condition) to 88.5% (wet condition) (Point C'').

The main result, obtained thanks to the simulations carried out at CO₂/CH₄ selectivity of 25, 50 and 100, is the humidity effect, which is less evident as much higher CO₂/CH₄ selectivities.

In particular, humidity reduced methane recovery of 4.4% with respect to dry conditions for CO₂/CH₄ selectivity of 25. At higher selectivities, methane recovery decreases progressively of 2.6% at CO₂/CH₄ selectivity of 50 and of 1.5% at CO₂/CH₄ selectivity of 100.

Water vapour effect is more evident on the permeate where the CO₂ rich stream is recovered, with respect to CH₄ concentration profile discussed before. The CO₂/CH₄ selectivity reduction affects the CO₂ permeate concentration significantly (Figure 34). Scholes et al [219] discussed the water effect in the polymeric matrix. The CO₂ permeability in wet condition is lower because of the very high solubility and fill capacity of the microvoids. By considering the CO₂ concentration correspondent to that of CH₄ equal to 90% in the retentate side (Point A), CO₂ permeate concentration reduces from 79.5% to 75.1% in the presence of water. In terms of separation, the CO₂ rich stream characteristics are equally important with respect to CH₄ rich stream to define if a downstream treatment is necessary to fit the targets of storage.

A low CH₄ permeate concentration allows CO₂ storage, otherwise other separation stages are required.

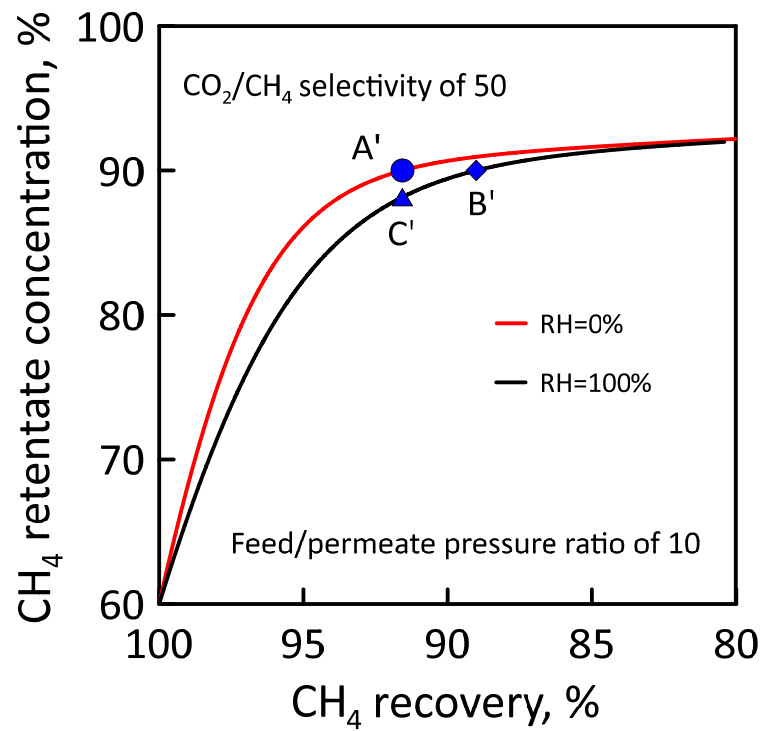


Figure 32 – CH₄ retentate molar concentration as a function of recovery in dry (red line) and wet (black line) condition. Pressure ratio of 10. CO₂/CH₄ selectivity of 50. Symbol: circle (A'), CH₄ retentate molar concentration of 90% at RH=0%; diamond (B'), CH₄ retentate molar concentration of 90% at RH=100%; triangle (C), CH₄ retentate molar concentration of 88.2% at RH=100%.

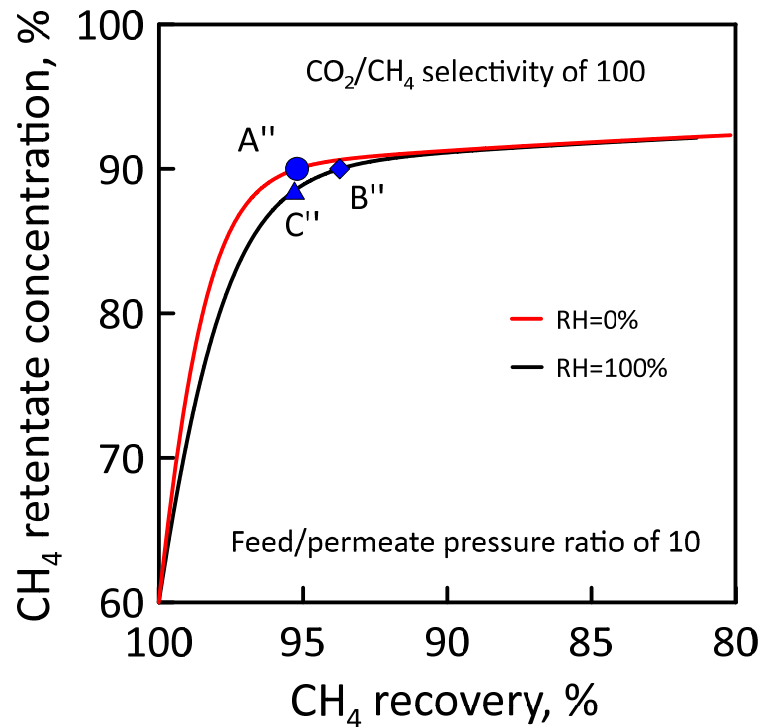


Figure 33 – CH₄ retentate molar concentration as a function of recovery in dry (red line) and wet (black line) condition. Pressure ratio of 10. CO₂/CH₄ selectivity of 100. Symbol: circle (A''), CH₄ retentate molar concentration of 90% at RH=0%; diamond (B''), CH₄ retentate molar concentration of 90% at RH=100%; triangle (C), CH₄ retentate molar concentration of 88.5% at RH=100%.

Table 16 reports the maximum CO₂ permeate concentration attainable at different CO₂/CH₄ selectivities for wet and dry stream.

Corresponding to Point A (CO₂/CH₄ selectivity of 25 and CH₄ concentration of 90%), CO₂ permeate concentration reduces from 92.7% in dry conditions to 90.2% at relative humidity (RH) of 100%. For the same recovery, methane retentate concentration reduces from 90% (dry condition) to 87.5% (wet condition) (Point C). When increasing the CO₂/CH₄ selectivity to 50 and 100, the maximum achievable CO₂ permeate concentration increases up to 96.2% (dry), 98.1% (dry), 94.8% (wet) and 97.3% (wet) in wet condition,

respectively (Table 16). As reported, humidity effect on separation performance is lower at higher selectivity.

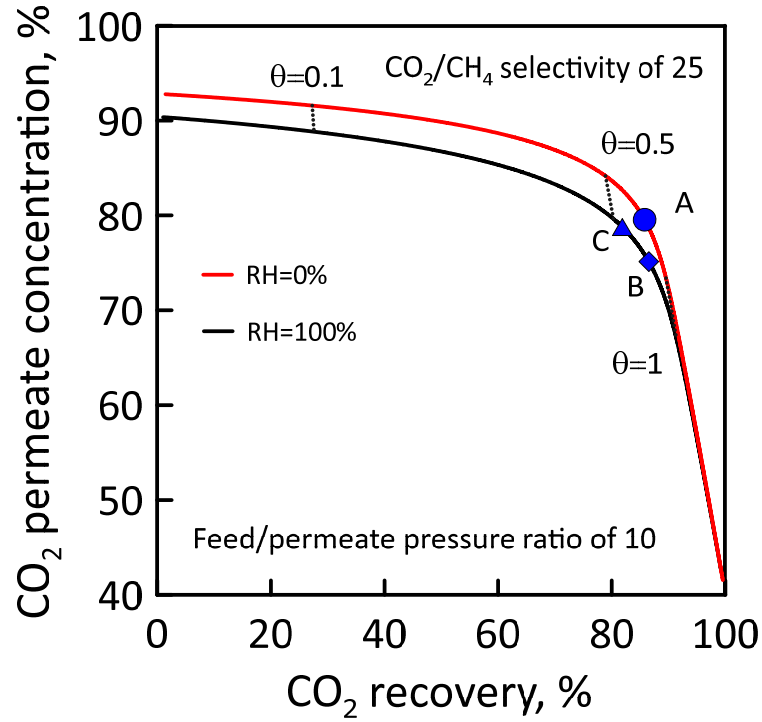


Figure 34 – CO₂ permeate molar concentration as a function of recovery in dry (red line) and wet (black line) condition. Pressure ratio of 10. CO₂/CH₄ selectivity of 25. Dashed line: permeation number. Symbol: circle (A), CH₄ retentate molar concentration of 90% at RH=0%; diamond (B), CH₄ retentate molar concentration of 90% at RH=100%; triangle (C), CH₄ retentate molar concentration of 87.5% at RH=100%.

Table 16 - Maximum CO₂ permeate concentration when CO₂ recovery close to 0% at different CO₂/CH₄ selectivity and humidity concentration in feed stream.

CO ₂ /CH ₄ selectivity, -	Maximum CO ₂ permeate concentration (@RH=0%), %	Maximum CO ₂ permeate concentration (@RH=100%), %	CO ₂ concentration difference, %
25	92.7	90.2	2.5
50	96.2	94.8	1.4
100	98.1	97.3	0.8

5.1.1. Effect of humidity at different pressure ratios

In industrial applications the separation pressure ratio is tuned and it is chosen as a function of economic evaluations and of the operating conditions available. In integrated membrane processes, feed and permeate pressure can be tied to upstream and downstream operations with respect to membrane separation system. In this case, the pressure ratio is bounded to upstream and downstream operating conditions. In this section, the effect of humidity at different pressure ratios was studied.

Figure 35 shows CH₄ retentate concentration as a function of CH₄ recovery in dry (red line) and wet (blue line) conditions, at a pressure ratio of 10 (solid line) and 20 (dashed line). At low CH₄ recovery the membrane selectivity does not affect the membrane module performance, and the permeate purity is controlled only by the pressure ratio. At a higher-pressure ratio, the absolute value of the limit slope is higher.

Table 17 reports CH₄ recovery in dry and wet conditions at CH₄ retentate concentration of 90% (Point A, Figure 35). At higher-pressure ratios, the separation is less affected by

humidity; in fact, CH₄ recovery variation at pressure ratio of 20 is 3.4%, which is lower than 4.4% obtained at a pressure ratio of 10.

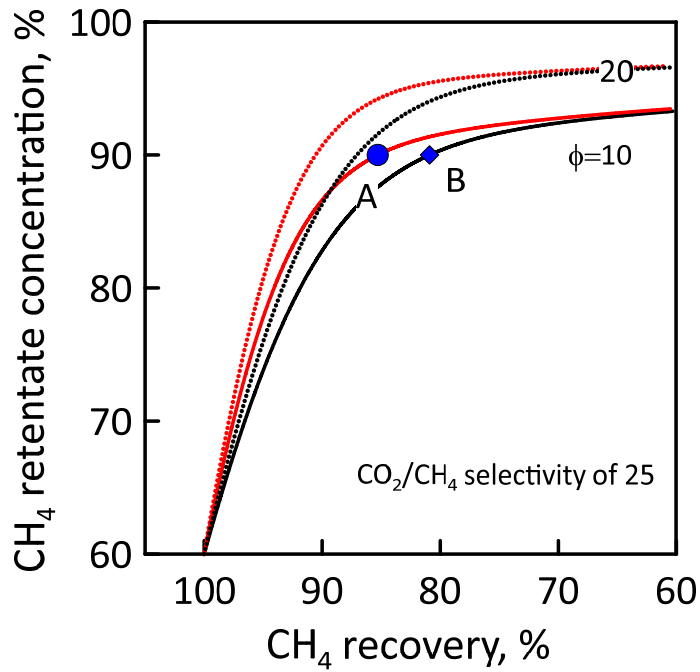


Figure 35 – CH₄ retentate concentration as a function of CH₄ recovery in dry (red line) and wet (black line) condition. CO₂/CH₄ selectivity of 25. Pressure ratio of 10 (solid line) and 20 (dashed line). Symbol: circle (A), CH₄ retentate molar concentration of 90% at RH=0%; diamond (B), CH₄ retentate molar concentration of 90% at RH=100%.

Table 17 – CH₄ recovery at CH₄ retentate concentration of 90% at different pressure ratio and humidity concentration in feed stream.

Pressure ratio, -	CH ₄ recovery (dry), %	CH ₄ recovery (@RH=100%), %	CH ₄ recovery difference, %
10	85.3	80.9	4.4
20	90.5	87.1	3.4

5.1.2. Effect of humidity on membrane area

Figure 36 shows CH₄ (a) and CO₂ (b) retentate concentration (solid line) and recovery (dashed line) as a function of feed flow rate/membrane area ratio. Design of the membrane modules in terms of membrane area must be opportunely modulated by considering CO₂/CH₄ selectivity reduction due to water presence in the feed stream, in order to obtain certain targets of recovery and purity.

Simulations were carried out at pressure ratio of 10 and CO₂/CH₄ selectivity of 25. At a given feed flow rate, all of the curves are shifted towards higher CH₄ retentate concentration and lower CH₄ recovery (Figure 36a) for higher membrane areas. At the same feed flow rate/membrane area ratio in dry conditions, the higher CH₄ amount remaining in retentate side induces a lower CH₄ recovery than in wet. CO₂ permeate concentration in dry condition is higher than in wet condition at higher feed flow rate/membrane area ratio. At a higher membrane area, CO₂ permeate concentration drastically decreases due to methane permeation through the membrane. In wet condition this behaviour is lower because CO₂ permeation driving forces are higher at the same feed flow rate/membrane area ratio (Figure 37). For this reason, at a low feed flow rate/membrane area ratio (lower than 0.133 dm³ s⁻¹ m⁻²) CO₂ permeate concentration in dry condition is lower than in wet.

Figure 37 shows CO₂ partial pressure (left) as a function of feed flow rate/membrane area ratio. CO₂ retentate partial pressure variation between dry and wet condition is more evident in retentate side. As discussed before, due to the reduction of CO₂/CH₄ selectivity in wet condition with respect to dry, the CO₂ average concentration in wet condition along the membrane module is higher than in dry. As a consequence, the CO₂ driving force is higher (Figure 37, right).

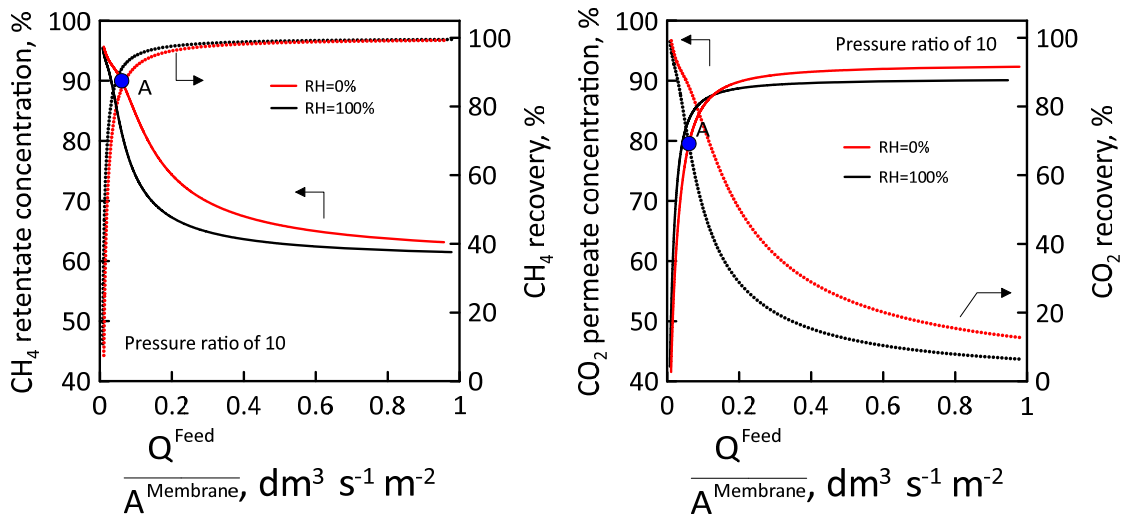


Figure 36 - CH_4 (left) and CO_2 (right) concentration (solid line) and recovery (dashed line) as a function of feed flow rate/membrane area ratio. Pressure ratio of 10. CO_2/CH_4 selectivity of 25.

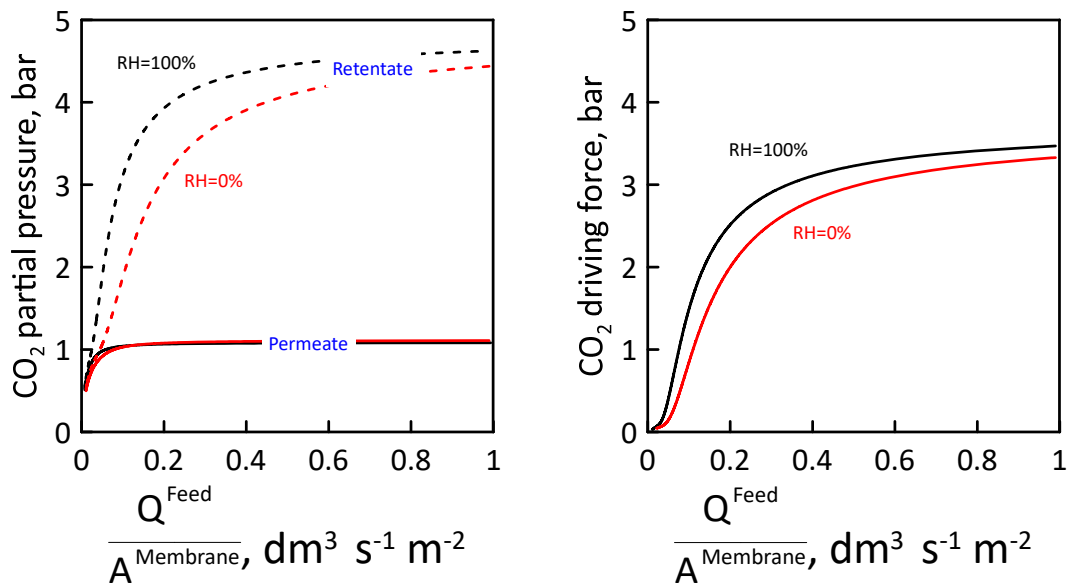


Figure 37 – CO_2 partial pressure (left) and CO_2 driving force (right) as a function of feed flow rate/membrane area ratio.

Figure 38 shows CH₄ retentate concentration (left) and CH₄ recovery (right) as a function of feed flow rate/membrane area ratio at different pressure ratio of 10 and 20. At higher pressure ratio, the humidity effect is more evident. In terms of concentration and recovery profiles, the driving force amplifies the effect of selectivity. At higher pressure ratios, the permeation driving force is higher and the humidity effect is more important.

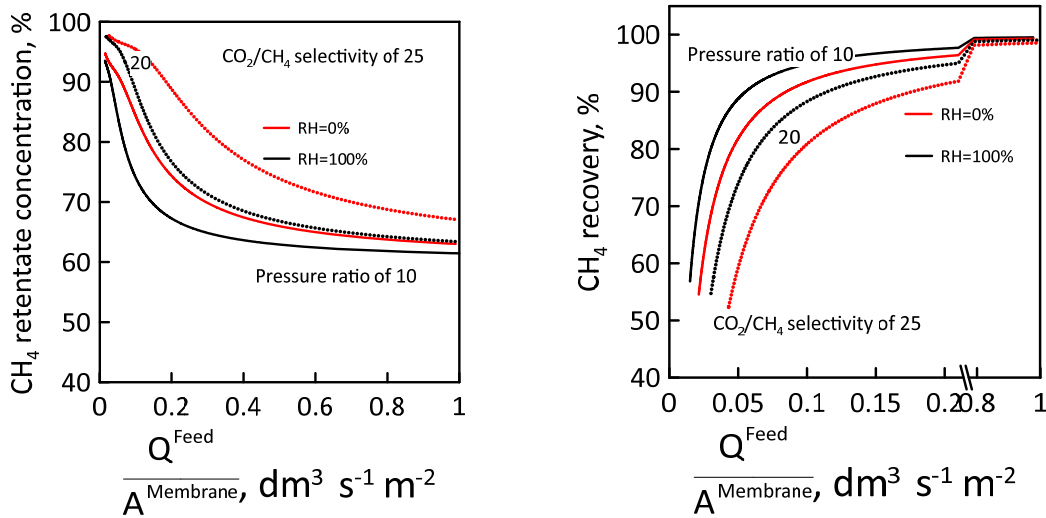


Figure 38 - CH₄ retentate concentration (left) and CH₄ recovery (right) as a function of feed flow rate/membrane area ratio. Pressure ratio of 10 (solid line) and 20 (dashed line). CO₂/CH₄ selectivity of 25.

5.2. Conclusion

The separation performance of a membrane unit for CH₄ enrichment in CO₂/CH₄ separation, by considering a feed stream composition of CO₂:CH₄= 40:60 in dry and humidified conditions, was analysed. The presence of water vapour in the gas mixture significantly changed the performance of the membrane unit, especially in terms of CO₂/CH₄ selectivity reduction (about 28%). A methane concentration target of 90% was used and, as a consequence, CH₄ retentate recovery of 85.3% obtained in dry condition

was reduced to 80.9% in wet, with a loss of 4.4%. At the same CH₄ retentate concentration, a CH₄ recovery difference of 3.4% at a pressure ratio equal to 10 was obtained, against a reduction of 4.4% at pressure ratio of 20.

Results show that higher membrane selectivity performances (in terms of higher CO₂/CH₄ selectivity) and lower pressure ratios allow to reduce the humidity effect on the membrane separation.

For industrial applications higher selectivity allows to work at lower pressure ratio and, consequently, to reduce the recovery loss between dry and wet condition.

6. Membrane Integrated Process for Trichloroethylene Mixture Separation

Removal of volatile organic compounds (VOCs) from industrial streams is an important challenge. Trichloroethylene, as toluene, methylene chloride, phenol and etc., are considered potential pollutants [220,221]. Trichloroethylene is used predominantly in chemical industry as a solvent for cleaning, metal degreasing, and various other activities and it represents an important source of air pollution, due to its volatility[220]. Membrane systems have become one of the most promising innovative technologies for VOCs abatement with respect to conventional ones as activated carbon adsorption or chemical oxidation [220,221,222,223].

Today, membrane technology has an important focus in chemical and petrochemical industry for VOCs concentration and recovery [6]. Particular attention is focused on rubbery polymers, such as PDMS, widely used for its selectivity to VOCs with respect to water and air [224,225].

In this chapter, the treatment of trichloroethylene/ N_2 mixture streams is considered. This mixture is usually present in the off-gases of vulcanization accelerating agent synthesis. Yeom et al. [224] investigated $C_2H_3Cl_3$ /Nitrogen separation with PDMS membranes. The main results obtained in this work is based on the VOCs effect in blocking nitrogen permeation. In other words, higher $C_2H_3Cl_3/N_2$ selectivity can be obtained at higher $C_2H_3Cl_3$ feed concentration.

The integrated membrane process for the treatment of C_2HCl_3 mixtures was compared to traditional gas treatments. Three case studies are considered: membrane integrated process (case study 1), high pressure-heat condenser (case study 2) and cryogenic

condenser (case study 3). Up to now, cryogenic treatment is the Best Available Technology (B.A.T.) used in VOCs treatment. However, new gas treatment solutions are highly desirable due to the high energy demand and the cost of liquid nitrogen. The simulations carried out focused to increase C_2HCl_3 recovery and reduce C_2HCl_3 concentration in the stream discharged into atmosphere.

Process intensification metrics were used to compare separation and energetic performances. In the last decades, efforts have been made for defining indicators to measure the industrial process sustainability in terms of environment, economy and society impact [226,227,228,229]. Drioli et al. [230] investigated the process intensification impact of membrane technologies in desalination. The authors used the metrics for the monitoring of the progress and improvement of membrane operations by taking into account plant size, weight, flexibility, modularity, etc.

In this work, a similar approach as the one developed by Drioli et al. [230] was followed in the trichloroethylene/nitrogen mixture gas separation. Mass and energy intensity, for system performance in various case studies are investigated and used for comparing the different technologies.

Table 18 summarizes the membrane properties considered for the simulations, while the operating conditions are listed in Table 19.

The mass transport properties used for simulations are those provided for PDMS membranes as reported by Yeom et al. [224]. On the basis of literature data, in most of cases, PDMS membranes show olefins/paraffins selectivity equal to 1-2 [231]. Therefore, here it was assumed that C_2HCl_3 has the same behaviour of $C_2H_3Cl_3$. As shown by Yeom et al. [224] and as mentioned before, VOCs are more permeable than N_2 and their

recovery occurs in the permeate side. In their work a range of VOCs/N₂ selectivity from 70 to 500 was reported.

Table 20 reports the heuristics parameters assumed for other devices simulation which have a compressor adiabatic efficiency of 75%. On the basis of literature data [232], we assumed a maximum stream temperature exiting from vacuum pump close to 70 °C and a vacuum pump energy requirement of 2 kW for a stream of 100 m³/h at 40 mbar. The pressure drop in the polymeric membrane module on feed/retentate side was assumed being negligible [231,233, 234].

Table 18 – Membrane properties [224]

C ₂ HCl ₃ permeability,	18.9
C ₂ HCl ₃ Permeance, $\mu\text{mol m}^{-2} \text{s}^{-1} \text{Pa}^{-1}$	38
C ₂ HCl ₃ /N ₂ Selectivity, -	100 - 500

Table 19 – Operating condition of the feed stream

Temperature, °C	40
Pressure, bar	1.2
Mixture volumetric flow rate	100 Nm ³ /h (~4.46 kmol/h)
Feed stream composition, molar %	C ₂ HCl ₃ :N ₂ =10:90

As mentioned previously, energy intensity and mass intensity (discussed into 1.3 Process intensification paragraph) approaches were used.

Results show that the membrane integrated process is the best solution in terms of energy intensity (61.6 kJ mol⁻¹) with respect to high pressure condensation and cryogenic systems which showed energy intensity of 142.9 and 110.7 kJ mol⁻¹, respectively.

Table 20 – Heuristic assumption in device design

Compressor adiabatic efficiency, %	75
Heat exchange pressure drop, kPa	13.8
Activated carbon pressure drop, kPa	1.24
Membrane pressure drop along feed/retentate side, kPa	Negligible

The results presented in this chapter have been published in (see reference [235]):

Melone L., Brunetti A., Giorno L., Barone M., Barbieri G. "Trichloroethylene/Nitrogen Mixture Separation via membrane operations: comparison with traditional technologies"; Sep. Pur. Tech. 251 (2020) 117344.

6.1. Results and Discussion

For a single gas separation unit at fixed feed/permeate pressure ratio of 30, the trend of C_2HCl_3 concentration in the permeate was studied for several C_2HCl_3/N_2 selectivity ranging from 100 to 500, as shown in Figure 39.

In the permeate, ca.70% of C_2HCl_3 was recovered corresponding to a concentration of 89.3%, by assuming C_2HCl_3/N_2 selectivity of 400 [224]. At the same time, C_2HCl_3 concentration detected in the retentate was 3.25%, therefore, to reduce it below 1% a further separation stage is required (low C_2HCl_3 concentration ensures longer life of the activated carbon adsorber system). In order to study the separation performance at lower energy request, the same measurements were carried out at feed/permeate pressure ratio of 20. As shown in Figure 40, similar trends were obtained as in the case of pressure ratio

20. Generally, a lower pressure ratio corresponds to a lower separation performance [27], therefore, a pressure ratio of 20 was allowed both lower C_2HCl_3 recovery (at the same C_2HCl_3 feed concentration) and lower C_2HCl_3 permeate concentration (at the same C_2HCl_3 recovery).

Assuming a C_2HCl_3 recovery target equal to 70% (point A' - Figure 40), the C_2HCl_3 concentration was 65.75%, lower than the value obtained at a pressure ratio of 30 (point A- Figure 12 , 89.3%). Similarly, at a C_2HCl_3 concentration of 89.3% (pressure ratio of 30) also the C_2HCl_3 recovery decreased from 70% to 53.4% at a pressure ratio 20.

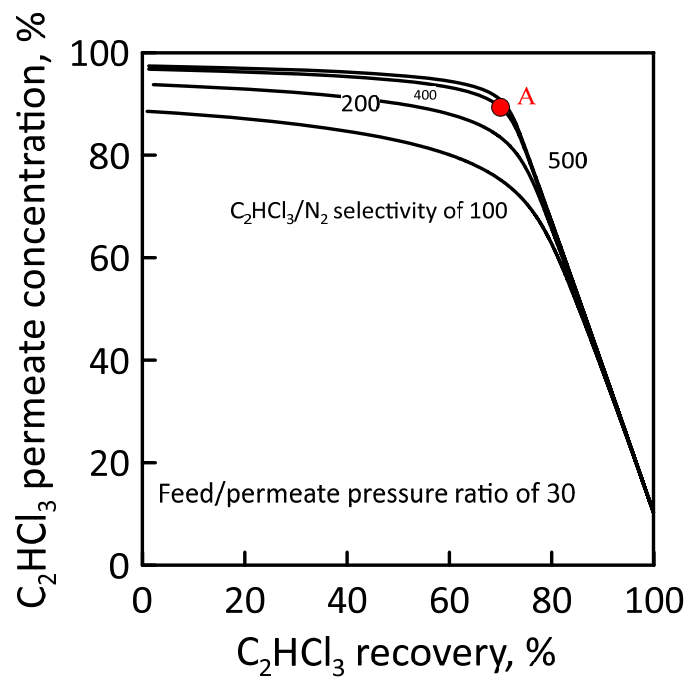


Figure 39 – C_2HCl_3 molar concentration as a function of recovery. $C_2HCl_3:N_2=10:90$. Feed/permeate pressure ratio of 30; C_2HCl_3/N_2 selectivity of 100, 200, 400 and 500; Point A: C_2HCl_3 recovery of 70%, pressure ratio of 30 and C_2HCl_3/N_2 selectivity of 400.

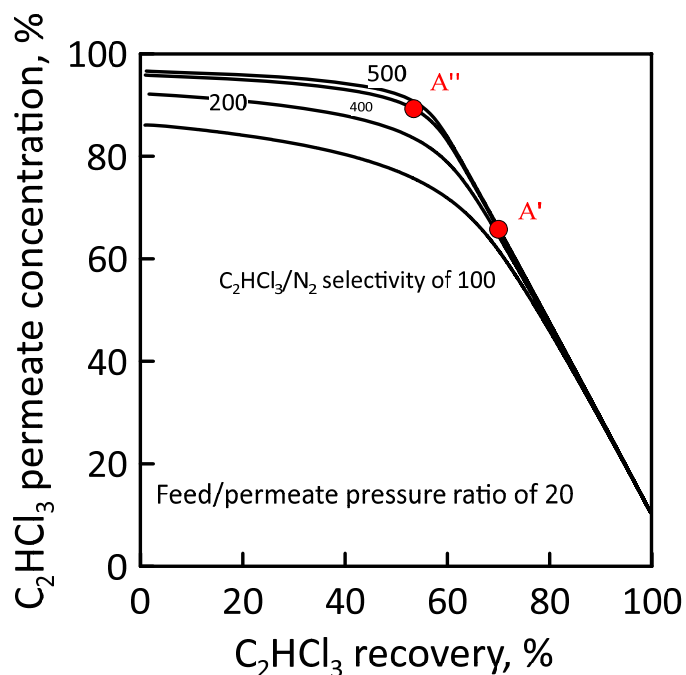


Figure 40 - C_2HCl_3 molar concentration as a function of recovery. $C_2HCl_3:N_2 = 10:90$. Feed/permeate pressure ratio of 20; C_2HCl_3/N_2 selectivity of 100, 200, 400 and 500. Point A': C_2HCl_3 molar concentration of 65.75% and C_2HCl_3 recovery of 70%. Point A'': C_2HCl_3 molar concentration of 89.3% and C_2HCl_3 recovery of 53.4%.

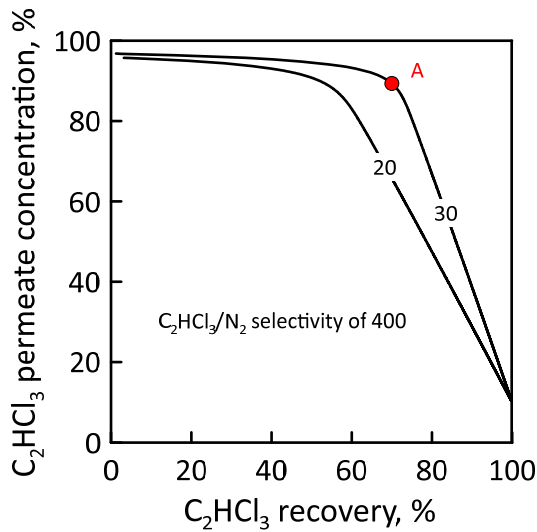
In order to examine the effect of the pressure ratio on the membrane performance, the C_2HCl_3 and N_2 molar concentration are reported as a function of recovery in Figure 41. Both pressure ratio values were selected by considering the lowest pressure that can be reached through the vacuum pump (40 mbar), corresponding to the pressure ratio of 30 at feed pressure of 1.2 bar.

At both the permeate and retentate side, the higher pressure ratio shifted the curves, getting higher purity and recovery [27].

By maintaining a fixed recovery of 70%, the permeate stream achieved a purity of 89.3%, higher than that gained by a pressure ratio of 20 (65.8%). Thus, just one stage was not enough to reach, in the meantime, the best results in terms of both C_2HCl_3 recovery in the permeate and C_2HCl_3 residual content in the retentate, close to 90% and lower than 1%

respectively. Therefore, to enhance the process performance, another stage was added. So to rise the C_2HCl_3 recovery, operatively the configuration system was changed by re-treating the stage I (point A - Figure 43) which became the feed of stage II. This adjustment permits to achieve a C_2HCl_3 recovery of 80% (Figure 44), corresponding to a total C_2HCl_3 recovery in the whole membrane system of 94%.

a) Stage I



b) Stage II

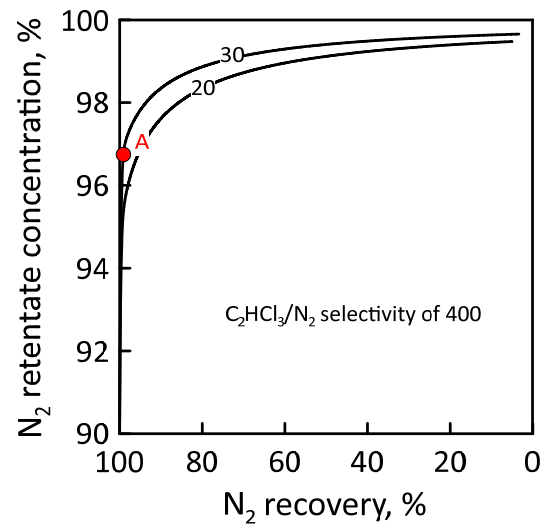


Figure 41 – C_2HCl_3 (a) and N_2 (b) molar concentration as a function of recovery. C_2HCl_3/N_2 selectivity of 400. Feed/permeate pressure ratio of 20 and 30. Point A: C_2HCl_3 recovery of 70%, pressure ratio of 30 and C_2HCl_3/N_2 selectivity of 400.

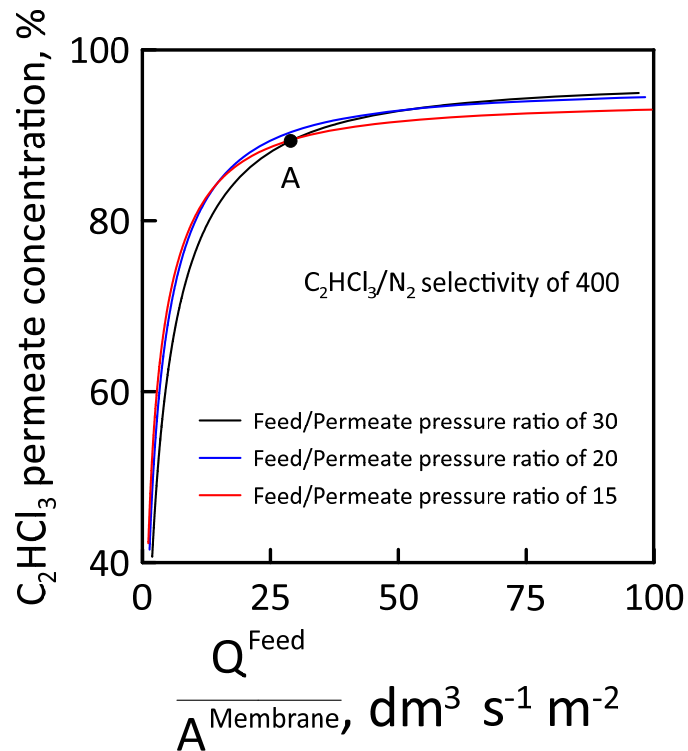


Figure 42 – C_2HCl_3 permeate concentration as a function of feed flow rate/membrane area ratio. C_2HCl_3/N_2 selectivity of 400. Pressure ratio of 40 (black), 60 (blue) and 80 (red)

Figure 42 shows C_2HCl_3 permeate concentration as a function of feed flow rate/membrane area ratio at different feed/permeate pressure ratio of 15, 20 and 30.

Simulations were carried out at pressure ratio of 15, 20 and 30 and C_2HCl_3/N_2 selectivity of 400. At a set feed flow rate and lower membrane area all the curves are shifted towards higher C_2HCl_3 permeate concentration. At a higher membrane area, C_2HCl_3 permeate concentration drastically decreases due to nitrogen permeation through membrane.

At low feed flow rates/membrane area ratio, higher feed/permeate pressure ratio allows to reach the same C_2HCl_3 permeate concentration, by using lower membrane area, at a given feed flow rate. Instead, the maximum C_2HCl_3 permeate concentration increases at higher pressure ratio [27]. Higher feed flow rate/membrane area ratio corresponds to low

membrane area for a given feed flow rate and the condition is close to initial membrane module (membrane length tends to 0). The C_2HCl_3 concentration tends to the maximum value allowed at the operating condition which is higher at higher pressure ratio (as shown in Figure 41).

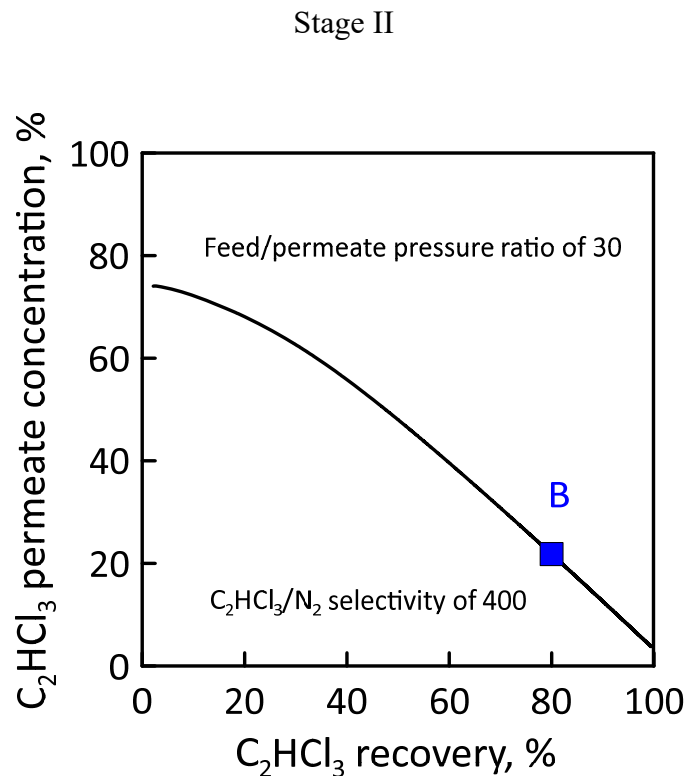


Figure 43 – C_2HCl_3 molar concentration as a function of recovery. $C_2HCl_3:N_2=3.25:96.75$. Feed/permeate pressure ratio of 30; C_2HCl_3/N_2 selectivity of 400; Point B: C_2HCl_3 recovery of 80%, pressure ratio of 30 and C_2HCl_3/N_2 selectivity of 400.

The flow diagram of the integrated membrane process (case study 1) for C_2HCl_3 separation from nitrogen mixture is shown in Figure 44. The stream to be treated is fed to the two-stage membrane system, whose performance were described above. The adjustment carried out permits to ensure a retentate stream containing only the 0.74% of

C_2HCl_3 , whereas the rest of C_2HCl_3 was recovered in the permeate (94%). The membrane units thus allowed to reach a composition of 49.87%, the rest being N_2 . Before releasing the stream in the atmosphere, an activated carbon adsorber was then used in the retentate to remove the residual C_2HCl_3 . Table 21 reports the data in both system configurations. This multistage membrane system, giving a final retentate stream with a lower C_2HCl_3 concentration, allowed to improve the performance of the process, to increase the life and to reduce the volume of activated carbon filter with respect to the case where no membranes were used.

In order to recover pure C_2HCl_3 , the permeate stream of the membrane system was then fed to a condenser. Table 22 reports vacuum pump operating conditions and streams molar composition.

Table 23 reports the data obtained from the outlet stream of the vacuum pump (at 120 kPa and 70 °C) which was fed to the condenser operating at -5 °C. Thanks to this further step, the C_2HCl_3 recovered in the liquid phase raised up to 96.7%, instead of the ca. 94% previously obtained, whereas the rest of vapour stream was fed to an activated carbon adsorber.

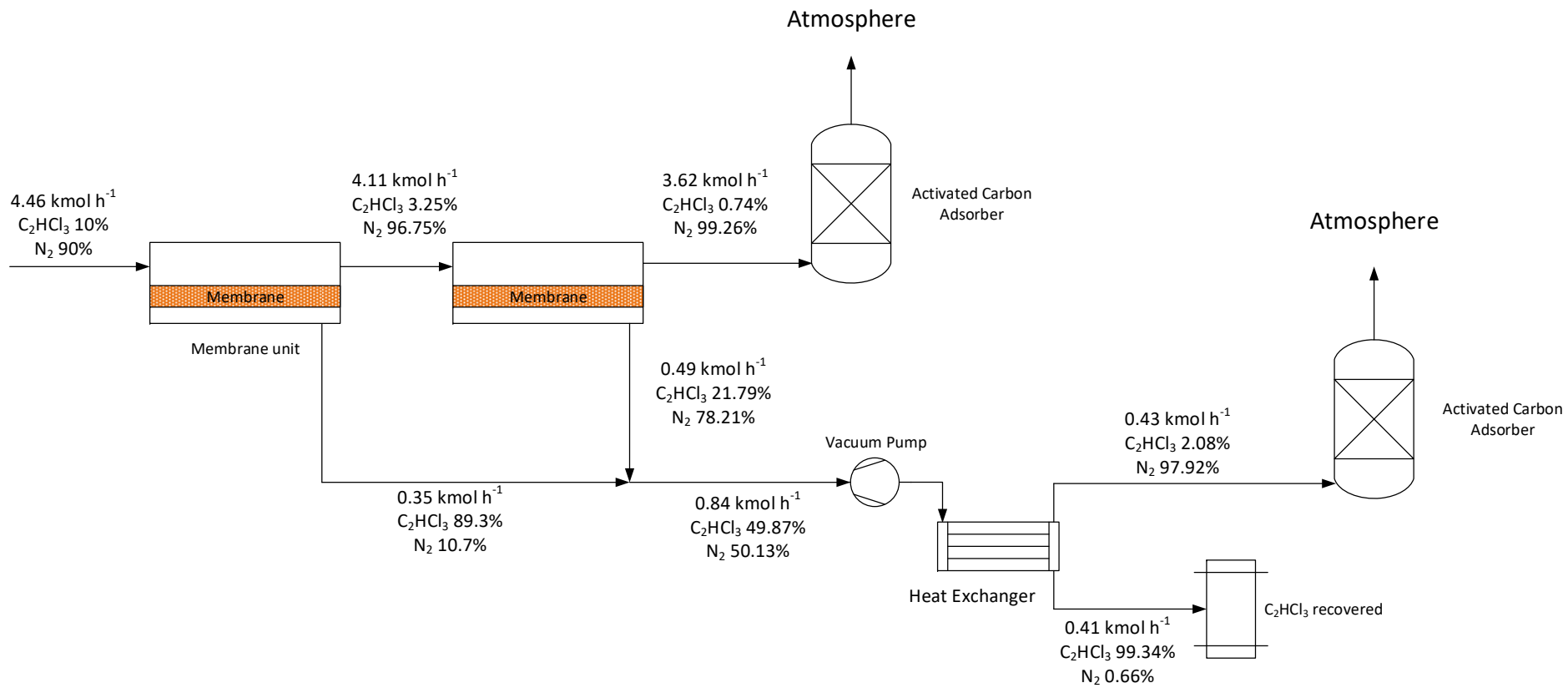


Figure 44 – Case Study 1: Flow sheet of integrated membrane process for N₂/C₂HCl₃ stream treatment.

Table 21 – Membrane units operating condition and streams molar composition.

	First membrane stage			Second membrane stage		
	Inlet	Retentate	Permeate	Inlet	Retentate	Permeate
Temperature, °C	40	40	40	40	40	40
Pressure, kPa	120	120	4	120	120	4
Molar Flow, kmol h ⁻¹	4.46	4.11	0.35	4.11	3.62	0.49
N ₂ :C ₂ HCl ₃ molar composition, %	90:10	96.75:3.25	10.7:89.3	96.75:3.25	99.26:0.74	78.21:21.79

Table 22 – Vacuum pump operating condition and streams molar composition.

	Inlet	Outlet
Temperature, °C	40	70
Pressure, kPa	4	120
Molar flow rate, kmol h ⁻¹	0.84	0.84
N ₂ :C ₂ HCl ₃ molar composition, %	49.87:50.13	49.87:50.13

Table 23 – Condenser operating condition and streams molar composition.

	Inlet	Vapour	Condensed
Temperature, °C	70	-5	-5
Pressure, kPa	120	106.2	106.2
Molar flow rate, kmol h ⁻¹	0.84	0.43	0.41
N ₂ :C ₂ HCl ₃ molar composition, %	49.87:50.13	97.92:2.08	0.66:99.34

In case study 2, instead, was considered the use of traditional technologies as showed in Figure 45. Here, the untreated stream was firstly fed to a heat exchanger, which allowed to condense and, consequently, to recover 80% of C₂HCl₃ with a purity of 99.34% (Table 24). Then, vapour stream exiting from the heat exchanger (4.1 kmol h⁻¹ at -5 °C and 106.2 kPa) was fed into the two-stage intercooler compressor, where the first one operated at 365 kPa and -5 °C (Table 25). This allowed to condense a stream containing 97.77% of C₂HCl₃. The rest of the vapour stream was fed to a second compressor where the pressure was increased up to 1200 kPa and the outlet stream reached 76 °C. At this point, through a second heat exchanger, the temperature was decreased from 76 °C to -5 °C (Table 26). In this way a vapour stream with a C₂HCl₃ concentration lower than 0.22% was obtained, which was then treated with an activated carbon adsorber before being discharged. The condensed stream concentrated at 93.45% in C₂HCl₃.

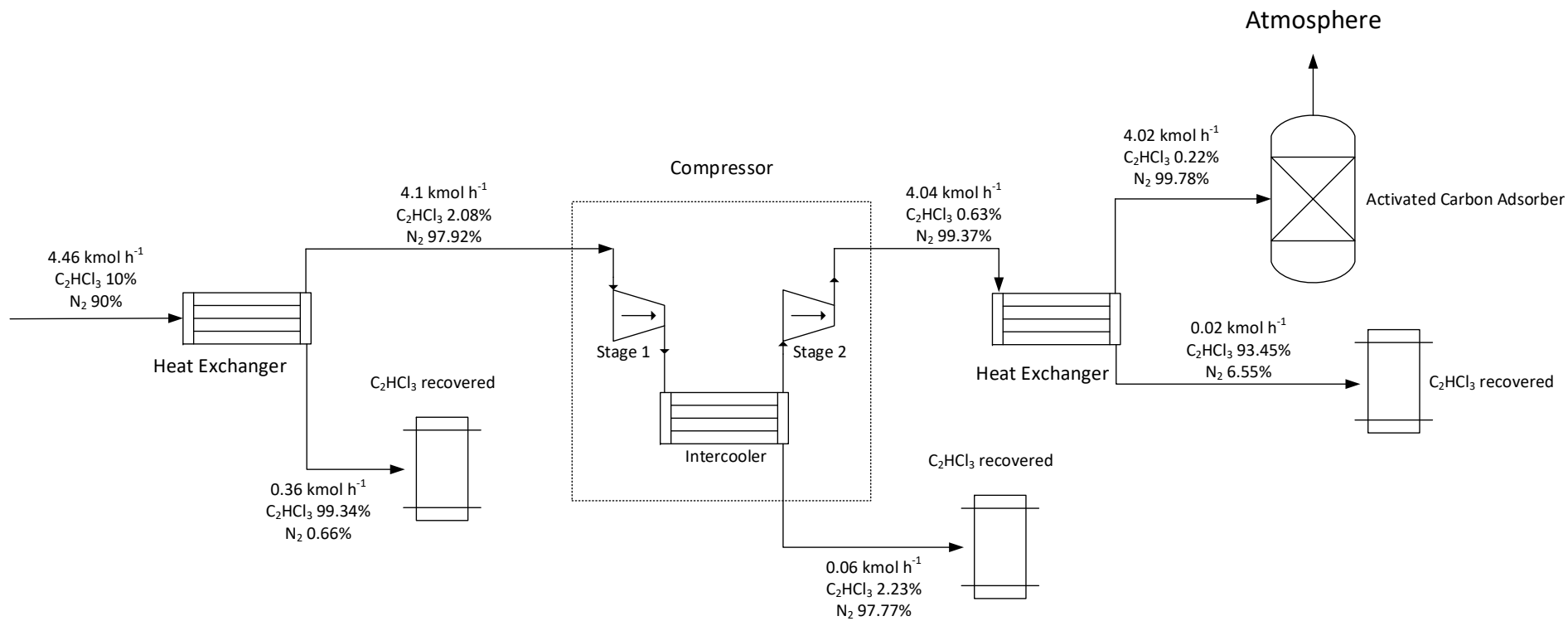


Figure 45 – Case Study 2: Flow sheet of traditional technologies for N₂/C₂HCl₃ stream treatment.

Table 24 – First heat exchanger unit operating condition and streams molar composition.

	Inlet	Vapour	Condensed
Temperature, °C	40	-5	-5
Pressure, kPa	120	106.2	106.2
Molar flow rate, kmol h ⁻¹	4.46	4.1	0.36
N ₂ :C ₂ HCl ₃ molar composition, %	90:10	97.92:2.08	0.66:99.34

Table 25 – Compressor operating condition and streams molar composition.

	Inlet	Intermediate condensed stream	Outlet
Temperature, °C	-5	-5	76
Pressure, kPa	106.2	365	1200
Molar flow rate, kmol h ⁻¹	4.1	0.06	4.04
N ₂ :C ₂ HCl ₃ molar composition, %	97.92:2.08	2.23:97.77	99.37:0.63

Table 26 – Second condenser unit operating condition and streams molar composition.

	Inlet	Vapour	Condensed
Temperature, °C	76	-5	-5
Pressure, kPa	1200	1186	1186
Molar flow rate, kmol h ⁻¹	4.04	4.02	0.02
N ₂ :C ₂ HCl ₃ molar composition, %	99.37:0.63	99.78:0.22	6.55:93.45

The third case study takes into account the use of cryogenic technologies which, up to now, are considered, the best available system for VOCs treatment. Figure 46 shows the scheme for N_2/C_2HCl_3 stream treatment. In this case study, in order to enhance the C_2HCl_3 recovery, the untreated stream was fed to the cryogenic heat exchanger set at $-80\text{ }^\circ\text{C}$ by using liquid nitrogen (because $-87.1\text{ }^\circ\text{C}$ is the C_2HCl_3 melting temperature) (Table 27). In this condition, C_2HCl_3 was totally recovered and, before to release the stream in the atmosphere, the non-condensable part was fed to a heat exchanger (Table 28). A fan was then added downstream to the heat exchangers to set the pressure above the atmospheric one (Table 29).

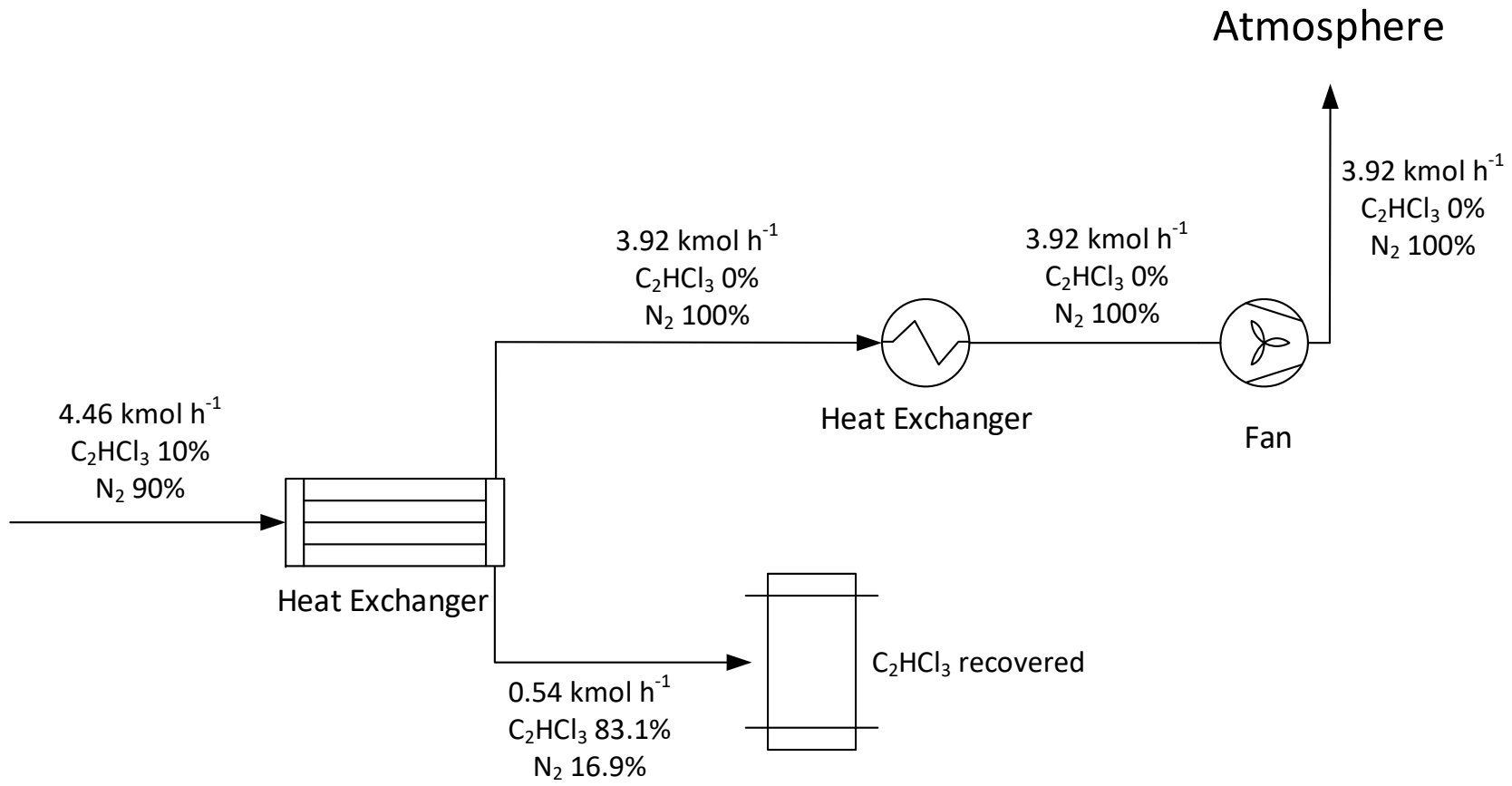


Figure 46 - Case Study 3: Flow sheet of cryogenic technology for N₂/C₂HCl₃ stream treatment.

Table 27 – Cryogenic heat condenser unit operating condition and streams molar composition.

	Inlet	Vapour	Condensed
Temperature, °C	40	-80	-80
Pressure, kPa	120	106.2	106.2
Molar flow rate, kmol h ⁻¹	4.46	3.92	0.54
N ₂ :C ₂ HCl ₃ molar composition, %	90:10	100:0	16.9:83.1

Table 28 – Heat condenser operating condition and streams molar composition.

	Inlet	Outlet
Temperature, °C	-80	20
Pressure, kPa	106.2	92.4
Molar flow rate, kmol h ⁻¹	3.92	3.92
N ₂ :C ₂ HCl ₃ molar composition, %	100:0	100:0

Table 29 – Fan operating condition and streams molar composition.

	Inlet	Outlet
Temperature, °C	20	29.1
Pressure, kPa	92.4	120
Molar flow rate, kmol h ⁻¹	3.92	3.92
N ₂ :C ₂ HCl ₃ molar composition, %	100:0	100:0

In order to properly compare all of the case studies and estimate the most sustainable one, an energetic analysis was performed.

As reported in Table 30, the integrated membrane process required a total energy demand of 7 kW with the heat exchanger consuming ca. 71.3% of the total energy. In case study 2, the compressor was the most energy demanding device, consuming 9.07 kW, correspondent to (Table 31) 52% of the energy request. The higher energy request of the case study 3 was equal to 10.26 kW, corresponding to the cryogenic unit, due to the heat flow for performing the C₂HCl₃ condensation, as reported in Table 32.

Globally, the advantage offered by the membranes use implies a significant reduction of energy consumption with respect to the other two traditional operations (7 kW with respect to 17.4 and 13.72 for case study 2 and 3, respectively).

Table 30 – Case Study 1. Operating condition and heat flow requirement of heat exchanger and vacuum pump.

	Inlet, °C	Outlet, °C	Pressure difference, kPa	Heat Flow, kW
Vacuum pump	40	70	116	2
Heat Exchanger	70	-5	-13.79	4.97

Table 31 – Case Study 2. Operating condition and heat flow requirement of heat exchangers and compressor.

	Inlet, °C	Outlet, °C	Pressure difference, kPa	Heat Flow, kW
Heat Exchanger	40	-5	-13.79	5.44
Compressor	-5	75.9	1094	9.07
Heat Exchanger	75.9	-5	-13.79	2.89

Table 32 – Case Study 3. Operating condition and heat flow requirement of heat exchangers and fan.

	Inlet, °C	Outlet, °C	Pressure difference, kPa	Heat Flow, kW
Cryogenic Heat Exchanger	40	-80	-13.79	10.26
Heat Exchanger	-80	20	-13.79	3.16
Fan	20	20	+27.6	0.3

Energy and mass intensity are two handy indexes to compare among these three technologies adopted in the case studies. These parameters are often used as process intensification metrics for highlighting the advantages of one technology to another.

Energy intensity (Eq. 71) is the ratio between power required to plant and the main compound (in this work is C_2HCl_3) product flow rate. At a low value of energy intensity corresponds higher energy. Mass intensity (Eq. 72) is defined as the recovery of main compound with respect to its total inlet stream. In our work, mass intensity is defined as the ratio between C_2HCl_3 product flow rate and total C_2HCl_3 inlet flow rate.

$$\text{Energy Intensity} = \frac{\text{Power required}}{C_2HCl_3 \text{ recovered flow rate}}, kJ \text{ mol}^{-1} \quad \text{Eq. 71}$$

$$\text{Mass Intensity} = \frac{C_2HCl_3 \text{ recovered flow rate}}{\text{Total } C_2HCl_3 \text{ inlet flow rate}}, - \quad \text{Eq. 72}$$

In particular, an intensified process was generally defined by a high mass intensity and a low energy intensity.

Figure 47 shows the energy intensity and the mass intensity versus the total C_2HCl_3 concentration before the activated carbon treatment, and the C_2HCl_3 concentration in the recover liquid stream, respectively.

Energy intensity was compared to “disposal in activated carbon” which was defined as the ratio between the C_2HCl_3 amount fed to the activated carbon adsorber and total C_2HCl_3 amount in the feed stream. Instead, the mass intensity was compared to “reuse liquid stream” which is the C_2HCl_3 amount condensed and stored during the gas treatment.

Firstly, we have to consider that both case study 1 (Figure 44) and case study 2 (Figure 45) require an adsorption system to reduce the C_2HCl_3 concentration close to 0 before discharge the stream in atmosphere.

On the contrary, in the case study 3 (Figure 46), thanks to cryogenic condensation, a total recovering of C_2HCl_3 was obtained in the liquid phase, therefore its mass intensity (mass intensity of 1) results higher compared with both case study 1 (mass intensity of 0.91) and 2 (mass intensity of 0.98). However, energy intensity of case study 1 (61.6 kJ mol^{-1}) was lower than that of case study 2 ($142.9 \text{ kJ mol}^{-1}$) and case study 3 (ca. $110.7 \text{ kJ mol}^{-1}$). These considerations highlights that the membrane integrated process requires lower energy to reach the same target of alternative technologies.

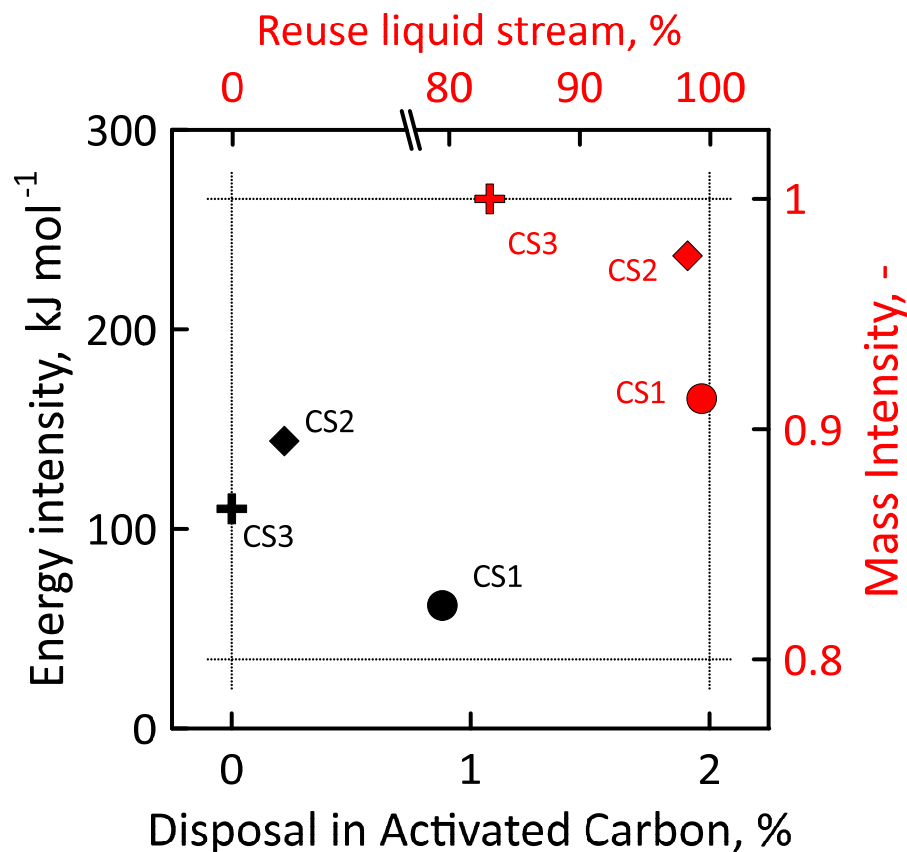


Figure 47 – Energy intensity and mass intensity as a function of average C_2HCl_3 concentration to disposal in activated carbon and average C_2HCl_3 concentration to reuse liquid stream, respectively. CS1: case study 1, membrane integrated system; CS2: case study 2, high pressure-heat condenser system; CS3: case study 3, cryogenic condenser.

From an industrial point of view, membrane integrated process assumes a relevant position. Other technologies could reach the same results but require high pressure systems, that need to follow pressure equipment directive (PED). In addition, the use of higher pressure systems implies higher capital costs and periodic and expensive maintenance. The membrane process, working at low pressure, is cheaper technology, more appealing than plants operating at high pressure, and preferred from an environmental point of view.

6.2. Conclusion

The separation of C_2HCl_3 from N_2/C_2HCl_3 mixtures was studied by considering three case studies: membrane integrated system (case study 1), high pressure-heat condenser system (case study 2) and cryogenic condenser (case study 3). The third case is today considered the best available technology for this application, allowing to fully recover C_2HCl_3 . Nevertheless, high energy demand, at least equal to 13.72 kW, is required to reach cryogenic temperature. In terms of energy consumption, the worst system is the high-pressure one (case study 2) which required the higher energy power ~ 17.4 kW. Membrane integrated process is the less energy intensive, with an energy requirement close to 7 kW and an energy intensity of 61.6 kJ mol^{-1} . However, the main disadvantage of this technology was the incomplete C_2HCl_3 recovery corresponding to a mass intensity value of 0.91. Cryogenic technologies, instead, allowed the total recovery with mass intensity of 1 despite the higher energy intensity value. On the other hand, the high pressure system showed the highest energy intensity due to the high energy demand of compressor and condenser devices.

This study underlined that membrane technology allows an important energy saving in terms of lower energy intensity with respect to traditional technologies for C_2HCl_3/N_2 gas separation. In addition, the membrane integrated system used for the total C_2HCl_3 recovery shows remarkable perspectives for its application.

7. Conclusions

In this dissertation, permeability properties of membranes for gas separation of industrial mixture streams were studied. A preliminary analysis of kinetic diffusivity measurements in the Sieverts apparatus was carried out. The aim was to evaluate the diffusivity and solubility of gases at high pressure and to improve the measurement accuracy when using small samples available on a research lab scale. Thermodynamics analysis was carried out for several gases by using cubic and state equations. The un-steady state analysis demonstrated the possibility of the Sieverts apparatus to be used in kinetic analysis but, due to the high number of possible parameters, the correct tuning of the measurements was crucial to obtain consistent results. The use of a volumetric system to investigate the transport properties of the materials permitted an extensive overview of the physics of the system. Experimental analyses were carried out for polymeric membranes, such as Matrimid and PIM, using pressure drop and concentration gradient methods. Matrimid membrane was studied in a wide temperature range from -25 °C to 150 °C. Membrane showed a good temperature resistance and in all the considered range followed an Arrhenius behaviour. The good membrane operability at different temperatures is promising for their use in different industrial fields. PIM-based membranes are more innovative materials with respect to Matrimid membranes and showed significant separative performances (high CO₂ permeability up to 1200 Barrer and good CO₂/N₂ selectivity up to 22.5). The membranes showed a good resistance to plasticization, as highlighted by the results obtained through high pressure measurements. The results showed a high potential of this new type of PIM-based polymers and, in particular,

indicated that this PIM-PI random copolymer membranes have remarkable potential to be used for CO₂ gas separation.

The analysis of the permeability properties was the basis to investigate membrane or integrated membrane system for industrial application. Two papers were published on these topics. The first one “Analysis of membrane unit performance in presence of wet CO₂-containing mixtures (see ref. [216]), dealt with the effect of saturation humidity on CO₂/CH₄ separation, by considering a feed stream composition of CO₂:CH₄=40:60 (composition approximate to biogas streams in the absence of the other species that are present in smaller quantities or traces). Owing to the high adsorption capacity, water and CO₂ competed for permeation, hence humidity drastically reduced the CO₂ permeance. CO₂/CH₄ selectivity decreased of about 28% going from dry to wet conditions. The work confirmed that the detrimental effect of humidity on the separation could be reduced by operating with membranes having high CO₂/CH₄ selectivity and low pressure ratios.

An important gas separation application is in the recovery of potential pollutants and/or high value vapours. An integrated membrane process and its comparison with traditional technologies was carried out for trichloroethylene recovery from N₂/trichloroethylene mixture (Trichloroethylene/Nitrogen Mixture Separation via membrane operations: comparison with traditional technologies, see ref. [235]). The analysis was carried out in terms of trichloroethylene recovery and comparison of energy requirement.

This study underlined that membrane technology allows important energy saving with respect to traditional technologies for C₂HCl₃/N₂ gas separation.

Appendix A – Publications

- 1) **Melone L.,** *Giorno L., Brunetti A., Barbieri G.* "Analysis of membrane unit performance in presence of wet CO₂-containing mixtures"; *Chem. Eng. Res. Des.* 153 (2020) 721–727. DOI: 10.1016/j.cherd.2019.11.034.

- 2) **Melone L.,** *Brunetti A., Giorno L., Barone M., Barbieri G.* " Trichloroethylene/Nitrogen Mixture Separation via membrane operations: comparison with traditional technologies"; *Sep. Pur. Tech.* 251 (2020) 117344. DOI: 10.1016/j.seppur.2020.117344.

Appendix B – Training PhD school activity

- 1) Metodologie avanzate di calcolo numeric.
- 2) Gestione della ricerca, della conoscenza dei sistemi di ricerca e dei sistemi di finanziamento.
- 3) Nonlinear structure analysis.
- 4) Scienza e tecnologia delle membrane – Applicazione di membrane.
- 5) Scienza e tecnologie delle membrane – Caratterizzazione di membrane.
- 6) Scienza e tecnologie delle membrane – Preparazione di membrane.
- 7) Corso di formazione “Formazione generale e specifica alto rischio”
- 8) Introduction to Hybrid, Multifunctional, Stimuli-Responsive Materials
- 9) Introduction to Informatics and Scientific Calculation using Matlab
- 10) Writing a scientific paper: Guidelines and Tips – Technical English Course

List of figures

Figure 1 - Milestone of membrane gas separation [7].

Figure 2– PermSelect module for the oxygen capture.

Figure 3– Scheme of PermSelect plant for the air separation and enrichment nitrogen stream [70].

Figure 4– VaporSep plant for the SynGas ratio adjustment [74].

Figure 5 – VaporSep plant for the Methanol enrichment [75].

Figure 6 – VaporSep plant for the hydrogen recovery by hydrotreater downstream [76].

Figure 7– Membrane recovery of hydrocarbon in a hydrocarbon/nitrogen plant [78].

Figure 8 – Membrane recovery of VOCs for clean air production by air/VOCs mixture [80].

Figure 9 - Scheme of natural gas sweetening membrane based technology [82].

Figure 10 – Scheme of the membrane system installed by Tecno Project Industriale srl in Italy.

Figure 11 – Driving force and concentration gradient through membrane according to solution-diffusion model.

Figure 12- Experimental plant scheme for single gas permeation measurements (Pressure drop method).

Figure 13 - Schematic of concentration gradient method experimental set-up used for measuring mixed gas permeation properties of membranes: MFC, mass flow controller; GC, gas chromatography.

Figure 14 – Membrane system geometry for model development

Figure 15 – CO₂ permeate concentration and CH₄ retentate concentration as a function of CO₂ and CH₄ recovery, respectively. Dashed line (red): Permeation number of 0.01, 0.02 and 0.05; Pressure ratio of 50; CO₂/CH₄ selectivity of 5, 10 and 50.

Figure 16 – CO₂ permeate concentration and CH₄ retentate concentration as a function of CO₂ and CH₄ recovery, respectively. Pressure ratio of 50; CO₂/CH₄ selectivity of 5, 10 and 50.

Figure 17 - Sieverts schematic apparatus

Figure 18 - Schematic Volumetric adsorption unit used during kinetic and adsorption measurements

Figure 19 - Packaging method. Left: stratified filling; right: dispersed filling. Blue circle: sample; grey circle: metal beads.

Figure 20 – CO₂ isotherm in terms of excess adsorption as a function of equilibrium pressure. Circle: excess adsorption obtained by cubic EoS data; Triangle: excess adsorption obtained by NIST webbook. Adsorption gas: CO₂; Sample: Polymer A; Temperature of 20 °C

Figure 21 – CO₂ excess adsorption deviation as a function of equilibrium pressure. Adsorption gas: CO₂; Sample: Polymer A; Temperature of 20 °C.

Figure 22 – Pressure decay as a function of time during open valve measurements. Gas: Helium; Diamond (red): experimental measurements; solid line (black): simulation dosing pressure. Temperature of 20 °C. Initial pressure of 31.33 kPa; Initial uptake pressure of 0.13 Pa. Valve constant χ : $2.2 \cdot 10^{-8} \text{ mol Pa}^{-1} \text{ s}^{-1}$.

Figure 23 – Pressure decay as a function of time during open valve measurements. Gas: Helium; Diamond (red): experimental measurements; solid line (black): simulation dosing pressure. Temperature of 20 °C. Initial dosing pressure of 80.4 kPa; Initial uptake pressure of 25.77 kPa. Valve constant χ : $4.7 \cdot 10^{-8} \text{ mol Pa}^{-1} \text{ s}^{-1}$.

Figure 24 – Dosing and uptake pressure as a function of times. Gas: CO₂. Diamond: experimental measurements; solid line (red): simulation dosing pressure; dashed line (blue): simulation uptake pressure. Initial dosing pressure: $13.28 \cdot 10^3 \text{ Pa}$; initial uptake pressure: 0.13 Pa. Temperature: 20 °C.

Figure 25 – Dosing pressure normalised as a function of times. Gas: CO₂. Diamond: experimental measurements; solid line (red): simulation dosing pressure. Initial dosing pressure: $13.28 \cdot 10^3 \text{ Pa}$; initial uptake pressure: 0.13 Pa. Temperature: 20 °C.

Figure 26 – CO₂ permeance as a function of temperature.

Figure 27 – Permeating flux of i-species as a function of correspondent partial pressure difference. Circle: CO₂; triangle: O₂; square: N₂. Single gas (black), Mixed gas (red)

Figure 28 – Permeating flux of i-species as a function of correspondent partial pressure difference. Circle: CO₂; triangle: O₂; square: N₂. Single gas (black), Mixed gas (red)

Figure 29 – Permeating flux of i-species as a function of correspondent partial pressure difference. Circle: CO₂; triangle: O₂; square: N₂. Single gas (black), Mixed gas (red)

Figure 30 – Robeson diagram for CO₂/N₂ for high free volume polymers. The lines represent the 2008 upper bounds for each gas pair.

Figure 31 – CH₄ retentate molar concentration as a function of recovery in dry (red line) and wet (black line) condition. Pressure ratio of 10. CO₂/CH₄ selectivity of 25. Dashed line: permeation number. Symbol: circle (A), CH₄ retentate molar concentration of 90% at RH=0%; diamond (B), CH₄ retentate molar concentration of 90% at RH=100%; triangle (C), CH₄ retentate molar concentration of 87.5% at RH=100%.

Figure 32 – CH₄ retentate molar concentration as a function of recovery in dry (red line) and wet (black line) condition. Pressure ratio of 10. CO₂/CH₄ selectivity of 50. Symbol: circle (A'), CH₄ retentate molar concentration of 90% at RH=0%; diamond (B'), CH₄ retentate molar concentration of 90% at RH=100%; triangle (C), CH₄ retentate molar concentration of 88.2% at RH=100%.

Figure 33 – CH₄ retentate molar concentration as a function of recovery in dry (red line) and wet (black line) condition. Pressure ratio of 10. CO₂/CH₄ selectivity of 100. Symbol: circle (A''), CH₄ retentate molar concentration of 90% at RH=0%; diamond (B''), CH₄ retentate molar concentration of 90% at RH=100%; triangle (C), CH₄ retentate molar concentration of 88.5% at RH=100%

Figure 34 – CO₂ permeate molar concentration as a function of recovery in dry (red line) and wet (black line) condition. Pressure ratio of 10. CO₂/CH₄ selectivity of 25. Dashed line: permeation number. Symbol: circle (A), CH₄ retentate molar concentration of 90% at RH=0%; diamond (B), CH₄ retentate molar concentration of 90% at RH=100%; triangle (C), CH₄ retentate molar concentration of 87.5% at RH=100%.

Figure 35 – CH₄ retentate concentration as a function of CH₄ recovery in dry (red line) and wet (black line) condition. CO₂/CH₄ selectivity of 25. Pressure ratio of 10 (solid line) and 20 (dashed line). Symbol: circle (A), CH₄ retentate molar concentration of 90% at RH=0%; diamond (B), CH₄ retentate molar concentration of 90% at RH=100%.

Figure 36 - CH₄ (left) and CO₂ (right) concentration (solid line) and recovery (dashed line) as a function of feed flow rate/membrane area ratio. Pressure ratio of 10. CO₂/CH₄ selectivity of 25.

Figure 37 – CO₂ partial pressure (left) and CO₂ driving force (right) as a function of feed flow rate/membrane area ratio.

Figure 38 - CH₄ retentate concentration (left) and CH₄ recovery (right) as a function of feed flow rate/membrane area ratio. Pressure ratio of 10 (solid line) and 20 (dashed line). CO₂/CH₄ selectivity of 25.

Figure 39 – C₂HCl₃ molar concentration as a function of recovery. C₂HCl₃:N₂=10:90. Feed/permeate pressure ratio of 30; C₂HCl₃/N₂ selectivity of 100, 200, 400 and 500; Point A: C₂HCl₃ recovery of 70%, pressure ratio of 30 and C₂HCl₃/N₂ selectivity of 400.

Figure 40 - C₂HCl₃ molar concentration as a function of recovery. C₂HCl₃:N₂ =10:90. Feed/permeate pressure ratio of 20; C₂HCl₃/N₂ selectivity of 100, 200, 400 and 500. Point A': C₂HCl₃ molar concentration of 65.75% and C₂HCl₃ recovery of 70%. Point A'': C₂HCl₃ molar concentration of 89.3% and C₂HCl₃ recovery of 53.4%.

Figure 41 – C₂HCl₃ (a) and N₂ (b) molar concentration as a function of recovery. C₂HCl₃/N₂ selectivity of 400. Feed/permeate pressure ratio of 20 and 30. Point A: C₂HCl₃ recovery of 70%, pressure ratio of 30 and C₂HCl₃/N₂ selectivity of 400.

Figure 42 – C₂HCl₃ permeate concentration as a function of feed flow rate/membrane area ratio. C₂HCl₃/N₂ selectivity of 400. Pressure ratio of 40 (black), 60 (blue) and 80 (red)

Figure 43 – C₂HCl₃ molar concentration as a function of recovery. C₂HCl₃:N₂=3.25:96.75. Feed/permeate pressure ratio of 30; C₂HCl₃/N₂ selectivity of 400; Point B: C₂HCl₃ recovery of 80%, pressure ratio of 30 and C₂HCl₃/N₂ selectivity of 400.

Figure 44 – Case Study 1: Flow sheet of integrated membrane process for N₂/C₂HCl₃ stream treatment

Figure 45 – Case Study 2: Flow sheet of traditional technologies for N₂/C₂HCl₃ stream treatment

Figure 46 - Case Study 3: Flow sheet of cryogenic technology for N₂/C₂HCl₃ stream treatment

Figure 47 – Energy intensity and mass intensity as a function of average C₂HCl₃ concentration to disposal in activated carbon and average C₂HCl₃ concentration to reuse liquid stream, respectively.

List of tables

Table 1 - Basic features of Process Optimization, Process synthesis , Process Intensification [108]

Table 2 – Feed condition and operating parameters

Table 3 – Instrumentation used in adsorption apparatus

Table 4 - Material properties

Table 5 – All system components geometry

Table 6 - EoS co-volumes and energy parameters for each gases

Table 7 – Deviation calculation between NIST data and cubic EoS

Table 8 – Dual-site Langmuir isotherm parameters

Table 9 - Operating condition and system geometry

Table 10 – Pre-exponential factor and activation energy of permeation.

Table 11 – Membranes size

Table 12 - Operating condition

Table 13 - PIM-based membrane separative properties

Table 14. Membrane properties of Matrimid® 5218 hollow fibres considered in the simulations [186]

Table 15 - Operating condition

Table 16 - Maximum CO₂ permeate concentration when CO₂ recovery close to 0% at different CO₂/CH₄ selectivity and humidity concentration in feed stream.

Table 17 – CH₄ recovery at CH₄ retentate concentration of 90% at different pressure ratio and humidity concentration in feed stream.

Table 18 – Membrane properties [224]

Table 19 – Operating condition of the feed stream

Table 20 – Heuristic assumption in device design

Table 21 – Membrane units operating condition and streams molar composition

Table 22 – Vacuum pump operating condition and streams molar composition.

Table 23 – Condenser operating condition and streams molar composition.

Table 24 – First heat exchanger unit operating condition and streams molar composition.

Table 25 – Compressor operating condition and streams molar composition.

Table 26 – Second condenser unit operating condition and streams molar composition.

Table 27 – Cryogenic heat condenser unit operating condition and streams molar composition.

Table 28 – Heat condenser operating condition and streams molar composition.

Table 29 – Fan operating condition and streams molar composition.

Table 30 – Case Study 1. Operating condition and heat flow requirement of heat exchanger and vacuum pump.

Table 31 – Case Study 2. Operating condition and heat flow requirement of heat exchangers and compressor.

Table 32 – Case Study 3. Operating condition and heat flow requirement of heat exchangers and fan.

References

- 1 Wijmans, J.G.; Baker, R.W. “The solution-diffusion model: a review”. *J. Membr. Sci.* 107 (1995) 1-21.
- 2 Alberto, M.; Bhavsar, R.; Luque-Alled, J. M.; Vijayaraghavan, A.; Budd, P. M.; Gorgojo, P. “impeded physical aging in PIM-1 membranes containing graphene-like fillers”. *J. Membr. Sci.* 563 (2018) 513-520.
- 3 <https://echa.europa.eu/substance-information/-/substanceinfo/100.001.062> (accessed 08/08/2020).
- 4 Górak, A.; Stankiewicz, A. (Eds.). (2011). *Research Agenda for Process Intensification: Towards a Sustainable World of 2050. Creative Energy - Energy Transition*. Retrieved from http://3me.tudelft.nl/fileadmin/Faculteit/3mE/Actueel/Nieuws/2011/docs/DSD_Research_Agenda.pdf.
- 5 Drioli, E.; Brunetti, A.; Di Profio, G.; Barbieri, G. “Process intensification strategies and membrane engineering”. *Green Chem.* 14 (2012) 1561–1572.
- 6 Brunetti, A.; Melone, L.; Drioli, E.; Barbieri, G. “Si-Containing Polymers in Membrane Gas Separation”, in: Y. Yampolskii and E. Finkelshtein (Eds), *Membrane Materials for Gas and Vapor Separation. Synthesis and Application of Silicon-Containing Polymers*, Wiley publishing, 2017. Reference to a chapter in an edited book: Chapter 11.
- 7 Kesting, R.E.; Fritzsche, A.K. “Polymeric gas separation membranes”. John Wiley & Sons, New York, 1993.
- 8 Mitchell, J.K. “On the penetrativeness of fluid”. *Am. J. Med. Sci.* 7 (1830) 36.
- 9 Mitchell, J.K. “On the penetration of fluid”. *Am. J. Med. Sci.* 13 (1833) 100.

-
- 10 Graham, T. "On the law of the diffusion of gases". *Phil. Mag.* 2 (1833) 175.
- 11 Fick, A. "Uber diffusion". *Ann. Physik.* 94 (1855) 59.
- 12 Graham, T. "On the absorption and dialytic separation of gases by colloid septa. Part I. Action of a septum of caoutchouc". *Phil. Mag.* 32 (1866) 401.
- 13 Wroblewski, S. V. *Wied. Ann. Phys.* 8 (1879) 29.
- 14 Kayser, R.E. *Wied. Ann. Phys.* 43 (1891) 544.
- 15 Daynes, H.A. "The process of diffusion through rubber membrane". *Proc. Roy. Soc. (London)*, 97A (1920) 286.
- 16 Bernado, P.; Clarizia, G. "30 years of membrane technology for gas separation". *Chem. Eng. Trans.* 32 (2013) 1999-2004
- 17 Baker, R. W. "Future directions of membrane gas separation technology". *Ind. Eng. Chem. Res.* 41 (2002) 1393-1411.
- 18 Basu, A.; Akhtar, J.; Rahman, M. H.; Islam, M. R. "A review of separation of gases using membrane systems". *Petroleum Sci. Tech.* 22 (2004) 1343-1368.
- 19 Caro, J. "Are MOF membranes better in gas separation than those made of zeolites?" *Current Opinion in Chemical Engineering* 1 (2011) 77-83.
- 20 Ismail, A.F.; Lorna, W. "Penetrant-induced plasticization phenomenon in glassy polymers for gas separation membrane". *Sep. Pur. Tech.* 27 (2002) 173-194.
- 21 Freemantle, M. "Membranes for gas separation". *Chem. Eng. News.* 43 (2005) 49-57.
- 22 Pandey, P.; Chauhan, R. S. "Membranes for gas separation". *Progress in Polymer Science*, 26 (2001) 853-893.
- 23 Brunetti, A.; Cersosimo, M.; Dong, G.; Woo, K. T.; Lee, J.; Kim, J. S.; Lee, Y. M.; Drioli, E.; Barbieri, G. "In situ restoring of aged thermally rearranged gas separation membranes". *J. Membr. Sci.* 520 (2016) 671-678.

-
- 24 Brunetti, A.; Cersosimo, M.; Kim, J. S.; Dong, G.; Fontananova, E.; Lee, Y. M.; Drioli, E.; Barbieri, G. “Thermally rearranged mixed matrix membranes for CO₂ separation: An aging study”. *I. J. Greenhouse Gas Cont.* 61 (2017) 16-26.
- 25 Drioli, E.; Romano, M. “Progress and new perspectives on integrated membrane operations for sustainable industrial growth”. *Ind. Eng. Chem. Res.* 40 (2001) 1277.
- 26 Simmonds, M.; Hurst, P.; Wilkinson, M.B.; Watt, C.; Roberts, C.A. “A study of very large scale post combustion CO₂ capture at a refining & petrochemical complex”. 2003. www.co2captureproject.org.
- 27 Brunetti, A.; Scura, F.; Barbieri, G.; Drioli, E. “Membrane Technologies for CO₂ separation”. *J. Mem. Sci.* 359 (2010) 115–125.
- 28 He, X. “A review of material development in the field of carbon capture and the application of membrane-based processes in power plants and energy-intensive industries”, *Ener. Sustain. Society.* 8 (2018) 34.
- 29 Ciferno, J.P.; Fout, T. E.; Jones, A. P.; Murphy, J.T. “Capturing carbon from existing coal-fired power plant”, *Chemical Engineering Progress*, April 2009, 33.
- 30 Herzog, H. “What future for carbon capture and sequestration?”, *Env. Sci. Tech.* 35 (2001)148
- 31 White, C.M. “Separation and capture of CO₂ from large stationary sources and sequestration in geological formations”, *J. Air Waste Manag. Ass.* 53 (2003) 645.
- 32 Favre, E. “Carbon dioxide recovery from post-combustion processes: Can gas permeation membranes compete with absorption?”, *J. Memb. Sci.* 294 (2007) 50.
- 33 Haider, S.; Lindbrathen, A.; Hagg, M.-B. “Techno-economical evaluation of membrane based biogas upgrading system: A comparison between polymeric membrane and carbon membrane technology”. *Green Ener. Environ.* 1 (2016) 222-234.

-
- 34 Saha, D.; Grappe, H. A.; Chakraborty, A.; Orkoulas, G. "Postextraction Separation, On-Board Storage, and Catalytic". *Chem. Rev.* 116 (2016) 11436-11499.
- 35 Nakayama, K.; Suzuki, K.; Yoshida, M.; Yajima, K.; Tomita, T. Method For Preparing DDR Type Zeolite Membrane, DDR Type Zeolite Membrane, And Composite DDR Type Zeolite Membrane, And Method For Preparation Thereof. U.S. Patent 20050229779 A1, October 20, 2005.
- 36 Kulprathipanja, S. "Zeolites in Industrial Separation and Catalysis". Wiley-VCH Verlag GmbH & Co.: Kga, Weinheim, 2010. (360) Gascon, J.; Kapteijn, F. Metal-Organic Framework Membranes-High Potential, Bright Future? *Angew. Chem., Int. Ed.* 49 (2010) 1530.
- 37 Denexter, M. J.; Vanbekkum, H.; Rijn, C. J. M.; Kapteijn, F.; Moulijn, J. A.; Schellevis, H.; Beenakker, C. I. N. "Stability Of Oriented Silicalite-1 Films In View Of Zeolite Membrane Preparation". *Zeolites* 19 (1997) 13 – 20.
- 38 Won, J. O.; Park, H. C.; Kang, Y. S. "Polymer Membranes For Gas Separation". *Polym. Sci. Technol.* 10 (1999) 170.
- 39 Ayala, D.; Lozano, A. E.; De Abajo, J.; Garcia-Perez, C.; De La Campa, J. G.; Peinemann, K.-V.; Freeman, B. D.; Prabhakar, R. "Gas Separation Properties Of Aromatic Polyimides". *J. Membr. Sci.* 215 (2003) 61.
- 40 Ma, C.; Urban, J.J. "Polymers of intrinsic microporosity (PIMs) gas separation membranes: A mini review". *Proc. Nature Res. Soc.* 2 (2018) 1-18
- 41 Mckeown, N. B.; Budd, M. "Polymers Of Intrinsic Microporosity (Pims): Organic Materials For Membrane Separations, Heterogeneous Catalysis And Hydrogen Storage". *Chem. Soc. Rev.* 35 (2006) 675 – 683.

-
- 42 Mckeown, N. B.; Makhseedab, S.; Budd, P. M. "Phthalocyanine-Based Nanoporous Network Polymers". *Chem. Commun.* (2002) 2780 – 2781.
- 43 Jeon, Y.-W.; Lee, D.-H. "Gas Membranes For CO₂/CH₄ (Biogas) Separation: A Review". *Environ. Eng. Sci.* 32 (2015) 71 – 85.
- 44 Pandey, P.; Chauhan, R. S. "Membranes for gas separation". *Prog. Polym. Sci.* 26 (2001) 853 – 893.
- 45 Muhammad, M.; Yeong, Y. F.; Lau, K. K.; Shariff, A. B. M. "Issues And Challenges In The Development Of Deca-Dodecasil 3 Rhombohedral Membrane In CO₂ Capture From Natural Gas". *Sep. Purif. Rev.* 44 (2015) 331 – 340.
- 46 Wadey, B.L. "Plasticizers". In: Mark, H.F. (Ed.), *Encyclopedia of Polymer Science and Technology*, vol. 3. Wiley-Interscience, New Jersey, pp. 498–524 (2005).
- 47 Roussenova, M.; Murith, M.; Alam, A.; Ubbink, J. "Plasticization, Antiplasticization, and Molecular Packing in Amorphous Carbohydrate-Glycerol Matrices". *Biomacromoleculs.* 11 (2010) 3237-3247
- 48 Xiao, Y.; Low, B.T.; Hosseini, S.S.; Chung, T.S.; Paul, D.R. "The strategies of molecular architecture and modification of polyimide-based membranes for CO₂ removal from natural gas—a review". *Progress in Polymer Science* 34 (2009) 561–580.
- 49 Lee, J.S.; Madden, W.; Koros, W.J. "Antiplasticization and plasticization of Matrimid asymmetric hollow fiber membranes—Part A. Experimental". *J. Membr. Sci.* 350 (2010) 232–241

-
- 50 Lee, J.S.; Madden, W.; Koros, W.J. “Antiplasticization and plasticization of Matrimid asymmetric hollow fiber membranes—Part B. Modeling”. *J. Membr. Sci.* 350 (2010) 242–251.
- 51 Larocca, N.M.; Pessan, L.A. “Effect of antiplasticisation on the volumetric, gas sorption and transport properties of polyetherimide”. *J. Membr. Sci.* 218 (2003) 69–92.
- 52 Maeda, Y.; Paul, D.R. “Effect of antiplasticization on gas sorption and transport. I Polysulfone”. *J. Polymer Sci. Part B: Polymer Physics. Ed. 25* (1987) 957–980.
- 53 Maeda, Y.; Paul, D.R. “Effect of antiplasticization on gas sorption and transport. II Poly(phenylene oxide)”. *J. Polymer Sci. Part B: Polymer Physics. Ed. 25* (1987) 981–1003.
- 54 Maeda, Y.; Paul, D.R. “Effect of antiplasticization on gas sorption and transport. III Free volume interpretation”. *J. Polymer Sci. Part B: Polymer Physics. Ed. 25* (1987) 1005–1016.
- 55 Maeda, Y.; Paul, D.R. “Effect of antiplasticization on selectivity and productivity of gas separation membranes”. *J. Membr. Sci.* 30 (1987) 1–9.
- 56 Horn, N.R.; Paul, D.R. “Carbon dioxide plasticization and conditioning effects in thick vs thin glassy”. *Polymer.* 52 (2011) 1619–1627.
- 57 Horn, N.R.; Paul, D.R.; “Carbon dioxide plasticization of thin glassy polymer films”. *Polymer.* 52 (2011) 5587–5594.

-
- 58 Cui, L.; Qiu, W.; Paul, D.; Koros, W. “Responses of 6FDA-based polyimide thin membranes to CO₂ exposure”. *Polymer*. 52 (2011) 5528–5537.
- 59 Xia, J.; Chung, T.-S.; Li, P.; Horn, R.N.; Paul, D.R. “Aging and carbon dioxide plasticization of thin polyetherimide films”. *Polymer*. 52 (2012) 2099–2108.
- 60 Immergut, E.H.; Mark, H.F. “Principles of plasticization”. In: Platzer, N.A. (Ed.), *Plasticization and Plasticizer Processes*, vol. 48. American Chemical Society, Washington, DC. 1–26 (1965).
- 61 Koros, W.J. “Gas separation”. In: Baker, R., Cussler, E., Eykamp, W., Koros, W., Riley, R., Strathmann, H. (Eds.), *Membrane Separation Systems—Recent Developments and Future Directions*, vol. II. William Andrew Publishing/Noyes, New Jersey. 189–241 (1991)
- 62 Drioli E.; Brunetti A.; Di Profio G.; Barbieri G. “Process intensification strategies and membrane engineering”. *Green Chemistry*. 14 (2012) 1561-1572.
- 63 Semenova S. I. “Polymer membranes for hydrocarbon separation and removal”. *J. Memb. Sci.* 231 (2014) 189-207.
- 64 Smitha, B.; Suhanya, D.; Sridhar, S.; Ramakrishna, M. “Separation of organic-organic mixtures by pervaporation - A review”. *J. Memb. Sci.* 241 (2004) 1-21.
- 65 Krea, M.; Roizard, D.; Mostefa, N. M. “Synthesis and characterization of rubbery highly fluorinated siloxane-imide segmented copolymers”. *Polymer Int.* 62 (2013) 1413-1424.
- 66 www.airproducts.no. (accessed 30/06/2020).
- 67 www.airproducts.com. (accessed 30/06/2020).

-
- 68 Yampolskii, Y.; Freeman, B. “Membrane gas separation”. Jhon Wiley & Sons, Ltd, Chichester (2010).
- 69 <https://permselect.com/markets/oxygen-enrichment>. (accessed 30/06/2020).
- 70
http://www.grasys.com/upload/iblock/a17/Membrane_nitrogen_plants_and_packages.pdf. (accessed 30/06/2020).
- 71 Advanced Prism® Membrane Systems” For Cost Effective Gas Separations”,
<http://www.airproducts.com/NR/rdonlyres/81FB384C-3DB5-4390-AED0-C2DB4EEDDB18/0/PrismPGS.pdf>. (accessed 30/06/2020).
- 72 <http://www.airproducts.com/~media/Files/PDF/products/supply-options/prism-membrane/en-process-gas-membrane-systems-ammonia-plants.pdf>. (accessed 30/06/2020)
- 73
http://www.mtrinc.com/pdf_print/refinery_and_syngas/MTR_Brochure_Hydrogen_Recovery_from_Ammonia_Plant_Purge_Gas.pdf. (accessed 30/06/2020)
- 74 http://www.mtrinc.com/hydrogen_separation_in_syngas_processes.html. (accessed 30/06/2020)
- 75 http://www.mtrinc.com/hydrogen_recovery_from_methanol_plant_purge_gas.html. (accessed 30/06/2020)
- 76 http://www.mtrinc.com/hydrogen_purification_in_refineries.html. (accessed 30/06/2020)
- 77 R.W. Baker, Membranes for vapor/gas separation, 2006.
http://www.mtrinc.com/publications/MT01%20Fane%20Mem%20for%20VaporGas_Sep%202006%20Book%20Ch.pdf. (accessed 30/06/2020)

-
- http://www.mtrinc.com/publications/MT01%20Fane%20Memb%20for%20VaporGas_Sep%202006%20Book%20Ch.pdf. (accessed 30/06/2020)
- 79 Melone L.; Brunetti A.; Giorno L.; Barone M.; Barbieri G. " Trichloroethylene/Nitrogen Mixture Separation via membrane operations: comparison with traditional technologies"; Sep. Pur. Tech., submitted.
- 80 <https://www.energy.gov/management/articles/department-energy-office-environmental-management-2016-year-review> (accessed: 01/08/2020)
- 81 Iulianelli, A.; Drioli, E. "Membrane engineering: Latest advancements in gas separation and pretreatment processes, petrochemical industry and refinery, and future perspectives in emerging applications". Fuel Processing Technology. 206 (2020) 106464.
- 82 Baker, R.W.; Low, B.T. "Gas separation membrane materials: a perspective". Macromolecules 47 (2014) 6999–7013.
- 83 MacDowell, N.; Florin, N.; Buchard, A.; Hallett, J.; Galindo, A.; Jackson, G.; Adjiman, C. S.; Williams, C.; Shah, N.; Fennel, P. "An overview of CO₂ capture technologies". Ener. Env. Sci. 3 (2010) 1645–1669.
- 84 Esposito, E.; Dellamuzia, L.; Moretti, U.; Fuoco, A.; Giorno, L.; Jansen, J.C. "Simultaneous production of biomethane and food grade CO₂ from biogas: an industrial case study". Ener. Environ. Sci. 12 (2019) 281–289.
- 85 Mohammed, I.Y. "Comparison of Selexol™ and Rectisol® Technologies in an Integrated Gasification Combined Cycle (IGCC) plant for clean energy production". Int. J. Eng. Res. 3 (2014) 742–744.

-
- 86 Vakharia, V.; Ramasubramanian, K.; Winston Ho, W.S. “An experimental and modelling study of CO₂-selective membranes for IGCC syngas purification”. *J. Membr. Sci.* 488 (2015) 56–66.
- 87 Jansen, D.; Dijkstra, J.W.; van den Brink, R.W.; Peters, T.A.; Stange, M.; Bredesen, R.; Goldbach, A.; Xu, H.Y. Gottschalk, A.; Doukelis, A. “Hydrogen membrane reactors for CO₂ capture”. *Energy Proc* 1 (2009) 253–260.
- 88 NanoGLOWA - FP6 EU Project, <https://cordis.europa.eu/project/id/26735/it> (accessed 31/07/2020)
- 89 Sandru, M.; Kim, T.-J.; Capala, W.; Huijbers, M.; Hägg, M.-B. “Pilot scale testing of polymeric membranes for CO₂ capture from coal fired power plants”. *Energy Procedia* 37 (2013) 6473–6480.
- 90 Hägg, M.B.; Lindbråthen, A.; He, X.; Nodeland, S.G.; Cantero, T. “Pilot demonstration reporting on CO₂ capture from a cement plant using hollow fiber process”. *Energy Procedia* 114 (2017) 6150–6165.
- 91 He, X. “A review of material development in the field of carbon capture and the application of membrane-based processes in power plants and energy-intensive industries”. *Ener. Sustain. Society* 8 (2018) 34.
- 92 Merkel, T.C.; Lin, H.; Wei, X.; Baker, R. “Power plant post-combustion carbon dioxide capture: an opportunity for membranes”. *J. Membr. Sci.* 359 (2010) 126–139.
- 93 Stankiewicz Andrzej, Moulijn Jacob A: *Re-engineering the Chemical Processing Plant: Process Intensification*. M. Dekker; 2004.
- 94 Rong B-G: *Process Synthesis and Process Intensification*. De Gruyter; 2017.

-
- 95 Stankiewicz A, van Gerven T, Giorgos Stefanidis: The Fundamentals of Process Intensification. Wiley; 2019.
- 96 Go' mez-Castro FI, Segovia-Herna' ndez G: Process Intensification: Design Methodologies. edn 1. De Gruyter; 2019.
- 97 Piemonte V, Falco M, de, Basile A: Sustainable Development in Chemical Engineering: Innovative Technologies. Wiley; 2013.
- 98 Huss R: Process Intensification Principles: Synergy – Focus on Reactive Distillation: Reactive Distillation: What, Why, and How? 2018
- 99 Harmsen, G.J. “Reactive distillation: the front-runner of industrial process intensification”. Chem. Eng. Process. Process. Intensif. 46 (2007) 774-780.
- 100 Luyben WL, Yu C-C: Reactive Distillation Design and Control. John Wiley & Sons; 2009.
- 101 Huss R: Process Intensification Principles: Synergy – Focus on Reactive Distillation: Reactive Distillation: What, Why, and How? 2018. (<https://www.aiche.org/academy/webinars/pi-principles-synergy-focus-on-reactive-distillation>)
- 102 Qian, Z.; Chen, Q.; Grossmann, I.E. “Optimal synthesis of rotating packed bed reactor”. Comput. Chem. Eng. 105 (2017)152-160.
- 103 Reay, D.; Ramshaw, C.; Harvey, A. “Process Intensification Engineering for Efficiency, Sustainability and Flexibility”. Elsevier; 2008.
- 104 Regatte, V.R.; Kaisare, N.S. “Propane combustion in non-adiabatic microreactors: 1. Comparison of channel and posted catalytic inserts”. Chem. Eng. Sci. 66 (2011) 1123-1131.

-
- 105 Kockmann, N.; Gottsponer, M.; Roberge, D.M. "Scale-up concept of single-channel microreactors from process development to industrial production". *Chem. Eng. J.* 167 (2011) 718-726.
- 106 Cremaschi, S. "A perspective on process synthesis: challenges and prospects". *Comput. Chem. Eng.* 81 (2015) 130-137.
- 107 Biegler, L.T. "New directions for nonlinear process optimization". *Curr. Opin. Chem. Eng.* 21 (2018) 32-40.
- 108 Keil, F. J. "Process Intensification". *Rev. Chem. Eng.* 34 (2018) 135-200.
- 109 Ohenoja, M.; Boodhoo, K.; Reay, D.; Paavola, M.; Leiviska, K. "Process control in intensified continuous solids handling". *Chem. Eng. Process. Process. Intensif.* 131 (2018) 59-69.
- 110 Tula, A.K.; Babi, D.K.; Bottlaender, J.; Eden, M.R.; Gani, R. "A computer- aided software-tool for sustainable process synthesis-intensification". *Comput. Chem. Eng.* 105 (2017) 74-95.
- 111 Tian, Y.; Demirel, S.E.; Hasan, M.M.F.; Pistikopoulos, E.N. "An overview of process systems engineering approaches for process intensification: state of the art". *Chem. Eng. Process. Process. Intensif.* 2018.
- 112 Keil, F. J. "Process Intensification". *Rev. Chem. Eng.* 34 (2018) 135-200.
- 113 Criscuoli, A.; Drioli, E. "New Metrics for Evaluating the Performance of Membrane Operations in the Logic of Process Intensification". *Ind. Eng. Chem. Res.* 46 (2007) 2268-2271.
- 114 Brunetti, A.; Sun, Y.; Caravella, A.; Drioli, E.; Barbieri, G. "Process intensification for greenhouse gas separation from biogas: More efficient process schemes based on membrane-integrated". *I. J. Greenhouse Gas Cont.* 35 (2015) 18-29.

-
- 115 Carvalho, A. I. C. S. G.; Gani, R.; Matos, H. A. S. "Design of sustainable chemical processes: systematic retrofit analysis and generation and evaluation of alternatives". AIChE Annual Meeting, Conference Proceedings; American Institute of Chemical Engineers: New York. (2005).
- 116 Sengupta, A.; Peterson, P. A.; Miller, B. D.; Schneider, J.; Fulk, C. W. "Large-scale application of membrane contactors for gas transfer from or to ultrapure water". *Sep. Purif. Technol.* 14 (1998) 189-200.
- 117 Ismail, A. F.; Kusworo, T. D.; Mustafa, A.; Hasbullah, H. "Understanding the solution-diffusion mechanism in gas separation membrane for engineering students". *Proceedings of the 2005 Regional Conference on Engineering Education.* (2005)
- 118 Paul D.R. Time Lag Method for Mass Transport Properties Evaluation in GS. In: Drioli E., Giorno L. (eds) *Encyclopedia of Membranes.* Springer, Berlin, Heidelberg. (2016)
- 119 Rutherford, S. W.; Do, D.D. "Review of time lag permeation technique as a method for characterisation of porous media and membranes" *Adsorption.* 3 (1997) 283-312.
- 120 Bounaceur, N.; Lape, N.; Roizard, D.; Vallieres, C.; Favre, E. "Membrane processes for post-combustion carbon dioxide capture: a parametric study, *Energy* 31 (2006) 2556-2570.
- 121 Kaldis, S.P.; Kapantaidakis, G.C.; Sakellariopoulos, G.P. "Simulation of multicomponent gas separation in a hollow fiber membrane by orthogonal collocation – Hydrogen recovery from refinery gases". *J. Membr. Sci.* 173 (2000) 61-71.
- 122 Chowdhury, M.H.M.; Feng, X.; Douglas, P.; Croiset E. "A new numerical approach for a detailed multicomponent gas separation membrane model and Aspen plus simulation". *Chem. Eng. Tech.* 28 (2005) 773-782.

-
- 123 Coker, D.T.; Allen, T.; Fleming, G.K. "Nonisothermal model for gas separation hollow fiber membranes". *AIChE Journal* 45 (1999) 1451-1468.
- 124 Matson, S. "Separation of gases with synthetic membranes". *Chem. Eng. Sci.* 38 (1983) 503-524.
- 125 Zanderighi L. "Evaluation of the performance of multistage membrane separation cascades". *Sep. Sci. Tech.* 31 (1996) 1291-1308.
- 126 Favre, E. "Carbon dioxide recovery from post combustion processes: Can gas permeation membranes compete with absorption?" *J. Membr. Sci.* 294 (2007) 50-59.
- 127 Favre, E.; Bounaceur, R.; Roizard, D. "A hybrid process combining oxygen enriched air combustion and membrane separation for postcombustion carbon dioxide capture". *Sep Pur. Tech* 68 (2009) 30-36.
- 128 Belaissaoui, B.; Favre, E. "Membrane separation processes for post-combustion carbon dioxide capture: state of the art and critical overview". *Oil&gas Sci. Tech.* 69 (2014) 1005-1020.
- 129 Tibbetts, G. G.; Meisner, G. P.; & Olk, C. H. "Hydrogen storage capacity of carbon nanotubes, filaments, and vapor-grown fibers". *Carbon.* 39 (2001) 2291–2301.
- 130 Brandani, S. "Analysis of the Piezometric Method for the Study of Diffusion in Microporous Solids: Isothermal Case". *Adsorption.* 4 (1998) 17-24.
- 131 Zielinski, J. M.; Coe, C. G.; Nickel, R. J.; Romeo, A. M.; Cooper, A. C.; Pez, G. P. "High pressure sorption isotherms via differential pressure measurements". *Adsorption.* 13 (2007). 1–7.
- 132 Brandani, S.; Mangano, E.; Luberti, M. "Net, excess and absolute adsorption in mixed gas adsorption". *Adsorption.* 23 (2017) 569–576.

-
- 133 Hu, X.; Mangano, E.; Friedrich, D.; Ahn, H.; Brandani, S. “Diffusion mechanism of CO₂ in 13X zeolite beads”. *Adsorption*. 20 (2014) 121–135.
- 134 Lee, J. S.; Kim, J. H.; Kim, J. T.; Suh, J. K.; Lee, J. M.; Lee, C. H. “Adsorption equilibria of CO₂ on zeolite 13X and zeolite X/activated carbon composite”. *J. Chem. Eng. Data*. 47 (2002) 1237–1242.
- 135 Chue, K. T.; Kim, J. N.; Yoo, Y. J.; Cho, S. H.; Yang, R. T. “Comparison of Activated Carbon and Zeolite 13X for CO₂ Recovery from Flue Gas by Pressure Swing Adsorption”. *Ind. Eng. Chem. Res.* 34 (1995) 591–598.
- 136 Harlick, P. J. E.; Tezel, F. H. “An experimental adsorbent screening study for CO₂ removal from N₂”. *Micro. Meso. Mat.* 76 (2004) 71–79.
- 137 Cavenati, S.; Grande, C. A.; Rodrigues, A. E. “Adsorption Equilibrium of Methane, Carbon Dioxide, and Nitrogen on Zeolite 13X at High Pressures”. *J. Chem. Eng. Data*, 49 (2004) 1095–1101.
- 138 Dasgupta, S.; Biswas, N.; Aarti, Gode, N. G.; Divekar, S.; Nanoti, A.; & Goswami, A. N. “CO₂ recovery from mixtures with nitrogen in a vacuum swing adsorber using metal organic framework adsorbent: A comparative study. *Int. J. Greenh. Gas Con.* (2012) 225–229.
- 139 Tibbetts, G. G.; Meisner, G. P.; Olk, C. H. “Hydrogen storage capacity of carbon nanotubes, filaments, and vapor-grown fibers”. *Carbon*, 39 (2001) 2291–2301.
- 140 Zlotea, C.; Moretto, P.; Steriotis, T. “A Round Robin characterisation of the hydrogen sorption properties of a carbon based material”. *Int. J. Hydrogen Energy*. 34 (2009) 3044–3057.

-
- 141 Parilla, P.A. “Hydrogen sorbent measurement qualification and characterization”. In: DOE Hydrogen and Fuel Cells Program Annual Merit Review and Peer Evaluation Meeting 2012, p. 12. National Renewable Energy Technology Laboratory (2012)
- 142 Sircar, S.; Wang, C.-Y.; Lueking, A.D. “Design of high pressure differential volumetric adsorption measurements with increased accuracy”. *Adsorption*. 19 (2013) 1211–1234.
- 143 Parambath, V.B.; Nagar, R.; Sethupathi, K.; Ramaprabhu, S. “Investigation of spillover mechanism in palladium decorated hydrogen exfoliated functionalized graphene”. *J. Phys. Chem. C*. 115 (2011) 15679–15685.
- 144 Parambath, V.B.; Nagar, R.; Ramaprabhu, S. “Effect of nitrogen doping on hydrogen storage capacity of palladium decorated graphene”. *Langmuir* 28 (2012) 7826–7833.
- 145 Webb, P.A.; Orr, C. “Corporation. Analytical Methods in Fine Particle Technology. Micromeritics Instrument Corporation” MI (1997).
- 146 Lee, Y.W.; Clemens, B.M.; Gross, K.J. “Novel Sieverts’ type volumetric measurements of hydrogen storage properties for very small sample quantities”. *J. Alloy. Compd.* 452 (2008) 410–413.
- 147 Lachawiec, A.J.; DiRaimondo, T.R.; Yang, R.T. “A robust volumetric apparatus and method for measuring high pressure hydrogen storage properties of nanostructured materials”. *Rev. Sci. Instrum.* 79 (2008).
- 148 Zhang, C.; Lu, X.S.; Gu, A.Z. “How to accurately determine the uptake of hydrogen in carbonaceous materials”. *Int. J. Hydrogen Energy* 29 (2004) 1271–1276.

-
- 149 Blach, T.P.; Gray, E.M. "Sieverts apparatus and methodology for accurate determination of hydrogen uptake by light-atom hosts". *J. Alloy. Compd.* 446 (2007) 692–697.
- 150 Blackburn, J.L.; Parilla, P.A.; Gennett, T.; Hurst, K.E.; Dillon, A.C.; Heben, M.J. "Measurement of the reversible hydrogen storage capacity of milligram Ti–6Al–4 V alloy samples with temperature programmed desorption and volumetric techniques". *J. Alloy. Compd.* 454 (2008) 483–490.
- 151 Zielinski, J.M.; Coe, C.G.; Nickel, R.J.; Romeo, A.M.; Cooper, A.C.; Pez, G.P. "High pressure sorption isotherms via differential pressure measurements". *Adsorpt. J. Int. Adsorpt. Soc.* 13 (2007) 1–7.
- 152 Qajar, A.; Peer, M.; Rajagopalan, R.; Foley, H.C. "High pressure hydrogen adsorption apparatus: design and error analysis". *Int. J. Hydrogen Energy* 37 (2012) 9123–9136.
- 153 Browning, D.J.; Gerrard, M.L.; Lakeman, J.B.; Mellor, I.M.; Mortimer, R.J., Turpin, M.C. "Studies into the storage of hydrogen in carbon nanofibers: proposal of a possible reaction mechanism". *Nano Lett.* 2 (2002) 201–205.
- 154 Bulow, M.; Micke, A. "Determination of Transport Coefficients in Microporous Solids," *Adsorption*, 1 (1995) 29–48.
- 155 Brandani, S.; Mangano, E.; Sarkisov, L. "Net, excess and absolute adsorption and adsorption helium". *Adsorption*. 22 (2016) 261-276.
- 156 Brandani, S.; Mangano, E.; Luberti, M. "Net, excess and absolute adsorption in mixed gas adsorption". *Adsorption*. 23 (2017) 569-576.
- 157 Keller, J.; Staudt, R. "Gas Adsorption Equilibria". Springer, New York (2005)

-
- 158 Banas, K.; Brandani, F.; Ruthven, D.M.; Stallmach, F.; Karger, J. “Combining macroscopic and microscopic diffusion studies in zeolites using NMR techniques.” *Magn. Reson. Imaging*. 23 (2005) 227-232.
- 159 Sircar, S. “Gibbsian surface excess for gas adsorption – revisited”. *Ind. Eng. Chem. Res.* 38 (1999) 3670-3682.
- 160 Sircar, S. “Measurement of Gibbsian surface excess”. *AIChE J.* 116 (2001) 1169-1176.
- 161 Myers, A.L.; Monson, P. “Adsorption in porous materials at high pressure: theory and experiment”. *Langmuir*. 18 (2002) 10261-10273.
- 162 Jacobsen, R.T.; Stewart, R.B. “Thermodynamic properties of nitrogen including liquid and vapour phases from 63K to 2000K with pressures to 10000 bar”. *J. Phys. Chem. Ref. Data*. 2 (1973) 757-922.
- 163 Span, R.; Wagner. “Equation of State for Technical Applications. I. Simultaneously optimized Functional Forms for Nonpolar and Polar Fluids” *I. J. Thermophys.* 24 (2003) 1-39.
- 164 Span, R.; Wagner. “Equation of State for Technical Applications. II. Results for Nonpolar Fluids” *I. J. Thermophys.* 24 (2003) 41-109.
- 165 Span, R.; Wagner. “Equation of State for Technical Applications. III. Results for Nonpolar Fluids” *I. J. Thermophys.* 24 (2003) 111-162.
- 166 Span, R.; Wagner, W.; Lemmon, E.W.; Jacobsen, R.T. “Multiparameter equations of state – recent trends and future challenges”. *Fluid Phase Equilibria*. 183-184 (2001) 1-20.

-
- 167 Kunz, O.; Wagner, W. "The GERG-2008 wide-range equation of state for natural gases and other mixtures: An expansion of GERG-2004". *J. Chem. Eng.* 57 (2012) 3032-3091.
- 168 Schmidt, R.; Wagner, W. "A new form of the equation of state for pure substance and its application to oxygen". *Fluid Phase Equilibria.* 19(3) (1985) 175-200.
- 169 Jacobsen, R.T.; Stewart, R.B.; Jahangiri, M. "Thermodynamic properties of nitrogen from the freezing line to 2000 K at pressures to 1000 MPa". *J. Phys. Chem. Ref. Data.* 15 (1986) 735-909.
- 170 Setzmann, U.; Wagner, W. "A new method for optimizing the structure of thermodynamic correlation equations". *Int. J. Thermophys.* 10 (1989) 1103-1126.
- 171 Setzmann, U.; Wagner, W. "A new equation of state and tables of thermodynamic properties for methane covering the range from the melting line to 625 K at pressures up to 100 MPa". *J. Phys. Chem. Ref. Data* 20 (1991) 1061-1155.
- 172 <https://webbook.nist.gov/> (accessed 02 June 2020)
- 173 Tang, X.; Ripepi, N.; Stadie, N. P.; Yu, L.; Hall, M. R. "A dual-site Langmuir equation for accurate estimation of high pressure deep shale gas resources". *Fuel*, 185 (2016) 10–17.
- 174 Mathias, P. M.; Kumar, R.; Moyer, J. D.; Schork, J. M.; Srinivasan, S. R.; Auvil, S. R.; Talu, O. "Correlation of multicomponent gas adsorption by the dual-site Langmuir model. Application to nitrogen/oxygen adsorption on 5A-zeolite". *Ind. Eng. Chem. Res.* 35(7) (1996) 2477–2483.
- 175 <https://webbook.nist.gov/> (accessed: 21/01/2016)
- 176 Van Atta, C. M. "Vacuum Science and Engineering". 1^o edition. New York: McGraw-Hill, 1965.

-
- 177 Swaidan, R.; Ghanem, B.S.; Litwiller, E.; Pinnau, I. "Pure- and mixed-gas CO₂/CH₄ separation properties of PIM-1 and an amidoxime-functionalized PIM1". *J. Memb. Sci.* 457 (2014) 95-102.
- 178 Choi, S.-H.; Jansen, J. C.; Tasselli, F.; Barbieri, G.; Drioli, E. "In-line formation of chemically cross-linked P84® co-polyimide hollow fiber membranes for H₂/CO₂ separation". *Sep. Pur. Tech.* 76 (2010) 132-139.
- 179 David, O. C.; Gorri, D.; Urriaga, A.; Ortiz, I. "Mixed gas separation study for the hydrogen recovery from H₂/CO/N₂/CO₂ post combustion mixtures using a Matrimid membrane". *J. Memb. Sci.* 378 (2011) 359-368.
- 180 David, O. C.; Gorri, D.; Nijmeijer, K.; Ortiz, I.; Urriaga, A. "Hydrogen separation from multicomponent gas mixture containing CO, N₂, and CO₂ using Matrimid asymmetric hollow fiber membranes". *J. Memb. Sci.* 419-420 (2012) 49-56.
- 181 Peer, M.; Kamali, S. M.; Mahdeyarfar, M.; Mohammadi, T. "Separation of hydrogen from carbon monoxide using a hollow fiber polyimide membrane: Experimental and simulation". *Chem. Eng. Tech.* 30 (2007) 1418-1425.
- 182 Shishatskiy, S.; Nistor, C.; Popa, M.; Nunes, S. P.; Peinemann, K. V. "Polyimide asymmetric membranes for hydrogen separation: influence of formation conditions on gas transport properties". *Adv. Eng. Mat.* 8 (2006) 390-397.
- 183 Kraftschik, B.; Koros, W. J.; Johnson, J. R.; Karvan, O. "Dense film polyimide membranes for aggressive sour gas feed separations". *J. Memb. Sci.* 428 (2013) 608-619.
- 184 Dong, G.; Li, H.; Chen, V. "Factors affect defect free Matrimid hollow fiber gas separation performance in natural gas purification". *J. Memb. Sci.* 353 (2010) 17-27.

-
- 185 Lee, J. S.; Madden, W.; Koros, W. J. “Antiplasticization and plasticization of Matrimid asymmetric hollow fiber membranes – Part A. Experimental”. *J. Memb. Sci.* 350 (2010) 232-241.
- 186 Falbo, F.; Tasselli, F.; Brunetti, A.; Drioli, E.; Barbieri, G. “Polyimide hollow fibre membranes for CO₂ separation from wet gas mixture”. *Braz. J. Chem. Eng.* 31 (2014) 1023–1034.
- 187 Ansaloni, L.; Minelli, M.; Giacinti baschetti, M.; Sarti, G.C. “Effects of thermal treatment and physucal aging on the gas transport properties in Matrimid”. *Oil&Gas Sci. Tech.* 70 (2015) 367-379.
- 188 Comer, A.C.; Kalika D.S.; Rowe, B.W.; Freeman B.D.; Paul, D.R. “Dynamic relaxation characteristics of Matrimid polyimide”. *Polymer.* 50 (20019) 891-897.
- 189 Lasseguette, E.; Malpass-Evans, R.; Carta, M.; McKeown, N.B.; Ferrari, M.C. “Temperature and pressure Dependence of Gasd Permeation in a Microporous Troger’s Base polymer”. *Membranes.* 8 (2018) 132.
- 190 Thomas, S.; Pinnau, I.; Du, N.; Guiver, M.D. “Pure- and mixed-gas permeation properties of a microporous spirobisindane-based ladder polymer (PIM-1)”. *J. Membr. Sci.* 333 (2009) 125–131.
- 191 Budd, P.M.; Msayib, K.J.; Tattershall, C.E.; Ghanem, B.S.; Reynolds, K.J.; McKeown, N.B.; Fritsch, D. “Gas separation membranes from polymers of intrinsic microporosity”. *J. Membr. Sci.* 251 (2005) 263–269.
- 192 Lasseguette, E.; Malpass-Evans, R.; Carta, M.; McKeown, N.B.; Ferrari, M.C. “Temperature and Pressure Dependence of Gas Permeation in a Microporous Troger’s Base polymer”. *Membranes.* 8 (2018) 132.

-
- 193 Bos, A.; Punt, I. G. M.; Wessling, M.; Strathmann, H. "CO₂-induced plasticization phenomena in glassy polymers". *J. Membr. Sci.* 155 (1999) 67-78.
- 194 Esposito, E.; Mazzei, I.; Monteleone, M.; Fuoco, A.; Carta, M.; McKeown, N.B.; Malpass-Evans, R.; Jansen, J.C. "Highly Permeable matrimid/PIM-EA(H₂)-TB Blend membrane for Gas Separation". *Polymers*. 11 (2019) 46.
- 195 Zhang, Q.; Chen, G.; Zhang, S. "Synthesis and properties of novel soluble polyimides having a spirobisindane-linked dianhydride unit". *Polymer* 48 (2007) 2250–2256.
- 196 Ghanem, B.S.; McKeown, N.B.; Budd, P.M.; Al-Harbi, N.M.; Fritsch, D.; Heinrich, K. Starannikova, L.; Tokarev, A.; Yampolskii Y. "Characterization, and gas permeation properties of a novel group of polymers with intrinsic microporosity: PIM-polyimides". *Macromolecules* 42 (2009) 7881–7888.
- 197 Shamsipur, H.; Dawood, B.A.; Budd, P.M.; Bernardo, P.; Clarizia, G.; Jansen, J.C. "Thermally rearrangeable PIM-polyimides for gas separation membranes". *Macromolecules* 47 (2014) 5595–5606.
- 198 Hossain, I.; Al Munsur, A.Z.; Kim, T.-H. "A Facile Synthesis of (PIM-Polyimide)-(6FDA-Durene-Polyimide) Copolymers as novel POolymer Membrnaes for CO₂ Separation". *Membranes*. 9 (2019) 113
- 199 Robeson, L.M. "The upper bound revisited". *J. Membr. Sci.* 320 (2008) 390-400.
- 200 Bermeshev, M., Bulgakov, B., Starannikova, L., Dibrov, G., Chapala, P., Demchuk, D., Yampolskii, Y., Finkelshtein, E. (2015) Synthesis and gas permeation parameters of metathesis polytricyclononenes with pendant Me₃E-groups (E=C, Si, Ge). *Journal of Applied Polymer Science*, DOI: 10.1002/app.41395.
- 201 Chapala, P.P., Bermeshev, M.V., Starannikova, L.E., Shantarovich, V.P., Gavrilova, N.N., Yampolskii, Y.P., Finkelshtein, E.S. (2015) Gas-transport properties of novel

-
- composites based on addition poly(3-trimethylsilyltricyclononene-7) and substituted cyclodextrines. *Polymer Composites*, 36, 1029-1038.
- 202 Belov, N., Nizhegorodova, Y., Bermeshev, M., Yampolskii, Y. (2015) Detailed study of the gas permeation parameters of a glassy poly(tricyclononene) with Si-O-Si side groups. *Journal of Membrane Science*, 483, 136-143.
- 203 Yampolskii, Y.P., Korikov, A.P., Shantarovich, V.P., Nagai, K., Freeman, B.D., Masuda, T., Teraguchi, M., Kwak, G. (2001) Gas permeability and free volume of highly branched substituted acetylene polymers. *Macromolecules*, 34, 1788-1796.
- 204 Starannikova, L., Pilipenko, M., Belov., Yampolskii, Y., Gringolts, M., Finkelshtein, E. (2008) Addition-type polynorborene with Si(CH₃)₃ side groups: Detailed study of gas permeation and thermodynamic properties. *Journal of membrane Science*, 323, 134-143.
- 205 Pinnau, I., Toy, L.G. (1996) Transport of organic vapors through poly(1-trimethylsilyl-1-propyne). *Journal of membrane Science*, 116, 199-209.
- 206 Toy, L.G., Nagai, K., Freeman, B.D., Pinnau, I., He Z., Masuda, T., Teraguchi, M., Yampolskii, Y.P. (2000) Pure-gas and vapor permeation and sorption properties of poly[1-phenyl-2-[p-(trimethylsilyl)phenyl]acetylene] (PTMSDPA). *Macromolecules*, 33, 2516-2524.
- 207 Chen, X.Y.; Vinh-Thang, H.; Ramirez, A.A.; Rodrigue, D.; Kaliaguine, S. “Membrane gas separation technologies for biogas upgrading”. *RSC Adv.* 5 (2015) 24399–24448.
- 208 Scholes, C.A.; Stevens, G.W.; Kentish, S.E. “Membrane gas separation applications in natural gas processing”. *Fuel* 96 (2012) 15–28.

-
- 209 Sahota, S.; Shah, G.; Ghosh, P.; Kapoor, R.; Sengupta, S.; Singh, P.; Vijay, V.; Sahay, A.; Vijay, V.K.; Thakur, I.S. "Review of trends in biogas upgradation technologies and future perspectives. *Bioresour. Technol. Rep.* 1 (2018) 79–88.
- 210 Scholz, M.; Melin, T.; Wessling, M. "Transforming biogas into biomethane using membrane technology". *Renew. Sustain. Energy Rev.* 17 (2013) 199–212.
- 211 Cersosimo, M.; Brunetti, A.; Drioli, E.; Fiorino, F.; Dong, G.; Woo, K.T.; Lee, J.; Lee, Y.M.; Barbieri, G. "Separation of CO₂ from humidified ternary gas mixtures using thermally rearranged polymeric membranes". *J. Membr. Sci.* 492 (2015) 257–262.
- 212 Scholes, C.A.; Stevens, G.W.; Kentish, S.E. "The effect of hydrogen sulfide, carbon monoxide and water on the performance of a PDMS membrane in carbon dioxide/nitrogen separation". *J. Membr. Sci.* 350 (2010) 189–199.
- 213 Zhao, W.; He, G.; Zhang, L.; Ju, J.; Dou, H.; Nie, F.; Li, C.; Liu, H. "Effect of water in ionic liquid on the separation performance of supported ionic liquid membrane for CO₂/N₂". *J. Membr. Sci.* 350 (2010) 279–285.
- 214 Pourafshari Chenar, M.; Soltanieh, M.; Matsuura, T.; Tabe-Mohammadi, A.; Khulbe, K.C.; "The effect of water vapor on the performance of commercial polyphenyleneoxide and Cardo-type polyimide hollow fiber membranes in CO₂/CH₄ separation applications". *J. Membr. Sci.* 285 (2006) 265–271.
- 215 Vrbova, V.; Ciahotny, K. "Upgrading biogas to biomethane using membrane separation". *Energy Fuels* 31 (2017) 9393–9401.
- 216 Melone L.; Giorno L.; Brunetti A.; Barbieri G. "Analysis of membrane unit performance in presence of wet CO₂-containing mixtures"; *Chem. Eng. Res. Des.*, 2020, 153, 721–727.

-
- 217 Syrtsova, D. A.; Kharitonov, A. P.; Teplyakov, V. V. "Improving gas separation properties of polymeric membranes based on glassy polymers by gas phase fluorination". *Desalination* 163 (2004) 273-279.
- 218 Zhao, J.; Xie, K.; Liu, L.; Liu, M.; Qiu, W.; Webley, P. A. "Enhancing plasticization-resistance of mixed-matrix membranes with exceptionally high CO₂/CH₄ selectivity through incorporating ZSM-25 zeolite". *J. Memb. Sci.* 583 (2019) 23-30.
- 219 Scholes, C. A.; Stevens, G. W.; Kentish, S. E. "The effect of hydrogen sulfide, carbon monoxide and water on the performance of a PDMS membrane in carbon dioxide/nitrogen separation". *J. Memb. Sci.* 350 (2010) 189-199.
- 220 Visvanathan, C.; Basu, B.; Mora, J.C. "Separation of Volatile Organic Compounds by Pervaporation for a Binary Compound Combination: Tricloroethylene and 1,1,1-Trichloroethane". *Ind. Eng. Chem. Res.* 34 (1995) 3956-3962
- 221 Chang, B.-J.; Chang, Y.-H.; Kim, D.-K.; Kim, J.-H.; Lee, S.-B. "New Copolyimide membranes for the Pervaporation of Trichloroethylene from Water". *J. Memb. Sci.* 248 (2005) 99-107.
- 222 Dotremont, C.; Brabants, B.; Geeroms, K.; Mewis, J.; Vandecasteele C. "Sorption and diffusion of chlorinated hydrocarbons in silicalite-filled PDMS membranes". *J. Memb. Sci.* 104 (1995) 109-117
- 223 Yeom, C. K.; Lee, S. H.; Song, H. Y.; Lee, J. M. "Vapor permeations for a series of VOCs/N₂ mixtures through PDMS membrane". *J. Memb. Sci.* 198 (2002) 129-143.
- 224 Yeom, C. K.; Lee, S. H.; Song, H. Y.; Lee, J. M. "Vapor permeations for a series of VOCs/N₂ mixtures through PDMS membrane". *J. Memb. Sci.* 198 (2002) 129-143.
- 225 Uragami, T. "Pervaporation and Evapomeation with Si-Containing Polymers", in: Y. Yampolskii and E. Finkelshtein (Eds), *Membrane Materials for Gas and Vapor*

-
- Separation. Synthesis and Application of Silicon-Containing Polymers, Wiley publishing, 2017. Reference to a chapter in an edited book: Chapter 10.
- 226 Sikdar, S. K. "Sustainable development and sustainability metrics" *AIChE J.* 49 (2003) 1928-1932.
- 227 A. Stankiewicz, J. A. Moulijn, *Process intensification: Transforming chemical engineering*, *Chem. Eng. Prog.* 96 (2000) 22-23.
- 228 Stankiewicz, A.; Moulijn J. A. "Process intensification". *Ind. Eng. Chem. Res.* 41 (2002) 1920-1924.
- 229 Van Gerven, T.; Stankiewicz, A. "Structure, Energy, Synergy, Time – The Fundamentals of Process Intensification". *Ind. Eng. Chem. Res.* 48 (2009) 2465-2474.
- 230 Drioli, E.; Ali, A.; Macedonio, F. "Membrane operations for process intensification in desalination". *Appl. Sci.* 7 (2017) 100
- 231 Melone, L.; Brunetti, A.; Drioli, E.; Barbieri, G. "An integrated membrane process for butenes production". *Process.* 4 (2016) 42.
- 232 http://multiprod-vacuum.ro/wp-content/uploads/2017/03/Manual-GP-M-eng-03-15-gp-11-21_.pdf (accessed 28 February 2020)
- 233 Wu, J.; Chen, V. "Shell-side mass transfer performance of randomly packed hollow fiber modules". *J. Membr. Sci.* 172 (2000) 59–74.
- 234 Seider, W. D.; Seader, J.D.; Lewin, D. R. "Product and Process Design Principles. Synthesis, Analysis and Evaluation". II edition. Jhon Wiley and Sons. 1999.
- 235 Melone L.; Brunetti A.; Giorno L.; Barone M.; Barbieri G. " Trichloroethylene/Nitrogen Mixture Separation via membrane operations: comparison with traditional technologies"; *Sep. Pur. Tech.* 251 (2020) 117344